Dissertation zur Erlangung des Doktorgrades
der Fakultät für Chemie und Pharmazie
der Ludwig-Maximilians-Universität München

Structural and functional characterization of the INO80 Arp8 module

Kilian Rupert Knoll
aus
Freising, Deutschland

2018

Erklärung

Diese Dissertation wurde im Sinne von §7 der Promotionsordnung vom 28. November 2011 von Herrn Prof. Dr. Karl-Peter Hopfner betreut.

Eidesstattliche Versicherung

Diese Dissertation wurde eigenständig und ohne unerlaubte Hilfe erarbeitet.

München, den 26.10.2018

_____

Kilian Rupert Knoll

Dissertation eingereicht am: 29.10.2018

1. Gutachter: Herr Prof. Dr. Karl-Peter Hopfner

2. Gutachter: Herr Prof. Dr. Roland Beckmann

Mündliche Prüfung am: 17.12.2018

This thesis was prepared from January 2015 to October 2018 in the laboratory of Prof. Dr. Karl-Peter Hopfner at the Gene Center of the Ludwig-Maximilians-Universität (LMU).

Parts of this thesis have been published:

Knoll K.R.*, Eustermann S.*, Niebauer V., Oberbeckmann E., Stoehr G., Schall K., Tosi A., Schwarz M., Buchfellner A., Korber, P., Hopfner K-.P. (2018). The nuclear actin-containing Arp8 module is a linker DNA sensor driving INO80 chromatin remodeling. Nature Structural & Molecular Biology 25, 823-832.

*These authors contributed equally.

Parts of this thesis have been presented at international conferences:

Poster presentation at the FASEB Science Research Conference: Machines on Genes - June 2018 in Aspen, USA.

Poster presentation at the EMBO Conference: The Nucleosome - August 2017 in Heidelberg, Germany.

Poster presentation at the EMBO Conference: Molecular Machines - November 2016 in Heidelberg, Germany.

Poster presentation at the 4th Munich Chromatin Symposium: Chromatin Dynamics March 2016 in Munich, Germany.

I think it was this curiosity about the natural world which awoke my early interest in science.

Paul Nurse

TABLE OF CONTENTS

1 Summary

DNA in eukaryotic cells is packed as chromatin, a protein DNA complex. The basic unit of chromatin is the nucleosome, in which DNA is wrapped around a core of histone proteins. ATP-dependent chromatin remodelers are key regulators of the chromatin architecture and thereby regulate the accessibility of genetic information. Consequently, chromatin remodelers are critical regulators of transcription, DNA replication and genome maintenance. Chromatin remodelers are typically large multi-subunit complexes that non-covalently alter nucleosomes, for example by sliding nucleosomes on the DNA. Notably, actin-fold proteins such as nuclear actin (N-actin) and actin-related proteins (ARPs) are key components of several chromatin-associated complexes. Interestingly, in all known chromatin remodeling complexes N-actin and Arp4 form a conserved heterodimer. The INO80 complex, a large multi-subunit chromatin remodeler, comprises four actin-fold proteins in total. In INO80, N-actin and ARPs are organized as a submodule, the INO80 'Arp8 module', which is critical for INO80 function. Although, the role of N-actin and ARPs has been studied intensively, little is known about their important function in chromatin remodeling, mainly due to a lack of information about the structural framework that organizes the actin-fold proteins within chromatin remodelers.

Therefore, the aim of this thesis was to structurally and functionally characterize the elusive actin-fold protein subunits of the INO80 remodeler. In particular, the INO80 Arp8 module was studied by X-ray crystallography and biochemical methods.

During this thesis, the crystal structure of the 180 kDa *Saccharomyces cerevisiae* Arp8 module of the INO80 remodeler was solved at 4 Å resolution. The structure reveals the molecular architecture of this important INO80 submodule. In the Arp8 module complex the helicase/SANT-associated (HSA) domain of the Ino80 subunit functions as a binding platform for three actin-fold proteins, Arp4, N-actin and Arp8. Thereby, Arp8 specifically recruits the conserved Arp4-N-actin heterodimer via a novel type of actin-fold interaction to the helical HSA domain. By binding to each barbed-end of the three actin-fold proteins the HSA domain extends over a distance of 120 Å. Remarkably, the solvent accessible side of the HSA domain is decorated with highly conserved positively-charged lysine and arginine residues. Electro mobility shift assays revealed that the INO80 Arp8 module binds nucleosomes at the extranucleosomal DNA overhang and identified the positively-charged side of the HSA domain as the responsible DNA binding element. Mutational analysis, performed in parallel to this study, of the Ino80 HSA domain in context of the entire INO80 complex revealed that binding of the Arp8 module to extranucleosomal DNA is required to couple Ino80 motor activity to INO80 nucleosome remodeling. Together with the recent cryoEM structure of the INO80^{Core}-nucleosome complex, the Arp8 module crystal structure

provides, a first structural model of the conserved and functional critical part of the INO80 complex bound to the nucleosome. Interestingly, the Arp8 module is located close to the Ino80 motor domain at the entry site of the nucleosomal DNA and binds to 40 bp of extranucleosomal linker DNA. These structural insights, together with the biochemical data, suggest a model in which the Arp8 module functions as a sensor for 40 bp of extranucleosomal DNA and thereby drives INO80 nucleosome remodeling.

Moreover, the characteristics of the Arp4-N-actin dimer were examined by using a nanobody that specifically probes the conserved heterodimer in its endogenous environment. Affinity enrichment mass spectrometry demonstrated that the nanobody binds to all complexes that contain the Arp4-N-actin heterodimer in *Saccharomyces cerevisiae*: INO80, SWR1 and NuA4. In addition, the crystal structure of the ternary 120 kDa nanobody-Arp4-N-actin complex was solved at 2.8 Å resolution. Interestingly, the structure reveals that the nanobody binds the ATP-bound state of N-actin. Overall, the crystal structure, together with the mass spectrometry results, suggests a conserved arrangement of the Arp4-N-actin dimer in chromatin-associated complexes in *Saccharomyces cerevisiae*. Furthermore, the results indicate that ATP binding by N-actin in chromatin remodeling complexes is a conserved and common feature.

In summary, this work revealed the architecture of the INO80 Arp8 module and suggests a model for how the Arp8 module directly contributes to the mechanochemical cycle of INO80 nucleosome remodeling by sensing 40 bp of extranucleosomal DNA.

2 Introduction

2.1 Chromatin

Genetic information is encoded in the DNA sequence. The central dogma of molecular biology describes the flow of genetic information; RNA polymerases transcribe DNA into RNA and ribosomes translate RNA into proteins (Crick, 1970). Key features of life, such as adaption to environmental changes, growth and differentiation of cells, depend on the fine-tuned regulation of transcription and translation. A multitude of factors and mechanisms help to control and regulate the flow of genetic information. In eukaryotes the DNA is organized as chromatin, a protein-DNA complex, where the negatively-charged DNA is wrapped around the basic histone proteins. In contrast to free DNA, chromatin can be highly compact, enabling storage of the whole genome in the nucleus. More importantly, the organization of DNA as chromatin restricts access of DNA-binding factors to the genetic information and accordingly functions as an critical layer of regulation for all DNA-dependent processes in a eukaryotic cell (Judith G. Voet 2012).

2.1.1 Basic unit of chromatin: The nucleosome

The basic repeating unit of chromatin is the nucleosome (Kornberg, 1974, 1977; Olins and Olins, 1974; Olins and Olins, 2003), which is composed of DNA wrapped around a core of histone proteins in a left-handed superhelix (Luger et al., 1997) (Figure 1). The canonical histone core is constructed from two copies each of the four highly conserved histone proteins: H2A, H2B, H3 and H4. One H3-H4 tetramer builds together with two H2A-H2B dimers the histone octamer core, around which is wrapped 147 bp of DNA, thereby forming the nucleosome core particle (NCP) (Cutter and Hayes, 2015; Luger et al., 1997) (Figure 1a). In the NCP the centre of the nucleosomal DNA, termed the dyad, contacts the symmetrical histone octamer at the H3-H3 interface with the minor groove turned outwards. This minor groove position is termed super helical location (SHL) 0, from here on seven SHLs (±1, ±2, ±3, ...), minor grooves, follow in both directions until the DNA reaches the end of the NCP and the start of the extranucleosomal linker DNA (Figure 1d). This forms a continuous connection between individual NCPs (Cutter and Hayes, 2015; Kornberg, 1977; Olins and Olins, 1974) (The orientation of the SHL, + or -, is arbitrary; see comment in section 2.6). DNA is highly bent by binding across the histone octamer and forming 14 histone-DNA contacts (Figure 1d). Sequence-dependent DNA deformability is hereby an important feature that leads to energetically preferred nucleosome positions on the DNA, which is observed for example at so called nucleosomal arrays around gene start sites (Clapier et al., 2017; Jiang and Pugh, 2009).

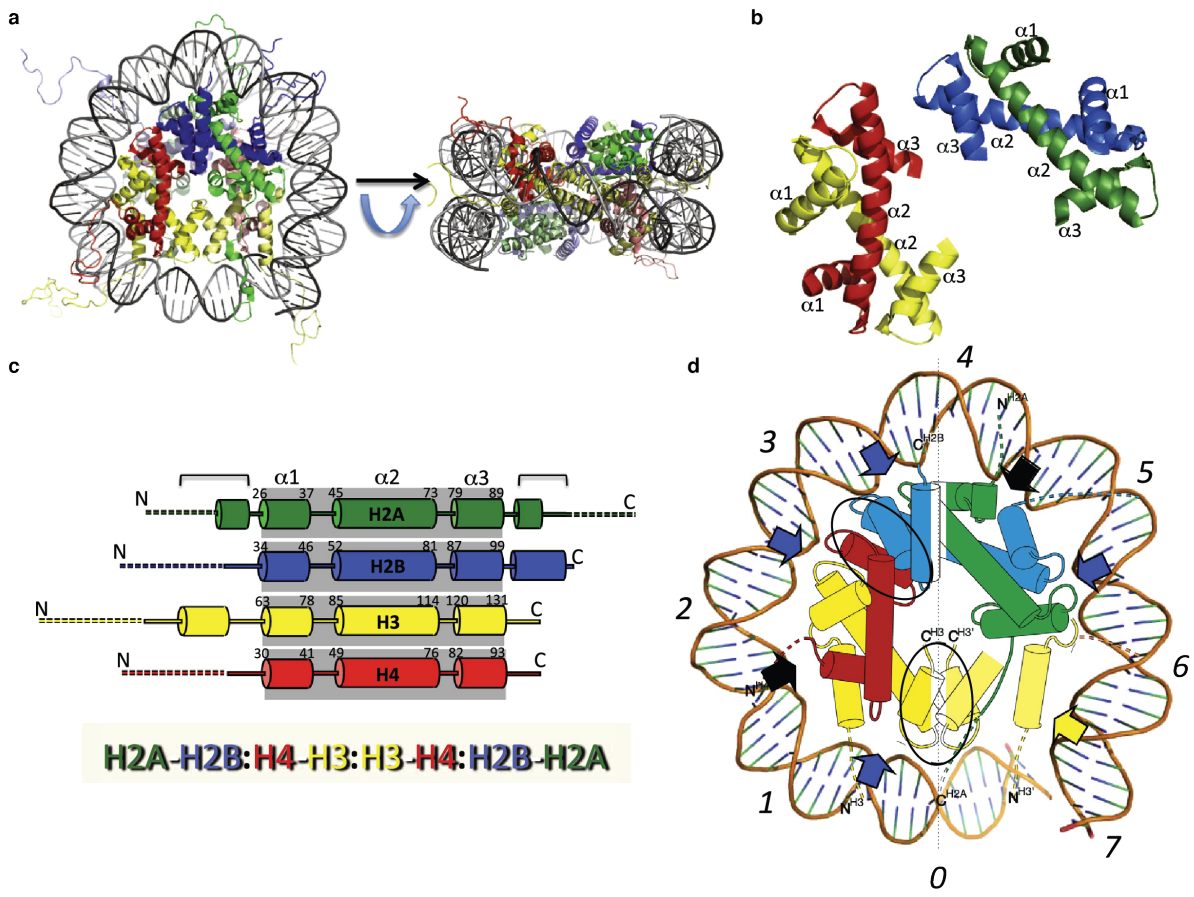

Figure 1 Structure of the nucleosome.

a, Crystal structure of the nucleosome core particle in two views (left side: top view; right side: side view looking at the dyad axis) shown in cartoon representation (PDB 1KX5). The four histone proteins are shown in green (H2A), blue (H2B), red (H4) and yellow (H3). The DNA is shown in black. **b**, Histone fold dimers H2A-H2B and H4-H3. Alpha helices of the conserved histone fold are labeled accordingly. Color code is the same as in panel a. **c**, Domain architecture of the canonical histones. Dashed stroke indicates regions that are not visible in the structure shown in panel a. Brackets indicate regions outside the conserved histone fold, shown in panel b. **d**, Top view of the nucleosome with all superhelical locations (SHLs) of one DNA gyre numbered accordingly. SHL 0 is located at the nucleosome dyad. Interactions between H3-H3 and H2B-H4 are indicated by ovals. Arrows indicate histone-DNA interactions of one DNA gyre. Adapted and modified from (Cutter and Hayes, 2015).

At the lateral surface of the histone octamer, which is not covered by the nucleosomal DNA, is the so-called acidic-patch, a region at the H2A-H2B dimer surface. This is an important interaction site for several NCP-binding factors and it might be also involved in the formation of higher-order chromatin structures (Kalashnikova et al., 2013). In addition to the structured histone-fold region, histone proteins harbour unstructured tail extensions that emerge from the NCP (Figure 1b and c). Posttranslational modifications (PTMs) of histone tails function as epigenetic marks. PTMs of histone tails coupled to 'reader', 'writer' and 'eraser' factors modulate the chromatin structure and control critical processes such as

DNA repair, transcription or DNA replication (Bannister and Kouzarides, 2011; Cutter and Hayes, 2015). Indeed, it was proposed that histone modifications sequentially and/or in combination form a 'histone code' that regulates diverse cellular events (Strahl and Allis, 2000). In addition to covalent histone tail modifications, histone variants play an important role in the regulation of many cellular processes (Venkatesh and Workman, 2015). For example, incorporation of the histone variant H2A.Z instead of H2A at promoter sites can lead to transcription activation (Sarma and Reinberg, 2005). In more compact chromatin an additional histone protein, the linker histone H1, binds the two extranucleosomal DNA strands next to their DNA exit sites from the NCP and thereby stabilizes the nucleosome and promotes formation of transcriptionally inactive chromatin (Cutter and Hayes, 2015).

2.1.2 Chromatin architecture

Chromatin can adopt differently compact states, ranging from a highly condensed metaphase chromosome, to individual nucleosomes on the DNA as 'beads on a string' during interphase. How chromosomes are assembled is still debated (Ou et al., 2017; Razin and Gavrilov, 2014; Woodcock and Ghosh, 2010). In the hierarchical chromatin-folding model it was proposed that chromatin forms secondary structure like elements, such as the "30 nm fibre", and sequential folding into higher-order structures leads to formation of a condensed chromosome (Woodcock and Ghosh, 2010). Indeed, the genome-wide formation of structural motifs such as, tri-or tetra-nucleosome structures was observed (Hsieh et al., 2015). However, the existence of strict higher-order elements in chromatin is questioned at present (Razin and Gavrilov, 2014). Chromatin electron microscopy tomography (ChromEMT) indicated that chromatin during interphase and also in mitotic chromosomes is organized into disordered chains with a diameter of 5 to 24 nm. Based on these new insights it was proposed that the organization of chromatin into different compact states depends on the chromatin volume concentration (CVC), rather than on higher-order structures (Ou et al., 2017).

Despite the controversial discussion about a hierarchical chromatin folding model it is nowadays clear that interphase chromosomes are organized into separate territories, so called chromosome territories (CT) (Cremer and Cremer, 2010). CTs are a major feature of chromatin architecture and recent technical progress revealed a distinct substructure of chromosomes, so called chromatin domains or topologically associated domains (TADs) (Dixon et al., 2016). Genome-wide chromosome conformation capture (3C) techniques revealed a defined organization of TADs that seems to be conserved between different cell types (Jost et al., 2017). TADs play important roles in transcription regulation, for example

genes within the same TAD are co-regulated by the same enhancer element, whereas genes in the neighbouring TAD are blocked from this co-regulation (Dixon et al., 2016). The organization of chromatin as TADs depends on formation of chromatin loop extrusions by structural maintenance of chromosome (SMC) protein complexes, such as Cohesion, and the adaptor protein CCCTC-binding factor (CTCF) (Yuen and Gerton, 2018).

An additional layer of chromatin organization is the compartmentalization into inactive/heterochromatin and active/euchromatin zones (Allshire and Madhani, 2018). Historically the terms heterochromatin and euchromatin originate from the staining behaviour of interphase chromatin; dark stained inaccessible regions are called heterochromatin and light stained open regions euchromatin. Heterochromatin is less dynamic than euchromatin and can be further divided into facultative heterochromatin (fHC) and constitutive heterochromatin (cHC). fHC is transcriptionally repressed and formed by Polycomb group (PcG) multiprotein complexes (PRC1 and PRC2). The formation of fHC is important in the regulation of cell differentiation (Trojer and Reinberg, 2007). cHC is static, transcriptionally inert and associates to the nuclear lamina. The formation of cHC depends on the methylation of the H3K9 (H3K9me), a histone mark which recruits the heterochromatin protein 1α (HP1α). HP1α binding leads to the formation of distinct cHC microcompartments (Rada-Iglesias et al., 2018). Euchromatin regions in contrast are transcriptionally active and highly dynamic. Interaction with multiple factors such as RNA polymerases, transcription factors or chromatin-associated complexes dynamically changes the chromatin organization (Jiang and Pugh, 2009; Rada-Iglesias et al., 2018).

2.1.3 Genic nucleosomal arrays

Not only transcriptionally repressed DNA but also actively transcribed genes are packed by nucleosomes. The organization of nucleosomes on eukaryotic genes is not random, but highly ordered. The positioning and composition of nucleosomes around gene starts affects the transcription of the respective genes. Improvement of DNA sequencing techniques allowed genome wide mapping of nucleosomes, for example by ChiP-Seq (Chromatin-immunoprecipitation followed by high-throughput DNA sequencing) experiments. Comparison of genome-wide nucleosome positions revealed a general organization of nucleosomes on genes, so called genic nucleosomal arrays, a hallmark of chromatin (Lai and Pugh, 2017; Stunkel et al., 1997; Zhao et al., 2001). Similarly, nucleosomes around origin of replications (ORI) adopt a conserved positioning pattern (Deal et al., 2010; Eaton et al., 2010; Lai and Pugh, 2017).

The overall organization of genic nucleosomal arrays is conserved between different species (Figure 2). Genes are bordered by upstream and downstream nucleosome-free regions (NFRs) or nucleosome-depleted regions (NDR) (NDRs are promoter sites where nucleosomes are actively removed by chromatin remodelers upon gene activation in contrast to NFRs, which are permanently nucleosome free). The upstream NFR is flanked by two tightly positioned nucleosomes. The -1 and +1 nucleosomes are positioned at the 5' and 3' ends of the NFR, respectively. In *Saccharomyces cerevisiae* (hereafter denoted as yeast) the +1 nucleosome is located at the transcription start site (TSS) of a gene, whereas in metazoans 30-50 bp downstream of the TSS (Schones et al., 2008). The +1 nucleosome is followed by an array of nucleosomes with a defined spacing, for example in yeast with a spacing of 165 bp from dyad to dyad. The nucleosomal array extends into the gene body, but diffuses into downstream direction of the gene. Furthermore, +1 and -1 nucleosomes often contain histone variants or PTMs that function as important regulatory signals (Jiang and Pugh, 2009; Lai and Pugh, 2017). For example, the histone variant H2A.Z is often incorporated into the +1 nucleosomes of actively transcribed genes (Sarma and Reinberg, 2005).

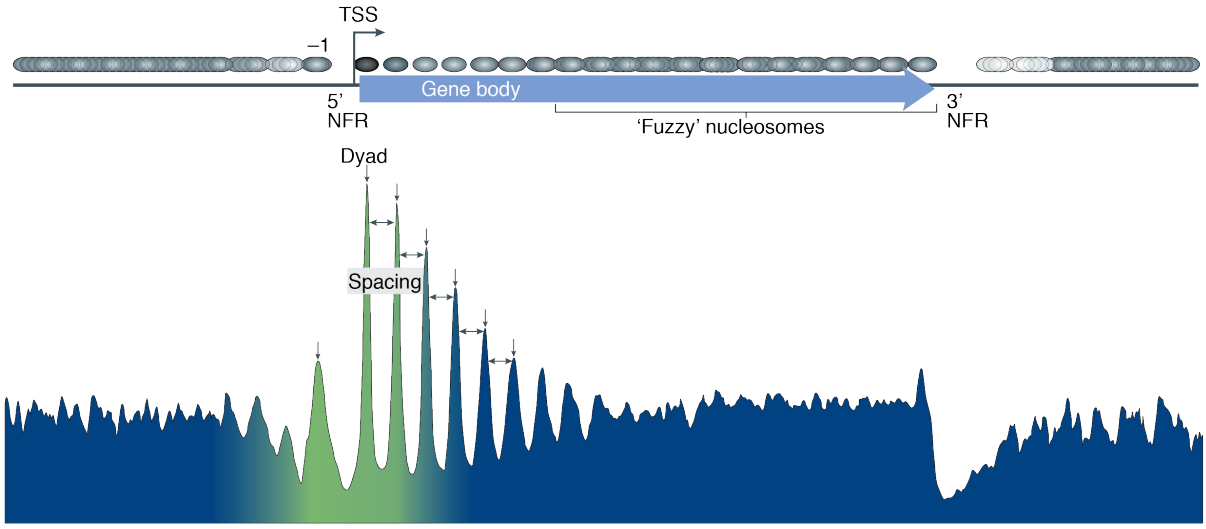

Figure 2 Organization of genic nucleosomal arrays in yeast.

On the top a schematic overview of the typical nucleosome organization around genes in yeast, with nucleosomes shown as grey ovals. The gene body is enclosed by nucleosome-free regions (NFRs) at the 5' and the 3' end. The 5' NFR is flanked by the -1 and the +1 nucleosomes. The +1 nucleosome is located at the transcription start site (TSS) and followed by an array of nucleosomes, that diffuses in 3' direction of the gene. The plot below shows a typical occupancy and positioning profile of nucleosomes on yeast genes, reflecting the schematic representation on the top. Top of peaks fit the dyad position of a particular nucleosome. The distance between the peaks corresponds to the spacing distance. In the green colored regions, the nucleosome composition is often altered, for example nucleosomes contain the histone variant H2A.Z instead of H2A. Adapted and modified from (Jiang and Pugh, 2009).

The positioning of nucleosomes on the DNA depends partially on the DNA sequence; indeed, sequences in the NFRs are unfavorable for nucleosome binding, whereas the +1 or -1 positions are highly favorable. However, the overall organization of nucleosomal arrays, composition, positioning and spacing of nucleosomes, is driven and regulated by chromatin-associated factors, such as chromatin remodelers, histone chaperones, nucleosome-organizing factors and histone-modifying enzymes (Clapier et al., 2017; Jiang and Pugh, 2009; Lai and Pugh, 2017). It was shown that ATP-dependent trans acting factors, such as chromatin remodelers, are necessary for the formation of genic nucleosomal arrays (Zhang et al., 2011). *In vivo* and *in vitro* studies demonstrated that during the formation of genic nucleosomal arrays different remodelers have specific functions for the nucleosome organization at the TSS, such as NFR formation, +1 nucleosome positioning, array formation and spacing of nucleosomes (Badis et al., 2008; Ganguli et al., 2014; Hartley and Madhani, 2009; Krietenstein et al., 2016; Ocampo et al., 2016). In addition 'barrier factors', specific DNA-binding proteins such Reb1 or Abf1, are important for the correct +1 nucleosome positioning (Jiang and Pugh, 2009; Krietenstein et al., 2016). Moreover, specialized chromatin remodelers and histone chaperones catalyze the exchange of histone variants at promoter sites (Venkatesh and Workman, 2015), particularly at the +1 and -1 nucleosomes (Jiang and Pugh, 2009; Malik and Henikoff, 2003).

Overall, fundamental cellular processes, such as transcription, replication and DNA repair, are regulated by the organization of nucleosomes at specific loci, such as genic nucleosomal arrays, which in turn are dependent on chromatin remodelers, major modulators of nucleosome positioning and composition.

2.2 Chromatin remodelers: A general overview

ATP-dependent chromatin remodelers form a large family of factors that alter the chromatin architecture non-covalently by positioning nucleosomes, the assembly/eviction of entire nucleosomes and changing the nucleosome composition (exchange of histone variants). All known chromatin remodelers belong to the superfamily 2 (SF2) class of helicases and share a conserved sucrose non-fermenting 2 (Snf2)-type ATPase domain (also termed motor domain or main ATPase). Intriguingly, it is assumed that the Snf2-type ATPase functions as the motor for all kinds of nucleosome remodeling reactions by simply translocating double stranded (ds) DNA in an ATP-dependent manner (SF2 helicases are described in more detail in section 2.3). A major challenge in decoding the molecular

mechanism of chromatin remodelers is to understand how the different domains, subunits and the architecture of a chromatin remodeler specify and convert the simple DNA translocation into a particular nucleosome remodeling reaction (Bartholomew, 2014; Clapier et al., 2017).

Table 1 Members of the four remodeler families in yeast and human.

Table shows the name of a particular remodeler complex, the name of the respective subunit harboring the Snf2-type ATPase and the number of subunits. Families highlighted in yellow contain N-actin and ARPs as subunits. Of note, in some of the human chromatin remodelers the complex composition varies between different cell types, which is why the stated number of subunits is not universal (Ho and Crabtree, 2010). Comment to the nomenclature: For yeast remodelers UPPERCASE letter names refer to the complex e.g. SWR1 and mixed case names to the subunit e.g. Swr1. In contrast, the human protein names and complex names are both written in in UPPERCASE, but protein names have a 'h' as prefix. Table is based on (Clapier and Cairns, 2009; Hodges et al., 2016; Hota and Bruneau, 2016).

Familiy		Organism					
		Yeast			Human		
SWI/SNF	**Complex name**	**SWI/SNF**	**RSC**		**BAF**	**PBAF**	
	Snf2-type ATPase	Swi2/Snf2	Sth1		hBRM or BRG1	hBRG1	
	number of subunits	12	17		14	14	
INO80	**Complex name**	**INO80**	**SWR1**		**INO80**	**SRCAP**	**TIP60**
	Snf2-type ATPase	Ino80	Swr1		hINO80	hSRCAP	hp400
	number of subunits	15	14		15	10	15
ISWI	**Complex name**	**ISW1a**	**ISW1b**	**ISW2**	**NURF**	**CHRAC**	**ACF**
	Snf2-type ATPase	Isw1		Isw2	hSNF2L	hSNF2H	
	# of subunits	2	3	2	3	4	2
CHD	**Complex name**	**CHD1**			**CHD1**	**NuRD**	
	Snf2-type ATPase	Chd1			hCHD1	hMi-2α/CHD3, hMi-2β/CHD3	
	number of subunits	1			1	10	

According to the domains flanking the Snf2-type helicase domain, chromatin remodelers can be classified into four different subfamilies (Clapier and Cairns, 2009; Flaus et al., 2006); the inositol auxotroph mutant 80 (INO80), switch/sucrose non-fermenting (SWI/SNF), imitation switch (ISWI) and chromodomain helicase DNA-binding (CHD) remodeler families (Figure 3) (see Table 1 for members of the four remodeler families in yeast and human). Remodelers of the INO80 and SWI/SNF families are typically large multi-subunit protein complexes, whereas the members of the ISWI and CHD families are small complexes or act as single subunits. Typically, the subunit harbouring the Snf2-type ATPase domain functions as binding platform for the other subunits. Most of the chromatin remodelers contain domains or subunits with so called 'reader-motifs' that recruit the complexes to specific PTMs of histone tails (Bartholomew, 2014; Clapier et al., 2017). A hallmark and long-standing puzzle of the large remodeler complexes from the INO80 and SWI/SNF families is that they contain nuclear actin (N-actin) and actin-related-proteins (ARPs) as conserved and critical subunits (Clapier et al., 2017; Olave et al., 2002).

Nuclear actin is itself identical to cytoplasmic actin and the term N-actin denotes only the location of actin. In both families a helicase/SANT-associated (HSA) domain N-terminal of the Snf2-type ATPase domain functions as a binding site for N-actin and/or ARPs (Szerlong et al., 2008).

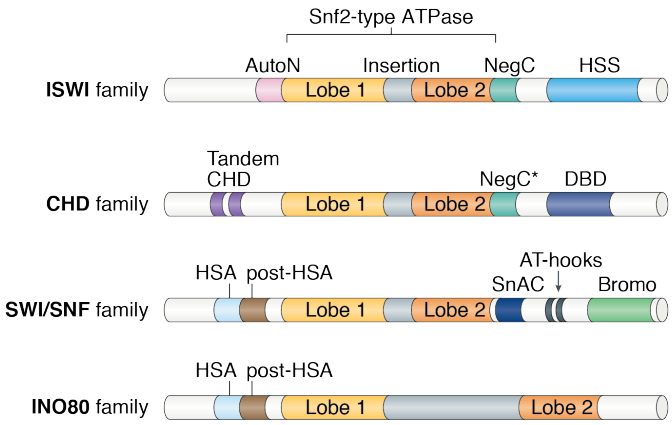

Figure 3 Chromatin remodeler subfamilies.

Schematic illustrations of the Snf2-type subunit domain architecture for the four chromatin remodeler families. Lobe1 and Lobe2 refer to the two RecA lobes of the Snf2-type ATPase domain (see section 2.3 for further information about the Snf2-type ATPase domain), adjacent domains are labeled accordingly. ISWI family: AutoN, autoinhibitory N-terminal domain; NegC, negative regulator of coupling domain; HSS, HAND–SANT–SLIDE domain. CHD family: Tandem CHD, tandem chromodomain; NegC*, NegC domain similar to the ISWI NegC domain; DBD, DNA-binding domain comprising SANT and SLIDE domains. SWI/SNF family: SnAC, Snf2 ATP-coupling domain; AT-hooks, DNA-binding motif with preference for A/T rich sequences; Bromo, bromodomain a reader domain for acetylated lysines SWI/SNF and INO80 family: HSA, helicase-SANT-associated domain; post-HSA, conserved region located between HSA domain and the Snf2-type ATPase domain. Adapted and modified from (Clapier et al., 2017).

Remodelers of the SWI/SNF family comprise typically 12 to 17 subunits. Besides N-actin and ARPs, SWI/SNF remodelers harbour a C-terminal bromo domain, which binds acetylated H3 and H4 tails, and AT-hooks, a DNA binding motif. Members of this remodeler family can slide and eject nucleosomes and seem to play an important role in cell differentiation (Clapier and Cairns, 2009; Wilson and Roberts, 2011). In addition, the human SWI/SNF homolog, the BAF complex, was identified as important tumour suppressor. Genes coding for subunits of the human SWI/SNF remodeler are highly mutated in cancer (Wilson and Roberts, 2011). ISWI remodelers form smaller complexes with 2 to 4 subunits and have specialized functions in nucleosome spacing and positioning. A unique feature of the ISWI remodelers is a C-terminal HAND-SANT-SLIDE domain, which binds the unmodified H3 tail and extranucleosomal DNA (Clapier et al., 2017).

Together with the 'barrier factors', Abf1 or Reb1, ISW2 and/or ISW1a position the +1 nucleosome. In addition, ISWI remodelers improve spacing of nucleosomes in preformed nucleosomal arrays (Krietenstein et al., 2016). The CHD family of remodelers consists in yeast of only one family member that acts as a single protein. CHD remodelers contain two N-terminal chromodomains that are followed by the Snf2-type ATPase and a C-terminal DNA binding domain (DBD). Remodelers of the CHD class space nucleosomes, expose promoter sites and incorporate the histone variant H3.3, and thus promote transcription in general (Clapier et al., 2017). The INO80 family of remodelers will be described in more detail in section 2.2.1.

2.2.1 The INO80 chromatin remodeler

The INO80 family consists in yeast of two members INO80 and SWR1, both of which are large protein complexes (Clapier and Cairns, 2009; Flaus et al., 2006). Whereas in humans the INO80 class comprises three complexes; INO80, SRCAP and TRRAP/Tip60 (Clapier and Cairns, 2009). Remarkably, the human TRRAP/Tip60 complex is a fusion of two yeast complexes, the SWR1 remodeler and the NuA4 histone acetyltransferase (Doyon and Cote, 2004). The unique feature of INO80 family members is a long insertion element within the Snf2-type ATPase. Interestingly, that insertion element functions in INO80 and SWR1 as a binding site for a heterohexamer of Rvb1 and Rvb2 (Chen et al., 2011; Chen et al., 2013; Tosi et al., 2013; Wu et al., 2005). In addition, both remodelers contain a dimer of N-actin and Arp4 that binds to the HSA domain on the respective Snf2-type ATPase subunit (Olave et al., 2002; Szerlong et al., 2008). Otherwise the two complexes do not share any similarities in terms of subunit composition, although both remodelers have a similar modular architecture (Gerhold and Gasser, 2014).

SWR1 has no nucleosome sliding, assembly or disassembly activity, but edits nucleosomes by incorporating the non-canonical H2A.Z-H2B dimer at promoter sites and thereby promotes transcription activation (Gerhold and Gasser, 2014; Krogan et al., 2003; Mizuguchi et al., 2004). It was reported that INO80 catalyses the reverse reaction to SWR1 by exchanging the histone variant dimer, H2A.Z-H2B for the canonical H2A-H2B dimer (Papamichos-Chronakis et al., 2011; Watanabe et al., 2013), albeit this function of INO80 is questioned (Wang et al., 2016). Nonetheless, during homologous recombination INO80 function is critical for the removal of H2A.Z from DNA double-strand breaks (Alatwi and Downs, 2015; Lademann et al., 2017). Moreover, INO80 is a highly processive chromatin remodeler (Schwarz et al., 2018; Zhou et al., 2018) that can slide (Shen et al., 2003), space (Udugama et al., 2011) and position nucleosomes (Krietenstein et al., 2016). The first

INO80 studies in yeast showed that INO80 function promotes transcription of the *PHO5* gene after phosphate depletion (Ebbert et al., 1999). Moreover, transcriptomic experiments revealed that the activity of INO80 alters transcription of a large portion of yeast genes into both directions (both up- and down-regulation). Transcript levels of around 20% of all yeast genes are changed in an INO80 deletion strain, with about 600 genes up- and 400 genes down-regulated (Poli et al., 2017; van Attikum et al., 2004). ChiP-exo mapping located the INO80 remodeler at the NFR and +1 nucleosome of genic nucleosomal arrays (Yen et al., 2013). Similarly, INO80 is the only remodeler known so far that positions +1 nucleosomes of most of the yeast genes on its own (Krietenstein et al., 2016), implying that INO80 intrinsically recognizes the promoter region in front of the TSS. The mechanism behind this, however, is so far not understood. In addition to +1 positioning, INO80 can form nucleosomal arrays and space nucleosomes, although spacing by INO80 is wider than the canonical nucleosome spacing (Krietenstein et al., 2016; Udugama et al., 2011). INO80's capacity to form nearly complete nucleosomal arrays around genes on its own is exceptional among chromatin remodelers, justifying its genome-wide impact on transcription regulation (Poli et al., 2017; van Attikum et al., 2004). In addition, INO80 has important functions in genome maintenance (Poli et al., 2017). *In vivo* and *in vitro* experiments indicated that INO80 is involved in the release of stalled replication forks (Falbo et al., 2009; Kurat et al., 2017; Shimada et al., 2008). It was proposed that INO80 removes nucleosomes ahead of the stalled replication fork and thereby promotes replication restart (Poli et al., 2017). During DNA repair, INO80 removes nucleosomes at DNA double-strand breaks (DSBs) to promote DNA end-resection during homologous recombination (Lademann et al., 2017). In fact, the expression of INO80 subunits is misregulated in several cancer types (Sheng et al., 2016; Zhou et al., 2016), reflecting its critical role in almost all DNA-dependent processes in eukaryotic cells.

2.3 SF2 family of helicases/translocases

Typically, helicases are enzymes that separate a duplex of nucleic acid strands. However, most members of the so-called helicase families are in fact translocases, enzymes that track along a nucleic acid, and the classical helicases are a subclass of those. Helicases/translocases remodel nucleic acids in an NTP-dependent manner and can be classified into six different superfamilies according to the similarity of conserved helicase-specific sequence motifs in the helicase domains. The helicase core of the two largest families, SF1 and SF2, comprises two similar protein domains that are structurally related to the recombination protein RecA (Singleton et al., 2007). The two RecA-like domains are also termed N- and C-lobe according to the terminus that flanks the respective domain (or

Lobe1 and Lobe2). The conserved 'helicase sequence motifs' in a cleft between the two lobes are important for NTP and nucleic acid binding. SF1 and SF2 members alter nucleic acids by an NTP-dependent conformational change of the two RecA lobes that leads to translocation of the nucleic acid bound between the two domains (Singleton et al., 2007). The best-studied SF2 helicase is the non-structural protein 3 (NS3), a bone-fide helicase that unwinds RNA-DNA duplexes. NS3 binds the ssDNA in a deep grove between the two RecA-like lobes and contacts the phosphodiester backbone mainly with residues of the helicase motif. In addition, hydrophobic residues outside of the helicase motif sandwich five bases of the DNA strand. ATP hydrolysis by NS3 leads to opening and closing of the two RecA lobes, resulting in alternating distances between the hydrophobic residues and leading to DNA translocation by a ratchet-like mechanism (Gu and Rice, 2010).

SF2 helicases/translocases that share sequence similarity in the helicase core to the Snf2 protein, the catalytic subunit of the SWI/SNF remodeler, are further sub-classified as Snf2-type helicases (Flaus et al., 2006; Hopfner et al., 2012). Snf2-type helicases/translocases remodel DNA-protein complexes by translocating dsDNA and applying torsional strain in an ATP-dependent manner (Singleton et al., 2007). Indeed, most of the Snf2-type family members are chromatin remodelers, but there are also members involved in other processes, such as Mot1 in transcription regulation (Flaus et al., 2006; Hopfner et al., 2012). Snf2-type helicases/translocases translocate dsDNA by tracking along the minor-groove in a 3' to 5' direction of one of the two DNA strands, the so-called tracking strand (Durr et al., 2005; Liu et al., 2017; Saha et al., 2002, 2005; Singleton et al., 2007). Models for dsDNA translocation by Snf2-type helicases/translocases rely on the well-studied NS3 helicase, since structural information on Snf2-type helicases for different DNA translocation states is so far missing (Gu and Rice, 2010; Liu et al., 2017). A prerequisite for dsDNA translocation by Snf2-type helicases/translocases is that the ATPase motor is fixed at a specific anchor point, otherwise the enzyme would simply track along the DNA (Clapier et al., 2017). For chromatin remodeling complexes it is assumed that they engage the nucleosome and provide a structural framework that anchors the Snf2-type ATPase on the DNA and allows for translocation of the DNA around the nucleosome (Bartholomew, 2014; Clapier et al., 2017; Hopfner et al., 2012). Our understanding of such a structural framework and how it specifies and facilitates a particular remodeling reaction was very limited, until recent high-resolution cryo-electron microscopy (cryoEM) structures of the Snf2 ATPase, CHD1, INO80^{Core} and SWR1^{Core} bound to the nucleosome were solved (Ayala et al., 2018; Eustermann et al., 2018; Farnung et al., 2017; Liu et al., 2017; Willhoft et al., 2018) (see section 2.5 and 2.6). A current model for INO80 nucleosome remodeling is described in section 2.6.

2.4 Actin and actin-related-proteins in the nucleus

2.4.1 Actin

Actin is one of the most abundant proteins in eukaryotes and highly conserved among different species. It is the main component of the cytoskeleton. By assembling into filaments (also termed microfilaments) actin forms extended networks in the cytoplasm. Actin is critical for diverse cellular processes such as cell migration, cell shape, intracellular transport and cytokinesis. Monomeric actin is a 43 kDa globular protein with a U-shaped fold that can be divided into two lobes or four sub-domains (SDs). Lobe1 is formed by SD2 and SD1 and lobe 2 by SD3 and SD4. A central nucleotide-binding pocket in which ATP is tightly bound by the two phosphate binding loops P1 (residues 11-16) and P2 (residues 154-161) is located between the two lobes (Dominguez and Holmes, 2011; Kudryashov and Reisler, 2013). This overall fold is a conserved structural motif, termed 'actin-fold', that is also found in other proteins of the actin superfamily, such as actin-related-proteins, heat-shock cognate protein 70 (HSC70), hexokinase B and glycerol kinase (Dominguez and Holmes, 2011; Kabsch and Holmes, 1995; Olave et al., 2002) (Figure 4a).

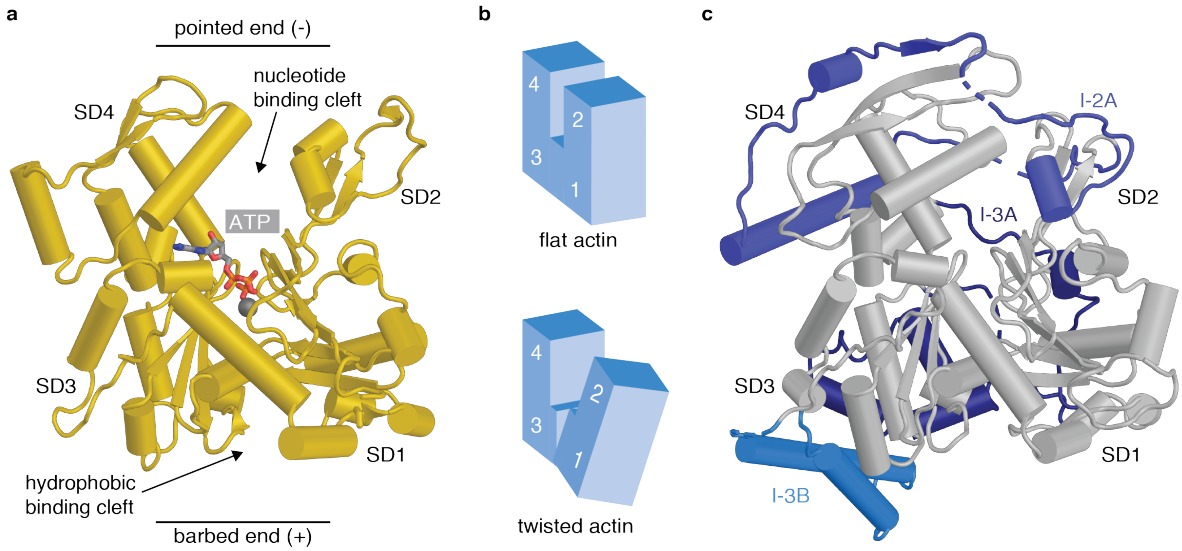

Figure 4 Structure of actin and the actin-related protein 8.

a, Crystal structure of actin (PDB 1ATN) shown as cartoon representation. Domains and features are labeled. **b**, Illustration of actin flattening during actin treadmilling. Adopted from (Dominguez and Holmes, 2011). **c**, Cartoon representation of the actin-related protein 8 (PDB 4AM6). The actin-core-fold is colored in grey, whereas the insertion elements are colored in different blue tones and are labeled accordingly.

In its monomeric form actin is a poor ATPase, but upon filament formation ATP hydrolysis is increased considerably. In a dynamic process called 'actin treadmilling', ATP-bound monomeric actin (G-actin) assembles into actin filaments (F-actin). For filament formation the concentration of actin monomers needs to be above the 'Critical Concentration' (Carlier and Shekhar, 2017). In addition, actin polymerization and ATPase activity are dependent on the concentration and type of divalent metal ions. Ca^{2+} inhibits actin filament formation and ATP hydrolysis, whereas Mg^{2+} triggers both processes (Dominguez and Holmes, 2011; Scipion et al., 2018). Actin filaments grow (assemble) at the barbed end of the actin-fold, formed by SD3 and 1, and shrink (disassemble) at the pointed end, formed by SD2 and 4 (Dominguez and Holmes, 2011). In the filament actin adopts three different nucleotide states: ATP-bound G-actin assembles at the barbed end, the post-hydrolysis ADP-Pi state in the middle and the ADP state at the pointed end. ADP bound F-actin disassembles at the pointed end of the filament into monomeric actin. During the transition from G- to F-actin the actin-fold undergoes a conformational change from a twisted form to a more flat state (Figure 4b). This flattening changes the orientation of critical residues in the nucleotide binding cleft, such as His161 and Glu137, and thereby triggers ATP hydrolysis (Dominguez and Holmes, 2011; Merino et al., 2018). Diverse small compound toxins, from for example fungi or sea sponges, target actin function. Those small molecules toxins have been successfully used as tools to manipulate and study actin dynamics. Latrunculins, one class of such molecules, bind into the nucleotide binding cleft of actin next to ATP and thereby prevent actin flattening and filament formation and consequently trap actin in an ATP state (Dominguez and Holmes, 2011; Morton et al., 2000). In addition, the dynamics of actin filament formation are modulated by diverse actin binding proteins (ABPs) that can, for example, sequester actin monomers, cap filament ends or branch filaments (Dominguez and Holmes, 2011).

The functions of N-actin are less well understood. Due to difficulties in detecting and distinguishing nuclear from highly abundant cytoplasmic actin filaments, the existence of nuclear actin-filaments has been questioned in the past (Fenn et al., 2011b; Misu et al., 2017; Olave et al., 2002; Virtanen and Vartiainen, 2017). However, recent findings could now link nuclear actin filament formation to chromatin dynamics during the homology-directed repair of DNA DSBs. The formation of N-actin filaments and the actin transporter myosin directly move DNA DSBs to the nuclear periphery for homology-directed DNA repair (Caridi et al., 2018; Schrank et al., 2018). Further studies are necessary to understand these new intriguing insights on nuclear actin filaments during chromatin dynamics and DNA repair in more detail.

Monomeric N-actin was found as a stably bound subunit in transcription factors (Qi et al., 2011), RNA polymerases (Hofmann et al., 2004; Hu et al., 2004; Obrdlik et al., 2008; Philimonenko et al., 2004) and chromatin remodeling complexes (Galarneau et al., 2000; Olave et al., 2002; Papoulas et al., 1998; Shen et al., 2000; Zhao et al., 1998). In chromatin remodelers N-actin forms together with Arp4 a conserved heterodimer that is critical for the remodeling function (Harata et al., 1994; Olave et al., 2002). It has been proposed that N-actin might function as a molecular switch that regulates the remodeler activity (Boyer and Peterson, 2000). In fact, addition of the actin-binding drug Latrunculin B to the N-actin containing human BAF complex inhibits the remodeler ATPase activity (Zhao et al., 1998), indicating that there is allosteric regulation of the remodeler via the N-actin nucleotide state. In a contradictory study, however, a more static and nucleotide-free role of N-actin in remodelers was described (Cao et al., 2016). Overall, the role and function of N-actin in chromatin remodeling is only poorly understood.

2.4.2 Actin-related proteins

Actin-related proteins (ARPs) belong to the superfamily of actin-fold proteins and share a moderate sequence similarity with actin (30 – 70%) (Schafer and Schroer, 1999). Crystal structures of individual ARPs, such as Arp4 and Arp8, and bioinformatic analyses revealed that the actin core-fold of ARPs contains a number of additional insertion elements (Fenn et al., 2011a; Gerhold et al., 2012; Saravanan et al., 2012; Schafer and Schroer, 1999) (Figure 4c). Based on their sequence similarity to actin, ARPs are numbered with increasing numbering for more sequence diverged ARPs. In contrast to actin, ARPs do not form filaments. In yeast there are ten ARPs; Arp1-Arp3 and Arp10 are located predominantly in the cytoplasm, whereas Arp4-Arp9 are found in the nucleus as subunits of large chromatin-associated complexes. Most ARPs are conserved from yeast to humans, the exceptions being Arp7 and Arp9, which are not present in higher eukaryotes. Cytoplasmic ARPs are involved in processes related to the cytoskeleton (Dion et al., 2010; Olave et al., 2002; Schafer and Schroer, 1999). Arp2 and Arp3 form together with additional proteins the Arp2/3 complex that is critical for actin filament branching (Swaney and Li, 2016). Arp1 and Arp10 are structural components of the of the dynactin complex that links the microtubule transporter dynein to its cargo (Urnavicius et al., 2015).

The nuclear ARPs are integral components of chromatin associated complexes. In yeast, ARPs and/or N-actin are present in the remodelers INO80, SWR1, SWI/SNF and RSC, and the histone acetyl transferase NuA4 (Olave et al., 2002). ARPs and/or N-actin bind in those complexes to a HSA domain and form ‘ARP module’ complexes, apart from Arp5 in INO80

and Arp6 in SWR1 (Szerlong et al., 2008). Crystal structures of the Arp7-Arp9-Snf2^{HSA} and the N-actin-Arp4-Swr1^{HSA} complexes and the cryoEM structure of the NuA4/Tip60 complex revealed that the actin-fold proteins bind via the hydrophobic pocket at their barbed end to the helical HSA domain in such 'Arp module' complexes (Cao et al., 2016; Schubert et al., 2013; Wang et al., 2018). In the SWR1 remodeler N-actin and Arp4 form a stable 'Arp module' complex with the Swr1 HSA domain. Whereas, in INO80 Arp8 is required as an additional subunit for stable association of the conserved Arp4-N-actin heterodimer to Ino80 HSA domain (Szerlong et al., 2008). Arp7 and Arp9 form a 'Arp module' complex with the Sth1 HSA domain, in the RSC remodeler, and with the Snf2 HSA domain, in the SWI/SNF remodeler. Notably, in RSC and SWI/SNF remodelers of higher eukaryotes the Arp7-Arp9 dimer is replaced by the Arp4-N-actin heterodimer (Figure 5). Consistent with Arp4 and N-actin forming together an integral part of the INO80, SWR1 and NuA4 complexes, the *ARP4* gene is essential in yeast (Bartholomew, 2013; Harata et al., 1994; Kapoor et al., 2013; Shen et al., 2003). Interestingly, the association of a second N-actin molecule to the HSA domain in SWR1 was described more recently (Lin et al., 2017). In contrast to the other actin-fold proteins, Arp5 in INO80 and Arp6 in SWR1 do not bind directly to the HSA domain of the Snf2-type ATPase subunit but to a hexameric ring of Rvb1/Rvb2 subunits (Jonsson et al., 2004; Szerlong et al., 2008; Wu et al., 2005).

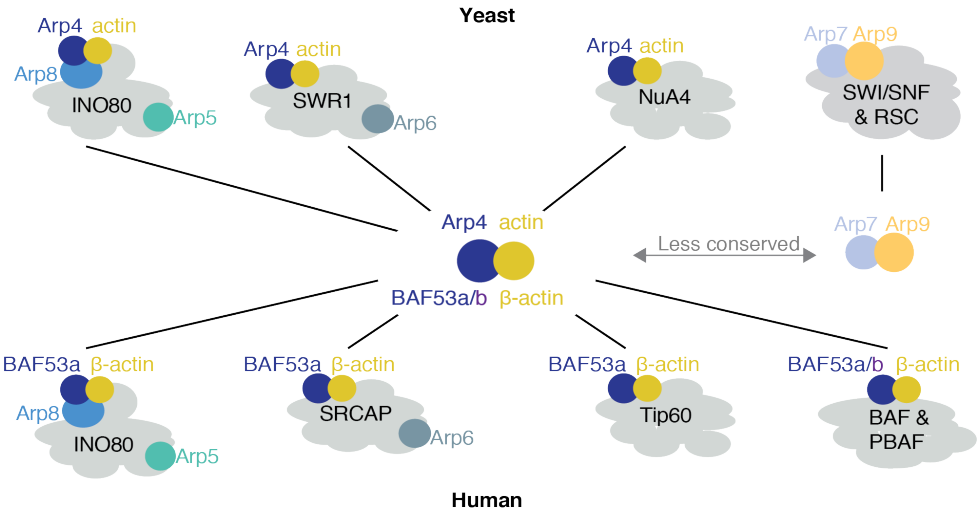

Figure 5 Arp4 and N-actin a conserved heterodimer.

Illustration of the conservation of the Arp4-N-actin heterodimer in yeast and human chromatin associated complexes. Interestingly SWI/SNF and RSC remodeler in yeast contain the Arp7-Arp9 dimer, whereas in higher eukaryotes this ARP dimer is replaced by the Arp4-N-actin dimer. Adapted and modified from (Bartholomew, 2013).

As integral components of chromatin remodelers, N-actin and nuclear ARPs are critical components in neuronal development and epigenetic control (Meagher et al., 2010; Son and Crabtree, 2014). In the human BAF complex, a tumour suppressor, the human Arp4 homolog hBAF53a/b is mutated and its expression is misregulated in cancer (Hodges et al., 2016). It was proposed that ARPs and N-actin function in chromatin remodelers as histone chaperones or DNA-binding components (Gerhold et al., 2012; Kapoor et al., 2013; Osakabe et al., 2014; Saravanan et al., 2012; Shen et al., 2003). Indeed, recent cryoEM structures revealed that Arp5 in INO80 (Ayala et al., 2018; Eustermann et al., 2018) and Arp6 in SWR1 interact in a similar way with nucleosomal DNA (Willhoft et al., 2018). However, the critical function and mode of action of the HSA domain-organized N-actin and/or ARPs in chromatin remodeling is largely unknown.

2.5 Architecture of the INO80 chromatin remodeling complex

The yeast INO80 complex exceeds 1 MDa in size and comprises 15 different subunits. Seven subunits of the INO80 remodeler are ATP-binding proteins and potential ATPases, and four of these are actin-fold proteins: N-actin, Arp4, Arp5 and Arp8 (Shen et al., 2000; Shen et al., 2003; Tosi et al., 2013). The versatile composition of INO80 implies a complex interplay of the different ATPases and subunits for INO80 function and regulation.

Biochemical experiments and protein cross-linking combined with mass-spectrometry analysis revealed the topology of the INO80 remodeler (Chen et al., 2011; Shen et al., 2003; Tosi et al., 2013). INO80 has a modular architecture and comprises three modules. The Ino80 subunit itself functions as a scaffold for the other subunits, binds all three modules and harbours the Snf2-type ATPase motor domain (Figure 6a). Two modules, the $INO80^{Core}$ module and the Arp8 module, are evolutionarily conserved and critical for INO80 function. The third module is species specific and not strictly required for INO80 nucleosome remodeling (Chen et al., 2011; Chen et al., 2013; Gerhold and Gasser, 2014; Shen et al., 2003; Tosi et al., 2013).

The $INO80^{Core}$ module is composed of a heterohexameric ring of the AAA^+ ATPases Rvb1 and Rvb2, Arp5, Ino eighty subunit (Ies) 6, Ies2 and the $Ino80^{ATPase}$, in total around 600 kDa in size (Chen et al., 2011; Chen et al., 2013; Shen et al., 2003; Tosi et al., 2013). Recent cryoEM studies on the conserved part of the *Chaetomium thermophilum* and human INO80 revealed the molecular architecture of the $INO80^{Core}$ module and its interaction with the NCP (Aramayo et al., 2018; Ayala et al., 2018; Eustermann et al., 2018) (Figure 6b). The Rvb1/Rvb2 heterohexamer encloses the Ino80 insertion domain and thereby positions the $Ino80^{ATPase}$ and Arp5 for NCP binding. In the crystal structure of the Rvb1/Rvb2

heterohexamer in an apo state, the oligonucleotide/oligosaccharide-binding (OB) domain layer adopts an open conformation, whereas in the INO80^{Core} cryoEM structure the Rvb1/Rvb2 heterohexamer is ADP-bound and the OB domains are closed and tightly surround the Ino80 insert (Aramayo et al., 2018; Ayala et al., 2018; Eustermann et al., 2018; Lakomek et al., 2015). Furthermore, the ATPase activity of the Rvb1/Rvb2 heterohexamer is clearly increased upon stimulation with Ino80 peptides (Zhou et al., 2017). Consequently, it was suggested that Ino80 insert binding induces Rvb1/Rvb2 ATP hydrolysis, leading to a conformational change that results in a closed conformation with the OB domains tightly enclosing the Ino80 insert (Eustermann et al., 2018). In this way, the Rvb1/Rvb2 heterohexamer appears to function as an assembly chaperone during biogenesis and as a 'stator' after INO80 complex assembly. Ino80^{ATPase}-Ies2 and Arp5-Ies6 bind the Rvb1/Rvb2 heterohexamer on the OB domains. A latch in the Ino80 insert introduces an asymmetry in the OB domain layer of the Rvb1/Rvb2 ring that allows precise binding of Arp5-Ies6 relative to the Ino80^{ATPase}. Arp5 contacts the Rvb1/Rvb2 hexamer with SD3 of its actin-fold and is additionally anchored by Ies6. The Ino80^{ATPase} domain binds the OB domains via its C-terminal ATPase lobe in addition to the Ino80 insert. INO80^{Core} binds the NCP by clamping it between the Ino80^{ATPase} and Arp5 (Ayala et al., 2018; Eustermann et al., 2018). The INO80^{Core}-NCP cryoEM structure matches previous DNA cross-linking studies, which showed that major nucleosomal DNA contacts are made between Arp5-Ies6 with SHL -2 and -3, and the Ino80^{ATPase}-Ies2 with the nucleosomal DNA entry site (Ayala et al., 2018; Brahma et al., 2017; Eustermann et al., 2018). INO80^{Core} contacts with the histone core are made by Ies6, Ies2 and a long insertion element of Arp5. The conserved SF2 helicase motifs of the Ino80^{ATPase} bind the nucleosomal DNA at SHL-6, thereby unwrapping the DNA from the histone-octamer and partially exposing the H2A-H2B dimer facing the Rvb1/Rvb2 hexamer. In addition, the N-lobe of Ino80^{ATPase} binds the upper gyre of the nucleosomal DNA at SHL+2. Ies2 binds the Rvb1/Rvb2 OB domains extends around the two DNA gyres and binds the acidic patch of the histone octamer opposite to the Rvb1/Rvb2 hexamer. Thereby, Ies2 stabilizes the N-lobe of Ino80^{ATPase} at SHL+2. Arp5-Ies6 bind the nucleosomal DNA opposite to the Ino80^{ATPase} (Ayala et al., 2018; Eustermann et al., 2018). Positively-charged residues in SD2 of the Arp5 actin-fold insert into the major groove between SHL-2 and SHL-3. Besides the conserved actin-fold, Arp5 contains a long insertion element in SD4, which forms a remarkable structure comprising several helices and is termed the 'grappler' (Eustermann et al., 2018). Helices of the grappler element contact the nucleosomal DNA at the nucleosomal dyad and SHL -7.5. In addition, the grappler contacts the acidic patch of the H2A-H2B dimer facing the Rvb1/Rvb2 hexamer. Since the grappler element can adopt different conformations and contacts H2A, it was proposed to function as a sensor that might regulate nucleosome editing in a histone variant-dependent manner

(Eustermann et al., 2018). Arp5 is further stabilized by Ies6 (Aramayo et al., 2018; Eustermann et al., 2018). The elongated structure of Ies6 wraps its N-terminal region around the actin-fold of Arp5, whereas its C-terminal region binds via a histidine triad (HIT) fold between the Rvb1/Rvb2 OB domains and the histone octamer, thereby contacting H2B.

The second module critical for INO80 remodeling function is the Arp8 module, which is around 200 - 240 kDa in size. The conserved core set of the Arp8 module comprises the Ino80^{HSA} domain and the three actin-fold proteins N-actin, Arp4 and Arp8 (N-actin and ARPs are described in more detail in section 2.4). In addition the Arp8 module contains subunits that are non-conserved, for example Ies4 and TBP associated factor 14 (Taf14) in yeast and Yin Yang 1 (hYY1) in metazoans (Chen et al., 2011; Klymenko et al., 2006). In the Ino80 subunit the HSA domain is located N-terminal to the Snf2-type ATPase domain (Figure 6a). Ino80^{HSA} is critical for the recruitment of the Arp8 module subunits (Szerlong et al., 2008). Deletion of either a partial segment of the Ino80^{HSA} domain or Arp8 leads to the loss of all other Arp8 module subunits (Kapoor et al., 2013; Shen et al., 2003; Szerlong et al., 2008; Tosi et al., 2013). The INO80 complex lacking the Arp8 module is defective in nucleosome remodeling but can still bind nucleosomes and its nucleosome-stimulated ATPase activity is comparable to wild-type levels (Shen et al., 2003; Tosi et al., 2013). In yeast, Arp8 or the partial Ino80^{HSA} deletion results in a phenotype that is similar to the complete Ino80 deletion and the cells are hypersensitive to genotoxic stress (Kapoor et al., 2013; Shen et al., 2003). In the cryoEM study of the conserved part of the *Chaetomium thermophilum* INO80 bound to the NCP, density with a low local resolution was observed for the Arp8 module close to the DNA entry site next to Ino80^{ATPase} (Eustermann et al., 2018) (Figure 6c). This is in line with ChiP-exo data, which located Arp8 in the extranucleosomal NFR region upstream of +1 nucleosomes (Yen et al., 2013). Despite crystal structures of the individual subunits Arp4 and Arp8 (Fenn et al., 2011a; Gerhold et al., 2012), and related complexes, such as Arp7-Arp9-Snf2^{HSA} and N-actin-Arp4-Swr1^{HSA} (Cao et al., 2016; Schubert et al., 2013), no structural and functional data is available that has been able to reveal the critical role of the Arp8 module in INO80 nucleosome remodeling.

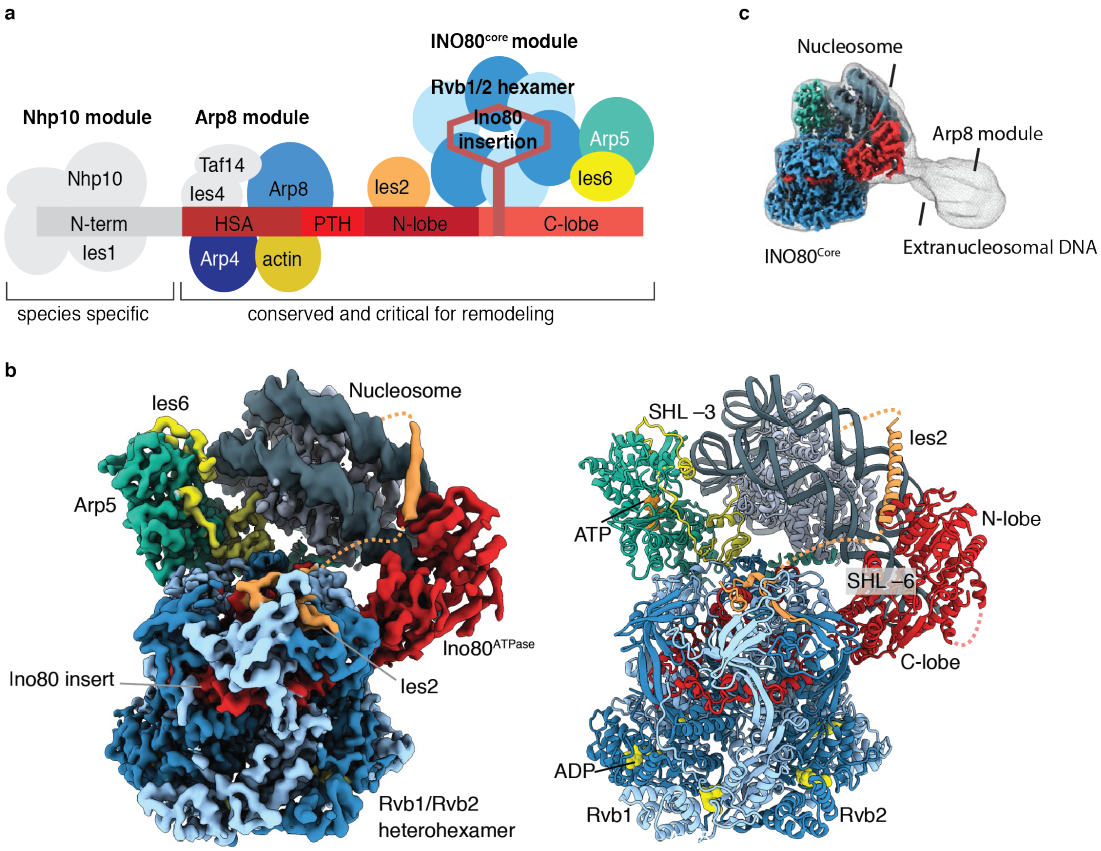

Figure 6 Architecture of the INO80 chromatin remodeler.

a, Schematic overview displaying the modular architecture of the yeast INO80 complex. Adopted and modified from (Knoll et al., 2018). N-term; N-terminal region; HSA, helicase-SANT-associated-domain; PTH, post-HSA domain; N-lobe and C-lobe, N-terminal and C-terminal RecA lobes of the Ino80 Snf2-type ATPase domain. **b**, CryoEM density map (left) and structure (right) of the INO80^{Core}-nucleosome core particle complex. Subunits and features are colored and labeled accordingly. **c**, Low resolution cryoEM density map indicating extranucleosomal localization of the Arp8 module. Panel b and c are adapted from (Eustermann et al., 2018).

The non-conserved subunits of the Arp8 module appear to have diverse regulatory functions in DNA repair or transcription regulation. Ies4 is important in INO80-dependent DNA damage checkpoint regulation. Upon DNA damage the Mec1/Tel1 kinases phosphorylate Ies4, which leads to recruitment of the checkpoint kinase Rad53 to the phosphorylated Ies4 and its activation (Kapoor et al., 2015; Morrison et al., 2007). Taf14 comprises a YEATS domain (a reader module for acetylated H3K9) and is also a subunit in complexes other than INO80, such as the transcription factors TFIID and TFIIF or chromatin-associated complexes SWI/SNF, RSC and NuA4. It was suggested that Taf14 regulates stress-induced genes, however the precise role in INO80 is unknown (Nemet et al., 2017). hYY1 is a transcription factor that regulates a large number of genes essential for cell-cycle control, proliferation, differentiation and apoptosis. In context of INO80 it was

suggested to recruit INO80 to hYY1 regulated genes, where INO80 functions as co-activator of hYY1 regulated genes by providing access to the hYY1 target sites (Cai et al., 2007).

The species-specific INO80 submodule is organized at the N-terminus of Ino80 (Chen et al., 2011; Tosi et al., 2013) (Figure 6a). Since the N-terminal module is not required for INO80 nucleosome remodeling it was proposed to have a regulatory function (Chen et al., 2013; Tosi et al., 2013). In the yeast INO80 remodeler the N-terminal module is termed 'Nhp10 module' and is composed of non-histone protein 10 (Nhp10), Ies1, Ies3 and Ies5 (Shen et al., 2000; Shen et al., 2003; Tosi et al., 2013). The yeast Nhp10 module has a high affinity for DNA and the Nhp10 protein recognizes a specific sequence motif often enriched in the NFR (Badis et al., 2008; Yen et al., 2013). In addition, ChiP-exo mapping located Ies5 in the NFR. Hence it was proposed that Nhp10 targets INO80 to the promoter site and might be involved in +1 nucleosome positioning (Yen et al., 2013). More recently, single molecule studies showed that the Nhp10 module recognises the length of extranucleosomal DNA and thereby modulates the INO80 nucleosome remodeling activity (Zhou et al., 2018). The N-terminal INO80 module in metazoans comprises hAmida, hIno80E, hIno80D, nuclear factor related to kappa-B-binding protein (hNFRKB), ubiquitin C-terminal hydrolyse 37 (hUch37) and hMcrs1 (Chen et al., 2011). The subunit composition is clearly different to the yeast module and although it was proposed to have regulatory roles, its role in nucleosome remodeling by the human INO80 complex is not yet characterized (Chen et al., 2011; Chen et al., 2013).

Overall, INO80 consists of three modules; the INO80^{Core}, the Arp8 module and the species-specific N-terminal module. The species-specific submodule is not required for INO80 nucleosome remodeling and only poorly characterized. INO80^{Core} and Arp8 module are sufficient for INO80 nucleosome remodeling. CryoEM studies on this conserved part of INO80 bound to the nucleosome resulted in high-resolution structures of the INO80^{Core} module bound to the NCP. These revealed that the INO80^{Core} alone binds the NCP directly and led to a first molecular model for INO80 nucleosome remodeling (described in section 2.6).

2.6 A mechanism for nucleosome remodeling by INO80

The translocase/helicase domain is the unifying feature of all chromatin remodelers and generates the driving force for the diverse nucleosome remodeling reactions. The structural framework around the motor is required to convert plain translocation of DNA into nucleosome remodeling, to specify the remodeling reaction and to regulate the remodeler

activity (Bartholomew, 2014; Clapier et al., 2017). Sliding of nucleosomes on DNA appears to be a simple process, however it is major puzzle how the DNA is propagated around the histone octamer and the 14 histone-DNA contacts are broken (Clapier et al., 2017). Different DNA propagation models have been proposed: DNA-loop formation, DNA-twist diffusion and histone octamer distortion (Mueller-Planitz et al., 2013).

At present, the assumed common principles for nucleosome sliding are that the Snf2-type ATPase of the remodeler is anchored at a specific location to the nucleosomal DNA and pumps DNA in 1-2 bp steps towards the nucleosome dyad (Clapier et al., 2017; Deindl et al., 2013; Harada et al., 2016; Singleton et al., 2007). Structures of the SWI/SNF ATPase motor domain, the CHD1 remodeler and INO80^{Core} bound to the nucleosome provided important insights into how the Snf2-type ATPase domain interacts with the nucleosome (Ayala et al., 2018; Eustermann et al., 2018; Farnung et al., 2017; Liu et al., 2017). Of note, regarding the position of the motor domain at the nucleosomal DNA INO80 is unique because the Ino80 Snf2-type ATPase binds at SHL-6, whereas the Snf2-type ATPase domain in all other remodelers characterized so far binds at SHL-2. Nevertheless, the main interactions between the Snf2-type ATPase and the nucleosome observed in the different remodeler structures are similar. The Snf2-type ATPase is positioned in an orientation to translocate DNA from the nucleosome entry site in the direction of the nucleosome dyad. The conserved helicase motifs in the DNA-binding cleft between the N- and C-lobes of the Snf2-type ATPase domain form the main contact points with the nucleosomal DNA. In addition, in all the structures the N-lobe forms a second DNA contact with the opposite DNA gyre (Ayala et al., 2018; Eustermann et al., 2018; Farnung et al., 2017; Liu et al., 2017). Mutation of this second contact point on the N-lobe led to decreased remodeling rates for Snf2 (Liu et al., 2017), indicating that this second DNA contact functions as an anchor to fix the ATPase during DNA translocation and positions the ATPase in the correct orientation (Liu et al., 2017; Winger et al., 2018).

Comment: The definition of the nucleosomal DNA SHL direction '±' is arbitrary, but in context of chromatin remodeling on a single NCP usually and hereafter defined by the side of the DNA overhang and the DNA translocation direction of the remodeler. On the 'entry site' of the NCP, the side with the DNA overhang that is pumped into the nucleosome by the translocase domain, SHL numbering starts with – prefix and continuous after the nucleosome dyad with + prefix until the DNA reaches the 'exit site' of the NCP.

The recent structures of the INO80^{Core} complex bound to the nucleosome together with biochemical and single-molecule data provided important mechanistic insights, which led

to a first molecular model for nucleosome remodeling by one of the large multi-subunit remodelers (Ayala et al., 2018; Brahma et al., 2017; Eustermann et al., 2018; Schwarz et al., 2018; Zhou et al., 2018) (Figure 7). In this model the Rvb1/Rvb2 hexamer functions as a stator to position the Ino80^{ATPase} and Arp5-Ies6 for nucleosome binding at SHL-6 and SHL-2/SHL-3, respectively, and to anchor the ATPase for DNA translocation (Brahma et al., 2017; Eustermann et al., 2018). In addition, the ATPase is fixed at the nucleosomal DNA by the secondary DNA contact of the N-lobe and Ies2, which reaches from the Rvb1/Rvb2 hexamer to the acidic patch on the distal side of the nucleosome (Eustermann et al., 2018). Importantly, the Ino80^{ATPase} at the nucleosomal entry site is orientated to pump DNA towards the nucleosome dyad, consistent with INO80s characteristic to center nucleosomes on a single DNA fragment (Jin et al., 2005; Shen et al., 2003). Binding of the Ino80^{ATPase} deforms the nucleosomal DNA at the H2A-H2B interface and partially exposes the histone dimer. (Ayala et al., 2018; Eustermann et al., 2018). Minor groove tracking of the Snf2-type ATPase in 1-2 bp steps and translocation of the DNA towards Arp5-Ies6 would lead to a bulge formation between the Ino80^{ATPase} and Arp5 and increased exposure of the H2A-H2B dimer. Indeed, displacement of the DNA from the H2A-H2B interface upon DNA translocation and bulge formation was observed for INO80 by hydroxyl radical footprinting (Brahma et al., 2017). Translocation-dependent displacement of the DNA from the H2A-H2B interface was proposed to play a role during the exchange of H2A.Z-H2B (Brahma et al., 2017; Papamichos-Chronakis et al., 2011). Interestingly SWR1, which catalyses the reverse histone exchange reaction but cannot slide nucleosomes (Luk et al., 2010; Mizuguchi et al., 2004; Ranjan et al., 2015), binds the nucleosome differently to INO80, with the Snf2-type ATPase at SHL-2 and Arp6 at SHL-6 (Willhoft et al., 2018).

DNA crosslinking and single molecule fluorescence resonance energy transfer (smFRET) experiments observed a large step size of around 10 bp for INO80 nucleosome sliding (Brahma et al., 2017; Zhou et al., 2018), but Snf2-type ATPases only translocate DNA in smaller steps of 1-2 bp (Clapier et al., 2017). Convincingly, the structural insights can explain the contradictory observations (Ayala et al., 2018; Eustermann et al., 2018). Continuous 1-2 bp minor groove tracking by Ino80 would build up tension between the Ino80^{ATPase} and Arp5-Ies6. After around 10 translocation steps the tension would be sufficient for the DNA to slip over the Arp5-Ies6 'counter grip', resulting in the observed step size of around 10-15 bp (Brahma et al., 2017; Zhou et al., 2018). Indeed, mutation of the Arp5 DNA-binding domain, which builds up the 'counter grip', abolishes INO80 nucleosome remodeling (Eustermann et al., 2018). During remodeling, the Arp5-Ies6 'counter grip' is held in place by the Rvb1/Rvb2 hexamer and multiple histone contacts with the Arp5-insertion and Ies6. Thereby, the acidic patch on the H2A-H2B dimer appears to be an important anchor point for INO80 on both sides of the nucleosome for either Arp5

by the Arp5-insertion or for Ino80^{ATPase} by Ies2. In fact, mutations of the acidic patch anchor point greatly decrease INO80 nucleosome sliding (Eustermann et al., 2018; Gamarra et al., 2018).

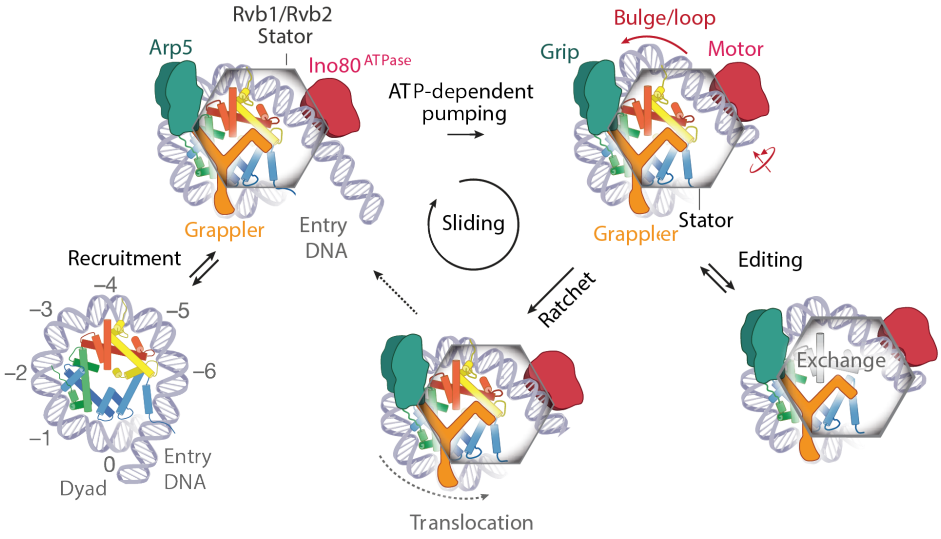

Figure 7 Ratchet model for INO80 nucleosome remodeling.

The illustration displays the proposed unifying model for INO80 nucleosome sliding and histone exchange (Eustermann et al., 2018). Binding of the INO80^{Core} to the nucleosome lifts off DNA from the H2A-H2B dimer. DNA translocation by the Ino80^{ATPase} would result in either nucleosome sliding by a ratchet like mechanism or might lead to H2A.Z-H2B exchange by H2A.Z increased Ino80^{ATPase} activity and complete exposure of the dimer. Adapted from (Eustermann et al., 2018).

INO80 function is controlled by several regulatory elements. The Arp5-insertion element appears to function as versatile nucleosome sensor. Structural insights suggest that Arp5-inserition element might be a switch-like sensor element, sensitive to the DNA path at the nucleosome exit end entry sites (Eustermann et al., 2018). Additionally, sensing of histone variant specific differences between H2A and H2A.Z as well as the H3 histone tail by the Arp5-insertion element seems to regulate the INO80 remodeling rate (Ayala et al., 2018; Eustermann et al., 2018; Schwarz et al., 2018; Willhoft et al., 2016).

Overall recent structural and functional insights into INO80 remodeling provided a unifying ‘ratchet’ model for INO80 nucleosome sliding and exchange with DNA translocation as the driving force. Nevertheless, the enigmatic role of the functionally critical Arp8 module has until now remained elusive owing to a lack of structural information.

2.7 Aim of the thesis

Already in the 1990's N-actin and ARPs had been identified as conserved, stably bound, critical subunits of chromatin-associated complexes (Olave et al., 2002; Schafer and Schroer, 1999; Shen et al., 2003). Despite that, our understanding about the mechanistic role of actin-fold proteins during chromatin remodeling is still limited. Nuclear ARPs have been characterized as individual proteins and structures of Arp4 and Arp8 have been solved (Fenn et al., 2011a; Gerhold, 2012; Gerhold et al., 2012). At the time the work on this thesis started, the only high-resolution structure available for an ARP-containing chromatin remodeler subcomplex was the crystal structure of $Snf2^{HSA}$-Arp7-Arp9 complex from the yeast SWI/SNF remodeler (Schubert et al., 2013). Although others subcomplexes have been solved subsequently (Cao et al., 2016), the lack of structural information still restricts the mechanistic understanding of actin-fold proteins in chromatin remodelers.

The function of actin-fold proteins in the INO80 chromatin remodeling complex is especially intriguing, as it comprises four actin-fold proteins (Shen et al., 2000; Shen et al., 2003; Szerlong et al., 2008) and is a bona-fide remodeler that can slide (Shen et al., 2003), space (Udugama et al., 2011) and edit (Papamichos-Chronakis et al., 2011) nucleosomes. Recent progress helped to propose a mechanistic model for INO80 nucleosome remodeling (Eustermann et al., 2018). However, the mysterious and functionally critical Arp8 module, which harbors with Arp4, N-actin and Arp8 three actin-fold proteins, is missing in that model. The intrinsic flexibility of the INO80 remodeler did not permit high resolution structural information on the Arp8 module to be obtained by cryoEM.

The aim of this thesis was to characterize the function of the Arp8 module in the INO80 chromatin remodeler by using a combined approach of structural biological and biochemical methods. A nanobody that specifically recognizes the Arp4-N-actin heterodimer in endogenous chromatin remodelers was used to structurally and functionally study the conserved heterodimer by affinity enrichment mass spectrometry and X-ray crystallography. Structural knowledge from these first studies was used to successfully solve the structure of the INO80 Arp8 module by X-ray crystallography. Insights into the molecular architecture of the INO80 Arp8 module were validated by mutational analysis and used to characterize the mechanistic function of the Arp8 module in INO80 chromatin remodeling by nucleosome binding and sliding assays. This work identified, together with the recent cryoEM structure of the $INO80^{Core}$-NCP complex, the INO80 Arp8 module as an allosteric sensor of linker DNA that drives INO80 nucleosome remodeling.

3 Results

3.1 Crystal structure of the INO80 Arp8 module

Actin-fold proteins, such as N-actin and ARPs, are central components of the INO80 remodeler, where they are mainly organized within the Arp8 module. The lack of structural information on the Arp8 module limits the understanding of its mechanistic and functional role during INO80 nucleosome remodeling. In order to fill this gap, X-ray crystallography was applied to a complex comprising the conserved components of the yeast Arp8 module.

3.1.1 Purification and crystallization of the INO80 Arp8 module

3.1.1.1 Construct optimization

The INO80 Arp8 module comprises the Ino80^{HSA}, N-actin, Arp4 and Arp8 and is in this respect conserved from yeast to man. In yeast, the Arp8 module contains along with Ies4 and Taf14, two additional species-specific subunits. Although the heterologous expression in insect cells and the purification of a stable Arp8 module complex was established in our and other laboratories (Gerhold et al., 2012; Szerlong et al., 2008; Tosi et al., 2013), structural studies on the Arp8 module have so far been unsuccessful. In order to screen for a stable and homogenous Arp8 module complex with fewer flexible regions that would be more suitable for crystallization, different subunit constructs and subunit combinations were examined in co-expression pull-down experiments.

Complex combinations of the yeast Arp8 module with the conserved part only, Arp4, N-actin, Arp8 and the Ino80^{HSA}, and with the species-specific subunits, Ies4 and Taf14, were examined. Moreover, different constructs of Arp8 and Ino80^{HSA} were designed and tested. Yeast Arp8 harbors a long (~250 residues) unconserved N-terminal region that is not part of its actin-fold. A construct comprising only the C-terminal domain of yeast Arp8 (Arp8CTD; residues 255-881) was crystalized successfully previously on its own (Saravanan et al., 2012). To obtain a more compact Arp8 module less prone to degradation and structural heterogeneity, complex formation with Arp8CTD was analyzed. In addition, previous studies demonstrated that the Ino80^{HSA} functions as a binding platform for Arp4, N-actin and Arp8 (Szerlong et al., 2008), however the exact binding sites of the actin-fold proteins were not known. To find a minimal stable HSA domain construct that allowed binding of all three actin-fold proteins, HSA domains with different lengths and affinity tags were designed. Using a combinatorial approach with two baculoviruses harboring the different Arp8 module subunits allowed fast screening for an optimized complex.

a

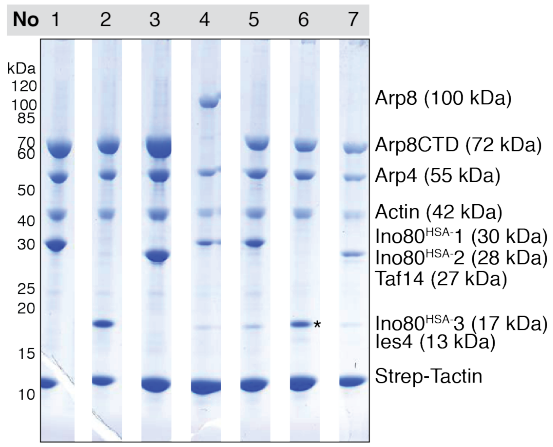

b

No	
1	Arp4, Actin, Arp8CTD, Ino80^{HSA}-1
2	Arp4, Actin, Arp8CTD, Ino80^{HSA}-3
3	Arp4, Actin, Arp8CTD, Ino80^{HSA}-2
4	Arp4, Actin, Ies4, Taf14, Arp8, Ino80^{HSA}-1
5	Arp4, Actin, Ies4, Taf14, Arp8CTD, Ino80^{HSA}-1
6	Arp4, Actin, Ies4, Taf14, Arp8CTD, Ino80^{HSA}-3
7	Arp4, Actin, Ies4, Taf14, Arp8CTD, Ino80^{HSA}-2

Figure 8 Test expressions of INO80 Arp8 module complex variants.

a, SDS-PAGE and Coomassie brilliant blue staining of INO80 Arp8 module test expressions. In small (10 mL) insect cell expression cultures different constructs of Arp8 module subunits were co-expressed by combining two baculoviruses (see panel b). Tryptic in-gel digestion and mass spectrometry analysis of the star marked band in expression No 6 identified peptides of Ies4 and Ino80^{HSA}-3. **b**, Table showing Arp8 module subunits expressed in panel a according to the numbering (for Ino80^{HSA} construct abbreviations see Table 2).

All virus combinations yielded Arp8 module complexes with Arp4, N-actin and Arp8 stably bound to the HSA domain of Ino80 (Figure 8). Similar to full-length Arp8, Arp8CTD formed complete Arp8 module complexes. Based on these initial pull-down experiments the N-terminal region of Arp8 does not seem to be required for Arp8 module complex formation. The three HSA domain constructs with various lengths clearly bind Arp4, N-actin and Arp8 in all expressions, indicating that all three Ino80^{HSA} constructs include the binding sites of the three actin-fold proteins (Figure 8 and Table 2). The binding of Ies4 was not unambiguous from the SDS-PAGE analysis, however mass spectrometry identified that Ies4 and Ino80^{HSA}-3 migrate in one band in expression No 6. Indeed, in expression samples No 4, 5 and 7, with longer HSA domain constructs, a faint band for Ies4 only was observed at the position equal to Ino80^{HSA}-3. Binding of Taf14 was not observed in any of the expression that included Taf14 (No 4-7). Expression No 3, comprising the Ino80^{HSA}-3 (here after simply termed Ino80^{HSA}), Arp4, N-actin and Arp8CTD, resulted in the smallest Arp8 module complex with a total weight of 180 kDa. This presumably contained the fewest flexible regions and would consequently have the most favorable properties for crystallization approaches. Consequently, the expression and purification of this 180 kDa Arp8 module complex (here after simply termed Arp8 module) was optimized to yield the complex in amounts and purity required for crystallization.

Table 2 Ino80^{HSA} constructs used in Arp8 module test expression.

Name	Residue range	Affinity tags	MW in kDa
Ino80^{HSA}-1	455-685	N-term: 6xHis; C-term: Strep-Tag II	30
Ino80^{HSA}-2	455-685	C-term: Strep-Tag II	28
Ino80^{HSA}-3	462-598	C-term: Strep-Tag II	17

3.1.1.2 Purification of the INO80 Arp8 module

Complex optimization led to a 180 kDa Arp8 module complex comprising yeast Arp4, N-actin, Arp8CTD (the N-terminal truncated version of Arp8 including residues 255-881) and the Ino80 HSA domain (residues 462-598) with a C-terminal attached Strep-Tag II. In order to increase the amount of protein and the purity for crystallization, these expression scale and purification procedure were adapted to these requirements.

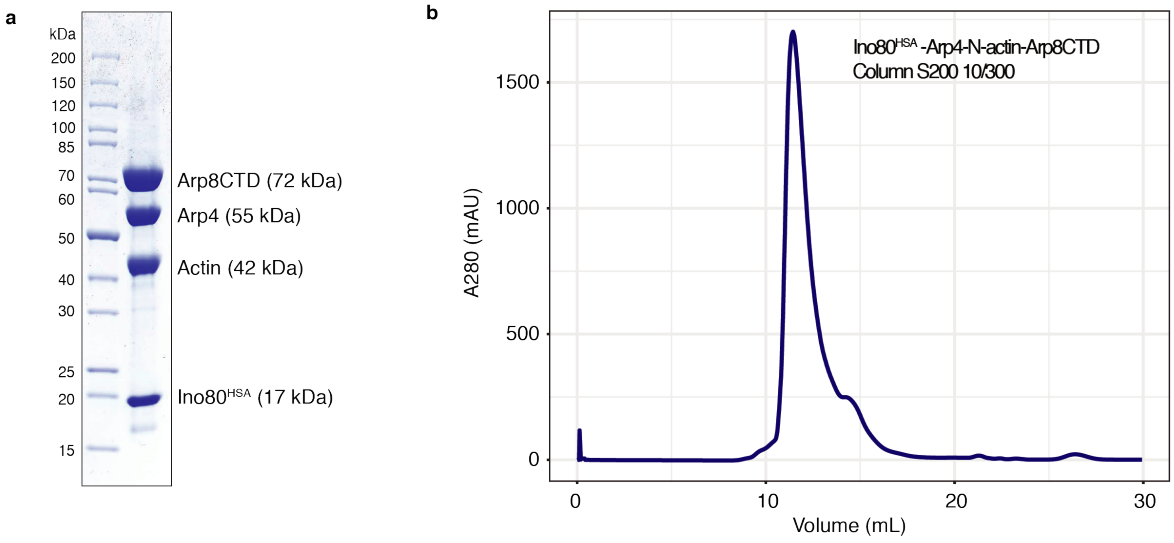

Figure 9 Purification of the Ino80^{HSA}-Arp4-N-actin-Arp8 complex for crystallization.

a, SDS-PAGE and Coomassie brilliant blue staining of the purified Arp8 module complex used for crystallization. **b**, Size-exclusion chromatography elution profile of the Arp8 module complex, comprising Ino80^{HSA}, Arp4, N-actin and Arp8CTD, on a S200 10/300 column. Adapted from (Knoll et al., 2018).

The expression scale was increased to 2 L of insect cell culture for a typical purification. The four subunits were co-expressed in insect cells by using two baculoviruses. To obtain a highly pure sample of the complex, the Arp8 module was purified from the lysate by Strep-

Tag affinity chromatography, anion-exchange chromatography with Q Sepharose and size-exclusion chromatography with Superdex 200 resin. Typically, 2 L of insect cell expression yielded 2 mg of a pure and monodisperse sample (Figure 9). Adapted expression and purification of the Arp8 module yielded sufficient amounts of highly pure sample appropriate for subsequent crystallization experiments.

3.1.1.3 Crystallization of the INO80 Arp8 module

Pure and monodisperse 180 kDa complex, comprising Ino80^{HSA}-Arp4-N-actin-Arp8CTD, was obtained from co-expression in insect cells and subsequent purification (Figure 9). Extensive high-throughput crystallization screening resulted in precipitation with a good appearance in a reasonable percentage of conditions, but did not result in any crystals.

To improve the homogeneity of the Arp8 module in crystallization trials, latrunculin A (LatA) was added to the Arp8 module crystallization screens to decrease potential intrinsic actin flexibility. Latrunculins are sea sponge toxins that were shown to inhibit the nucleotide exchange in actin and prevent actin filament formation in the cytoplasm (Dominguez and Holmes, 2011). In fact, several crystal structures of monomeric actin were solved before together with small actin binding toxins, such as latrunculins (Dominguez and Holmes, 2011). 29 actin crystal structures bound to latrunculins are deposited in the Protein Data Bank (PDB) (Dominguez and Holmes, 2011). Latrunculins bind actin in the nucleotide binding cleft and inhibit thereby actin dynamics (Morton et al., 2000; Yarmola et al., 2000). Furthermore, an early study on the N-actin containing BAF complex showed that the addition of latrunculin allosterically inhibits the remodeler ATPase (Zhao et al., 1998). In this particular case, the addition of LatA to the crystallization screens led to the formation of Arp8 module crystals, whereas no crystals where obtained under the same conditions without LatA.

Conditions for Arp8 module crystal growth were found using high throughput crystallization screening. Arp8 module protein solution with a concentration of 14 mg/mL was mixed with LatA (for the LatA stock solution LatA was dissolved in 100% dimethylsulfoxide to a final concentration of 10 mM) in molar ration of 1:1.5 (complex : LatA) prior crystallization. Initial crystals were grown by sitting-drop vapour-diffusion in 0.2 M sodium citrate tribasic dihydrate and 20% (w/v) polyethylene glycol 3,350 with a drop size of 200 nL protein solution + 200 nL of reservoir solution. Crystals appeared after 8 days at 6°C. Further refinement crystallization screens led to the optimized final conditions for crystal growth by hanging-drop vapour-diffusion in 0.1 M sodium citrate tribasic dihydrate

and 18% (w/v) polyethylene glycol 3,350. Crystals were harvested after 30 days at 4°C and cryo-protected with 20% glycerol.

3.1.2 Crystal structure determination of the Arp8 module

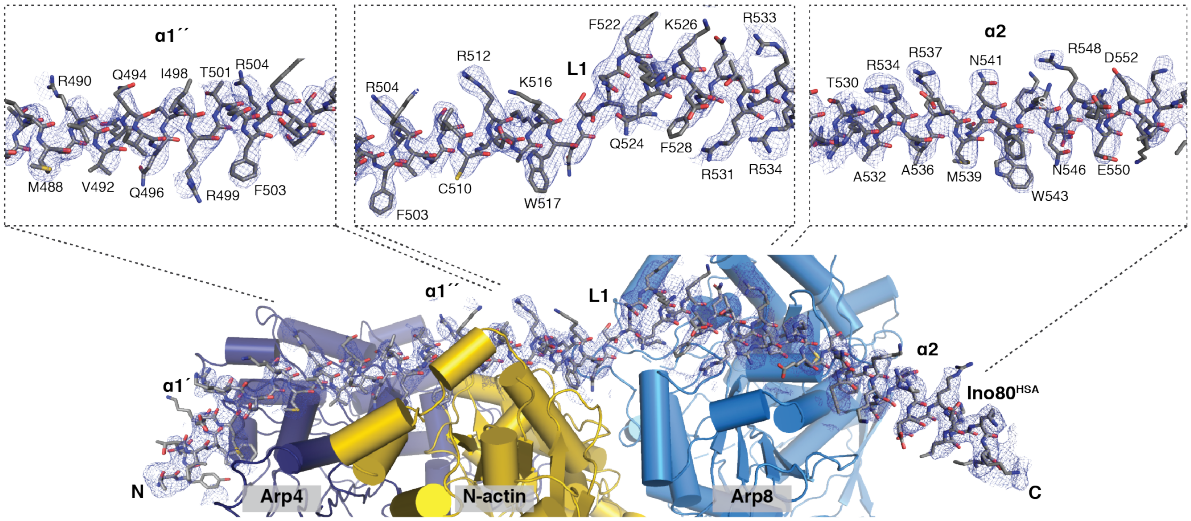

Figure 10 Ino80^{HSA} electron density.

Electron density for the Ino80^{HSA}. Shown is a feature-enhanced map (FEM) (Afonine et al., 2015) calculated by phenix.fem (Adams et al., 2010) at a contour level of 1 sigma (blue mesh). The Ino80^{HSA} model is shown in a stick representation and Arp4, N-actin and Arp8 as cartoon representation. Adapted from (Knoll et al., 2018).

Diffraction data from a single Arp8 module crystal was used to solve the structure. The crystal in space group C 2 2 2_1 diffracted up to 4 Å resolution and the structure was determined by molecular replacement (see section 5.2.3.6) using the structure of the Arp4-N-actin dimer (see section 3.4.2) and yeast Arp8CTD (PDB 4AM6) as search models. One single solution with two Arp4-N-actin-Arp8 complexes was found per asymmetric unit. Difference density for the Ino80^{HSA} was immediately visible. Despite the relatively low resolution, unambiguous assignment of the sequence register and model building for most of the sidechains of the Ino80^{HSA} was possible through the use of B-factor sharpened and feature enhanced maps (Afonine et al., 2015) (Figure 10).

Several rounds of model building and refinement led to a final model for the Ino80^{HSA}-Arp4-N-actin-Arp8CTD complex at 4 Å resolution with R_{work}/R_{Free} values of 19.3%/24.2% (see Table 3). Coordinates and structure factors were deposited in the PDB with the identifier 5NBN.

Table 3 Data collection and refinement statistics.

	NactNB-Arp4-N-actin(ATP) (PDB 5NBM)	NactNB-Arp4-N-actin(apo) (PDB 5NBL)	Ino80^{HSA}-Arp4-N-Actin-Arp8 (PDB 5NBN)
Data collection			
Space group	P 6_5	P 6_5	C 2 2 2_1
Cell dimensions			
a, b, c (Å)	190.58 190.58 220.62	191.22 191.22 221.97	172.29 263.91 241.40
α, β, γ (°)	90.00 90.00 120.00	90.00 90.00 120.00	90.00 90.00 90.00
Resolution (Å)	47.73-3.40 (3.50-3.40)[a]	49.43-2.80 (2.90-2.80)	49.40-4.00 (4.10-4.00)
R_{merge}	0.160 (1.081)	0.146 (1.107)	0.236 (1.336)
$I/\sigma(I)$	12.61 (2.19)	12.08 (2.09)	8.71 (1.87)
$CC_{1/2}$	0.996 (0.719)	0.995 (0.617)	0.996 (0.605)
Completeness (%)	100 (100)	100 (100)	100 (100)
Redundancy	6.5 (6.8)	5.9 (5.4)	9.6 (10.0)
Refinement			
Resolution (Å)	47.73-3.40 (3.50-3.40)	49.43-2.80 (2.90-2.80)	49.40-4.00 (4.10-4.00)
No. reflections	62264 (6206)	112476 (11263)	46675 (4625)
R_{work} / R_{free}	0.152 (0.231) / 0.193 (0.281)	0.171 (0.276) / 0.204 (0.316)	0.193 (0.254) / 0.242 (0.288)
No. atoms			
Protein	13949	14000	23029
Ligand/ion	128	64	186
Water	-	119	-
B factors			
Protein	92.30	58.50	121.87
Ligand/ion	85.97	38.80	101.03
Water	-	48.77	-
RMSD			
Bond lengths (Å)	0.004	0.004	0.002
Bond angles (°)	0.66	0.70	0.68

Diffraction data from one NactNB-Arp4-N-actin(ATP), one NactNB-Arp4-N-actin(apo) and one Ino80^{HSA}-Arp4-N-Actin-Arp8 crystal were used to solve the structures. [a]Values in parentheses are for the highest-resolution shell.

3.1.3 Overall organization of the Arp8 module

The biological unit in the crystal, the Ino80^{HSA}-Arp4-N-actin-Arp8 complex, could be directly discriminated from crystal packing interactions based on prior knowledge of the Arp8 module composition (Szerlong et al., 2008). Arp4, N-actin and Arp8 form a compact complex with the alpha-helical Ino80^{HSA} binding the barbed ends of the three actin-folds proteins (Figure 11a and b). By this the Ino80^{HSA} spans a distance of 120 Å in total. The binding sequence along Ino80^{HSA}, from N- to C-terminus, is Arp4, N-actin and Arp8. N-actin is bound between Arp4 and Arp8 and displays large contacts to both ARPs. In agreement with related structures of the Snf2^{HSA}-Arp7-Arp9 and the Swr1^{HSA}-Arp4-N-actin complexes, the orientation of the actin-folds of Arp4 and N-actin is "front-to-back" in contrast to the classical filamentous (F) actin "front-to-front" interaction (Figure 11c). Nevertheless, the overall assembly is similar to F-actin. In principle Arp4 is 180° rotated on an axis defined by SD3 to SD2 compared to its corresponding actin molecule in F-actin (Figure 11c). Using secondary structure matching (Krissinel and Henrick, 2004) in COOT (Emsley et al., 2010), the Arp8 module Arp4-N-actin dimer superimposes with the Swr1^{HSA} Arp4-N-actin with a backbone RMSD (root-mean-square deviation) of 0.97 Å and number of aligned residues (N_{align}) 727. The low RMSD value implies that the Arp8 module interactions between N-actin and Arp4 are highly similar to those in the structure of the Swr1^{HSA}-Arp4-N-actin complex. In contrast, Arp8 binds N-actin in a completely new type of interaction for actin-fold proteins; the lateral side of SD1 and SD2 in Arp8 binds the backside of SD3 and SD4 in N-actin (Figure 11c).

Overall Arp4, N-actin and Arp8 adopt a compact architecture, with the Ino80^{HSA} forming an elongated helical element that binds to the barbed ends of each of the three actin fold proteins.

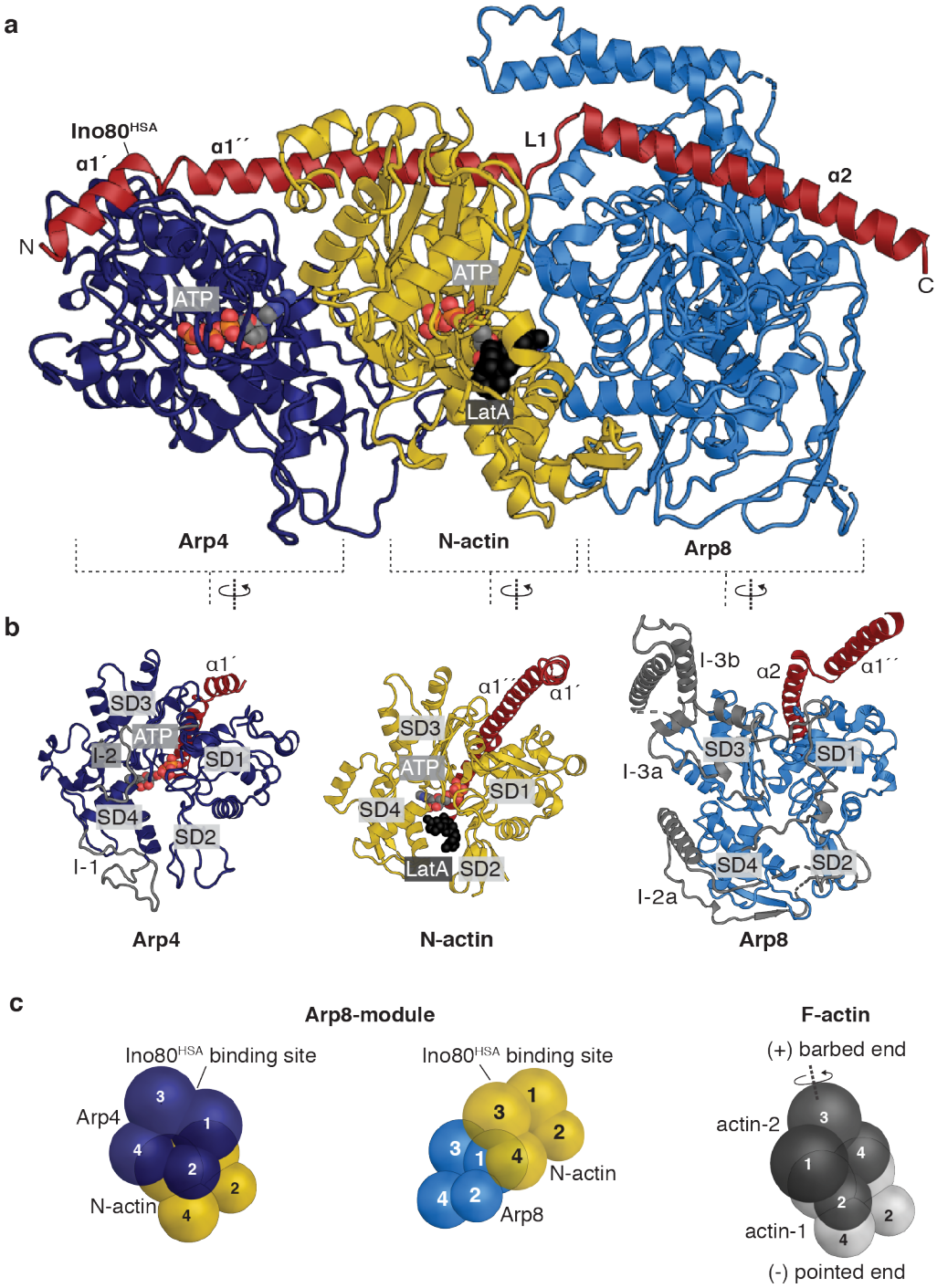

Figure 11 Crystal structure of the INO80 Arp8 module.

a, Structure of the INO80 Arp8 module comprising Arp4, N-actin, Arp8 and Ino80^{HSA}. Arp4 and N-actin are ATP-bound (colored spheres), whereas Arp8 is nucleotide-free. LatA (black spheres) is bound next to ATP in the N-actin nucleotide-binding cleft. **b**, Front views of the actin-fold proteins Arp4, N-actin, and Arp8. The Ino80^{HSA} binds to the barbed end of each of the actin folds. Actin fold insertions of Arp4 and Arp8 are shown in grey. **c**, Interaction of Arp4 with N-actin, and N-actin with Arp8 in the Arp8 module is compared with two lateral interacting actin molecules in F-actin. Schematic representations display the actin-fold proteins with the individual subdomains shown as spheres. Adapted and modified from (Knoll et al., 2018).

3.1.4 Nucleotide states of N-actin, Arp4 and Arp8

A hallmark of the 'actin-fold' is the nucleotide-binding pocket in the middle of the protein enclosed by the four actin subdomains (Kabsch and Holmes, 1995). The Arp8 module contains three actin-fold proteins and potential nucleotide binder.

Electron density in the nucleotide binding pocket of Arp4 could be clearly interpreted as ATP (Figure 12a). The coordination of ATP is similar to that observed previously for Arp4 in isolation (Fenn et al., 2011a). The two phosphate binding loops P1 (residues 22-25) and P2 (residues 159-164) enclose the nucleotide, with P1 Ser23^{Arp4} and P2 Asp163 ^{Arp4} coordinating the ATP gamma phosphate and Tyr24 ^{Arp4} stacking on the ribose, leading to tight binding of ATP by Arp4. In addition, the ATP phosphate moiety and Asp159 ^{Arp4} coordinate the divalent metal ion. ATP binding matches previous observations, which showed that Arp4 lacks detectable ATPase activity but that ATP binding is essential for Arp4 stability (Fenn et al., 2011a; Gerhold et al., 2012).

Interestingly, no electron density for a bound nucleotide was visible in the Arp8 nucleotide binding pocket. Previous studies showed that Arp8 binds ATP and possess a low ATPase activity (Gerhold et al., 2012; Saravanan et al., 2012), indicating that Arp8 hydrolysed any possibly bound ATP during the purification and crystallization process.

Electron density in the nucleotide-binding cleft of N-actin could be interpreted as ATP and LatA (Figure 12b). Binding of LatA to actin inhibits intrinsic actin flexibility and ATPase activity by stabilizing the ATP state (Yarmola et al., 2000). Accordingly, the addition of LatA to the Arp8 module for crystallization led to the ATP bound state of N-actin. In contrast, the structure of the Swr1^{HSA} bound Arp4-N-actin heterodimer contained N-actin in a nucleotide-free state. ATP is coordinated as in previous actin structures. Ser14$^{N\text{-}actin}$ of P1 (residues 13-16) and Asp157$^{N\text{-}actin}$ of P2 (residues 154-159) coordinate the phosphate moiety, while the catalytically important Gln137 (Merino et al., 2018) coordinates the metal ion. Interestingly, in the nucleotide free Swr1^{HSA} N-actin structure Asp157 $^{N\text{-}actin}$ blocks the nucleotide-binding pocket (Cao et al., 2016), whereas it is moved outwards in this structure to accommodate the gamma phosphate (Figure 12b and c). LatA binds actin in direct proximity to ATP between SD2 and SD4. Similar to earlier structures of LatA bound to actin, Tyr69 $^{N\text{-}actin}$ of SD2 and Arg210 $^{N\text{-}actin}$ of SD4 form specific contacts to LatA (Morton et al., 2000). LatA binding thereby prevents movement between SD2 and SD4 and leads to stabilization of actin in the ATP-bound state (Figure 12b). Of note, despite the addition of LatA the ATP present in the nucleotide binding pockets of both N-actin and Arp4 must have been co-purified from the expression host, High Five insect cells, since no additional nucleotide was added during protein purification and crystallization. LatA was only added

after purification for co-crystallization. The Arp8 module structure shows that N-actin can bind ATP and LatA, providing further evidence for the significance of ATP binding by N-actin in chromatin-associated complexes.

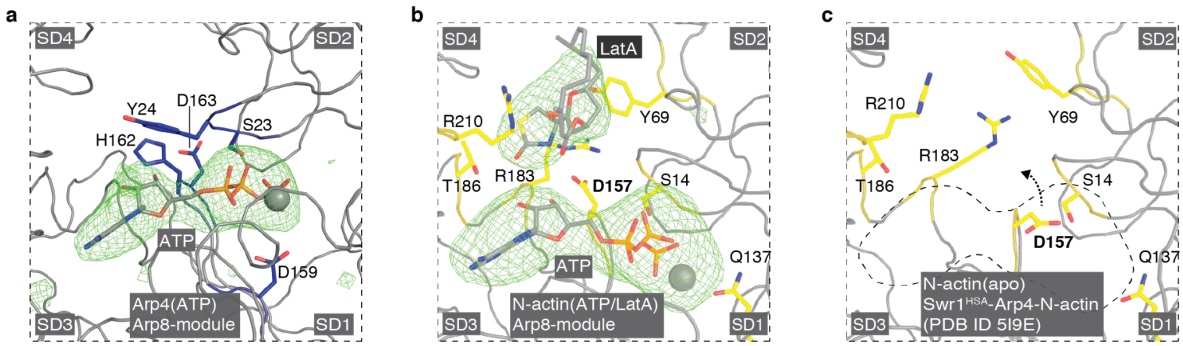

Figure 12 Ligand binding by Arp4 and N-actin.

a, and **b**, Close-up images of the Arp8 module Arp4(ATP) and N-actin(ATP/LAR) nucleotide-binding pockets showing electron density (green mesh) for the bound ligands (mFo-DFc difference map with a carving radius of 20 Å around each ligand; contoured at 3 sigma; resulting from structure refinement with phenix.refine (Adams et al., 2010) lacking ligands). **c**, Close-up of the Swr1^{HSA}-Arp4-N-actin crystal structure N-actin(apo) nucleotide-binding pocket (PDB 5I9E). Dotted line illustrates the canonical ATP-binding site of actin. Interestingly, Asp157 would block ATP binding in the apo N-actin structure, whereas it is moved outwards in the ATP-bound N-actin structure shown in panel b (indicated by the dashed arrow). Adapted from (Knoll et al., 2018).

3.1.5 N-actin and Arp8 form a novel type of actin-fold interaction

Compared to so far known arrangements between actin-fold proteins, the observed interaction between Arp8 and N-actin is new. Arp8 contacts N-actin opposite to Arp4, through its actin-core-fold and one of its insertion elements. Thereby the Arp8 actin-core-fold contacts the lateral side of the N-actin SD4-SD3 lobe with two major interaction-sites (Figure 13). SD1 and SD2 of Arp8 bind SD3 and SD4 of N-actin through several electrostatic interactions. Hydrogen bonds are formed between Glu473^{Arp8} and Lys238$^{N\text{-}actin}$ and Arg254$^{N\text{-}actin}$. Additionally, Lys427^{Arp8} contacts the backbone carbonyl groups of Glu237$^{N\text{-}actin}$, Ser235$^{N\text{-}actin}$ and Ser234$^{N\text{-}actin}$. Hydrophobic interactions are formed between the C-terminal region of Arp8 and the N-actin hinge between SD1 and SD3. Additionally, the conserved Arg871^{Arp8} binds a negatively-charged pocket in N-actin formed by Glu334$^{N\text{-}actin}$ and Asp25$^{N\text{-}actin}$. Besides the interactions made by the Arp8 actin-core-fold, Arp8 carries three long insertion elements (Figure 11b and Figure 13). Insertion 3A (I-3A; residues 621-699) originates from SD3 and covers most of the lateral face of all Arp8 subdomains.

Intriguingly, I-3A makes several hydrophobic interactions with N-actin SD3 and SD4 (Figure 13).

In summary, Arp8 forms multiple interactions with N-actin, rationalizing its central function in the recruitment of the Arp4-N-actin dimer to the Ino80^{HSA}.

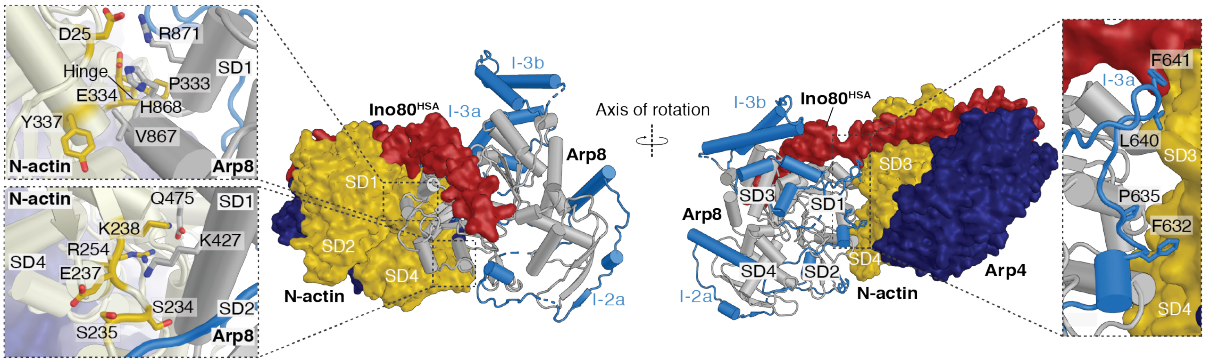

Figure 13 Arp8 binds N-actin in a bipartite interaction.

Cartoon and surface representations of the Arp8 module crystal structure displaying contact sites between Arp8 and N-actin. The Arp8 actin-fold is colored in gray and the insertions in blue. Arp8 contacts N-actin SD3 and SD4 via its actin-fold, with SD1 and SD2 (close up in the left panel), and its actin-fold insertions 3a (close up in the right panel). Adapted from (Knoll et al., 2018).

3.1.6 Ino80^{HSA}: The binding platform for N-actin and the ARPs

The central element in the Arp8 module is the highly conserved Ino80^{HSA}, which provides binding sites for Arp4, N-actin and Arp8 in the INO80 remodeler. In structures of related complexes (Swr1^{HSA}-Arp4-N-actin and Snf2^{HSA}-Arp7-Arp9), the Swr1^{HSA} and Snf2^{HSA} forms a single continuous helix that binds to the barbed ends of the actin-fold proteins (Cao et al., 2016; Schubert et al., 2013) (Figure 14a). Surprisingly, in the Arp8 module crystal structure the Ino80^{HSA} adopts a segmented conformation (Figure 14b). Ino80^{HSA} comprises two helices (α1 and α2) that are connected by a loop region L1 (residues 519-521). The N-terminal helix α1 (residues 472-518) is further divided by a kink at position 483-485 into two segments (α1.1 and α1.2). Interestingly, the Ino80^{HSA} shows a distinct amphipathic character, which appears to be highly conserved based on sequence alignments (Figure 14b). The segmented organization of Ino80^{HSA} enables binding of the helical segments via the hydrophobic side to the barbed ends of the actin-fold proteins.

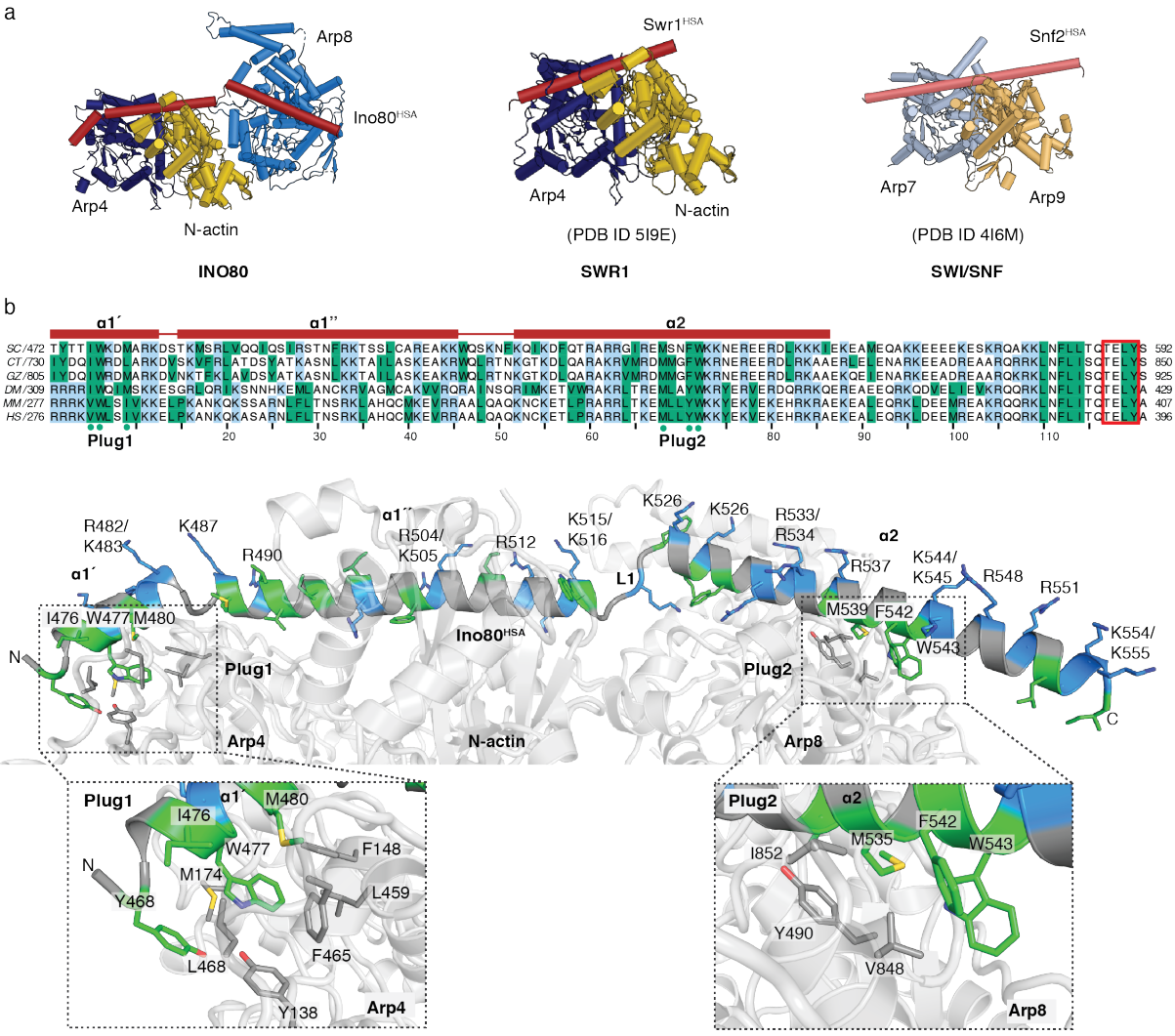

Figure 14 Organization of the Ino80^{HSA}.

a, Structures of the Ino80^{HSA}-Arp4-N-actin-Arp8 complex, the Swr1^{HSA}-Arp4-N-actin complex (PDB 5I9E) and the Snf2^{HSA}-Arp7-Arp9 complex (PDB 4I6M) shown as cartoon representations. **b**, Sequence alignment of Ino80^{HSA} from different species (*SC*, *Saccharomyces cerevisiae*; *CT*, *Chaetomium thermophilum; GZ, Gibberella Zeae; DM, Drosophila Melanogaster*; *MM*, *Mus Musculus*; *HS*, *Homo sapiens*), with positively-charged residues (Arg and Lys) colored in blue and hydrophobic residues (Ile, Leu, Trp, Val, Phe, Tyr, and Met) in green. The region and secondary structure of Ino80^{HSA} visualized in the Arp8 module structure is indicated above the sequence alignment. The highly conserved TELY motif (Shen et al., 2000) is highlighted by a red rectangle. Green dots below the sequences highlight the conserved hydrophobic residues of Plug1 and Plug2 that bind to Arp4 and Arp8, respectively. Below, cartoon representation of the Arp8 module. The Ino80^{HSA} domain is shown, with hydrophobic residues colored in green and positively-charged residues colored in blue. Boxed zoom images show the interactions of Plug1 with Arp4 (left box) and Plug2 with Arp8 (right box). Adapted and modified from (Knoll et al., 2018).

A cluster of conserved residues at α1.1, Tyr468^{Ino80}, Ile476^{Ino80}, Trp477^{Ino80} and Met480^{Ino80} (plug 1), binds into a hydrophobic pocket formed by Tyr138^{Arp4}, Phe148^{Arp4}, Phe465^{Arp4} and Leu459^{Arp4} at the barbed end of Arp4 (Figure 14b). Interestingly, Swr1^{HSA} binds Arp4 with

the same hydrophobic pocket (Cao et al., 2016). Furthermore, *in vivo* mutations of the hydrophobic residues Leu462^{Arp4}, Phe465^{Arp4} and Leu468^{Arp} located at the barbed end of the Arp4 Ino80^{HSA} binding site results in a severe growth defect of yeast under genotoxic stress. This is comparable to the phenotype of Ino80 deletion (Gerhold, 2012) (see section 3.7.2), confirming the relevance of the observed interactions. The central region at α1.2 (residues 494 to 518) of the Ino80^{HSA} binds to the barbed end of N-actin. Ino80^{HSA} adapts to the unusual binding mode of Arp8 to N-actin via formation of the pronounced loop region L1 and thereby facilitates binding of a second cluster of conserved hydrophobic residues, Met535^{Ino80}, Phe542^{Ino80} and Trp543^{Ino80} (plug 2), on the C-terminal α2 part of Ino80^{HSA} into a pocket at the barbed end of Arp8 (Figure 14b). The overall binding mode of the Ino80^{HSA} with the two hydrophobic plugs captures the sandwich-like architecture of Arp4, N-Actin and Arp8. Hereby, the distance between the two hydrophobic plugs appears to determine the specificity of the Ino80^{HSA} for Arp4, N-actin and Arp8.

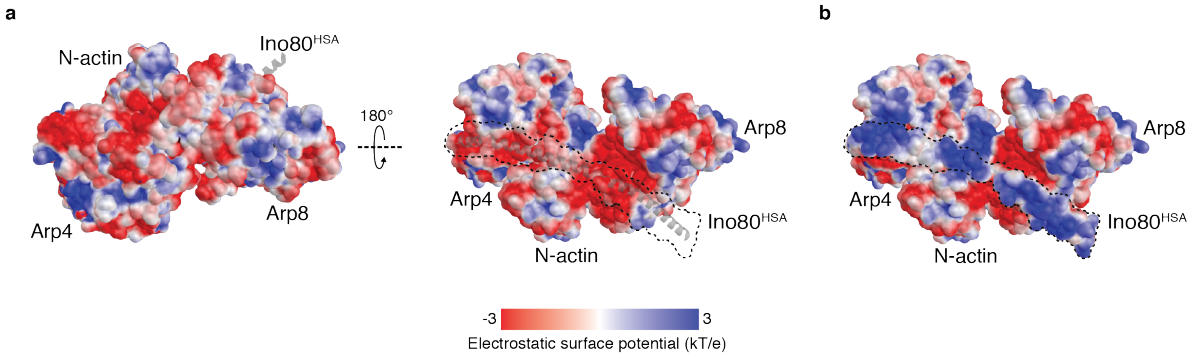

Figure 15 Electrostatic surface of the Arp8 module.

a and **b**, Electrostatic surface potential of the Arp8 module (calculated with the APBS PyMol plugin (Baker et al., 2001)) shown as surface representation. **a**, Ino80^{HSA} was not included in the electrostatic surface potential calculation but its profile is indicated by a dotted line. **b**, Ino80^{HSA} was included in the electrostatic surface potential calculation, showing the highly positively-charged surface of Ino80^{HSA}. Adapted from (Knoll et al., 2018).

While the hydrophobic side of the helical Ino80^{HSA} functions as important binding site for Arp4, N-actin and Arp8, the opposite side is solvent exposed in the Arp8 module crystal structure. Conserved pairs of lysine and arginine residues on this side of the Ino80^{HSA} helices lead to positively-charged patches on the surface of the Arp8 module (Figure 15), indicating a potential DNA-binding site. In order to investigate the Ino80^{HSA} as potential binding site for DNA, further experiments were performed (see section 3.5).

3.2 Characterization of yeast INO80 binding nanobodies

Five INO80 binding nanobodies were previously generated to probe functional states of INO80 and INO80 sub-modules. To reveal the specificity of the nanobodies, pull-down experiments were performed.

Camelids have in addition to the conventional antibodies (with two light and two heavy chains) heavy-chain-only antibodies (with only two heavy chains). Single-domain antibody fragments derived from these heavy-chain-only antibodies, termed nanobodies, are easy to generate by recombinant expression in *E. coli* (Muyldermans, 2013). Due to their small size, solubility, stability and high antigen binding affinity they are used for various research applications such as proteomics, super-resolution microscopy or intrabodies (de la Mata and Grosshans, 2018). Furthermore, nanobodies can be used as crystallization chaperones to trap the functional states of proteins, as for example in the case of G-protein coupled receptors (Rasmussen et al., 2011). To generate nanobodies specific for yeast INO80, alpacas were immunized with endogenous cross-linked entire 1.2 MDa INO80 complex and recombinantly overexpressed INO80 submodules: the Arp8 module (Arp8-Arp4-N-actin-Ies4-Ino80^{HSA}), the Nhp10 module (Nhp10-Ies3-Ies4), and Arp5-Ies6. The initial characterization of the nanobody clones identified five nanobodies that specifically recognize the entire INO80 complex in yeast lysate (Tosi, 2013). Further characterization of two of the nanobodies revealed that one nanobody specifically recognizes the Arp4-N-actin heterodimer and the second nanobody binds to subunits of the Nhp10 module (work done by Dr. Sebastian Eustermann).

In order to determine the sub-module specificity of the remaining three INO80 binding nanobodies, additional pull-down experiments were performed with all five nanobodies. Ten yeast INO80 subunits Arp4, Arp8, actin, Taf14, Ies1, Ies2, Ies3, Ies4, Ies5 and Nhp10 were recombinantly overexpressed in insect cells (see section 5.2.2.4). Of note, without Ino80, the main scaffold protein of the INO80 complex, the overexpressed proteins exist as individual entities or form smaller sub-complexes. Pull-down experiments were performed with the nanobodies covalently coupled to agarose-beads (generated by Chromotek GmbH) and analysed by SDS-PAGE (Figure 16). Surprisingly four out of the five nanobodies (995, 996, 998 and 1001) bind Ies3, Nhp10 and presumably Ies5, i.e. proteins of the Nhp10-module. In agreement with the previous analysis, the remaining nanobody (997) binds Arp4 and N-actin, subunits of the Arp8 module.

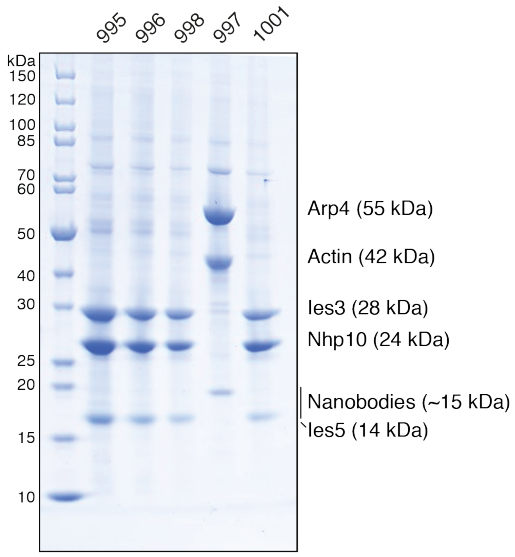

Figure 16 Sub-module specificity of INO80 binding nanobodies.

SDS-PAGE and Coomassie brilliant blue staining of pull-down experiments with INO80 specific nanobodies. Pull-downs were performed with insect cell lysate containing recombinantly overexpressed yeast Arp4, Arp8, actin, Taf14, Ies1, Ies2, Ies3, Ies4, Ies5 and Nhp10 (nanobodies are named according to their clone number). Four nanobodies (995, 996, 998 and 1001) showed binding to, Ies3, Nhp10 and presumably Ies5, proteins of the Nhp10 module. Due to the similar size of the Nhp10 module binding nanobodies and Ies5 further validation e.g. via mass spectrometry will be required to confirm the presence of Ies5. Nanobody 997 binds to Arp4 and N-actin, subunits of the Arp8 module.

With knowledge of the sub-module specificity, the nanobodies could be used for the further characterization of the respective sub-modules. Since this work focused on the characterization of the INO80 Arp8 module, the nanobody that recognises the Arp4-N-actin heterodimer (here after termed NactNB) was used for the further characterization of the Arp4-N-actin dimer in chromatin-associated complexes.

3.3 Arp4 and N-actin: A conserved heterodimer in chromatin-associated complexes

In order to confirm NactNB specificity and to investigate the conserved nature of the Arp4-N-actin heterodimer in endogenous chromatin-associated complexes, NactNB was used to perform affinity enrichment high-resolution mass spectrometry (AE MS) from yeast whole cell extract. For a quantitative approach, the pull-down experiments from yeast lysate were performed using a specific (NactNB) and an unspecific (GFP binding nanobody

(Kirchhofer et al., 2010); hereafter termed GFP-NB) binder and analyzed by a label-free quantification approach using mass spectrometry analysis (Cox et al., 2014).

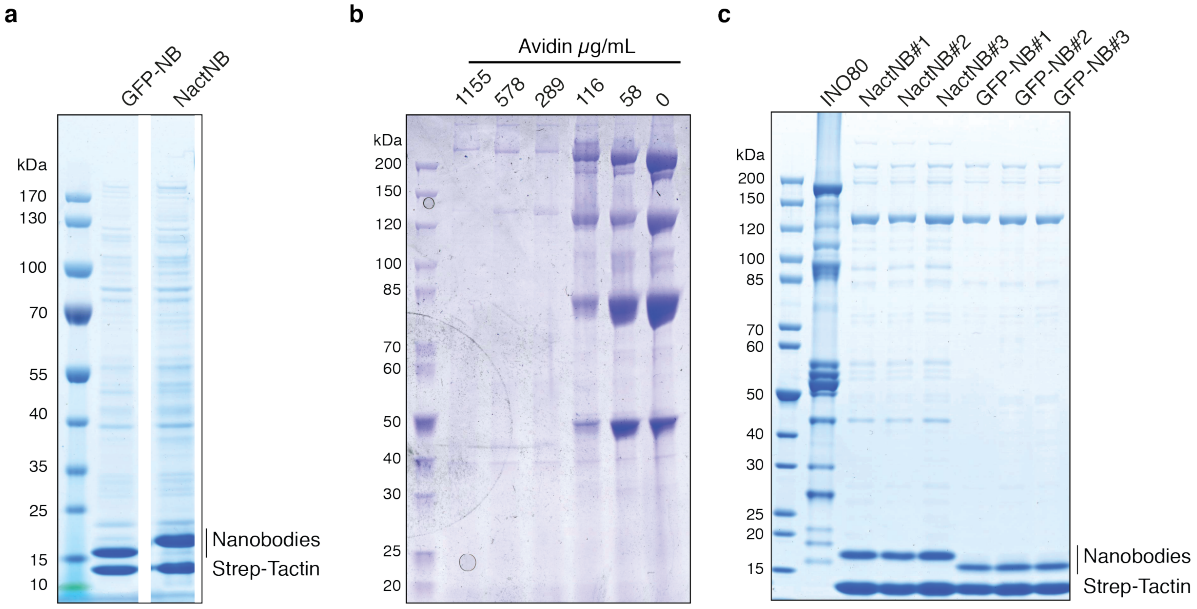

Figure 17 Nanobody pull-downs from yeast whole cell extract.

a, SDS-PAGE and SimplyBlue staining of purified GFP-NB and NactNB bound to Strep-Tactin resin. **b**, SDS-PAGE and Coomassie brilliant blue staining of Strep-Tactin resin incubated with yeast whole cell extract and washed. Increasing amounts of avidin were titrated against the yeast whole cell extract to determine the optimal avidin concentration for blockage of biotinylated proteins. **c**, SDS-PAGE and SimplyBlue staining of pull-down experiments from yeast whole cell extract used for AE MS (Figure 18). Three experiments were performed for each of the binders NactNB and GFP-NB. Purified INO80 complex is shown for comparison.

Nanobodies for AE MS experiments were successfully expressed in *E. coli* Rosetta cells and purified via a C-terminal Twin-Strep-Tag (Figure 17a). Strep-Tactin resin saturated with nanobody was directly used for the pull-down experiments. Initial pull-down experiments showed a high background of biotinylated proteins on SDS-PAGE. It became clear that a high amount of free biotin and biotinylated proteins compete with the Twin-Strep-Tag tagged nanobodies for Strep-Tactin binding sites in the yeast whole cell extract. Due to the higher affinity of biotin for Strep-Tactin, compared to the Twin-Strep-Tag to Strep-Tactin, the pull-down yielded mostly biotinylated proteins (Schmidt and Skerra, 2007). To overcome this, free biotin and biotinylated proteins were blocked by the addition of avidin. Avidin binds biotin with very high affinity, the strongest known non-covalent interaction for a protein so far, but not the Twin-Strep-Tag (Schmidt and Skerra, 2007). The optimal avidin concentration for the blockage of biotinylated proteins in yeast lysate was determined in titration experiments. Yeast whole cell extract was supplemented with

increasing amounts of avidin, subsequently incubated with Strep-Tactin resin, washed and the resin analyzed by SDS-PAGE. A concentration of 250 µg avidin per mL of yeast whole cell extract was sufficient to prevent binding of most of the biotinylated contaminants (Figure 17b).

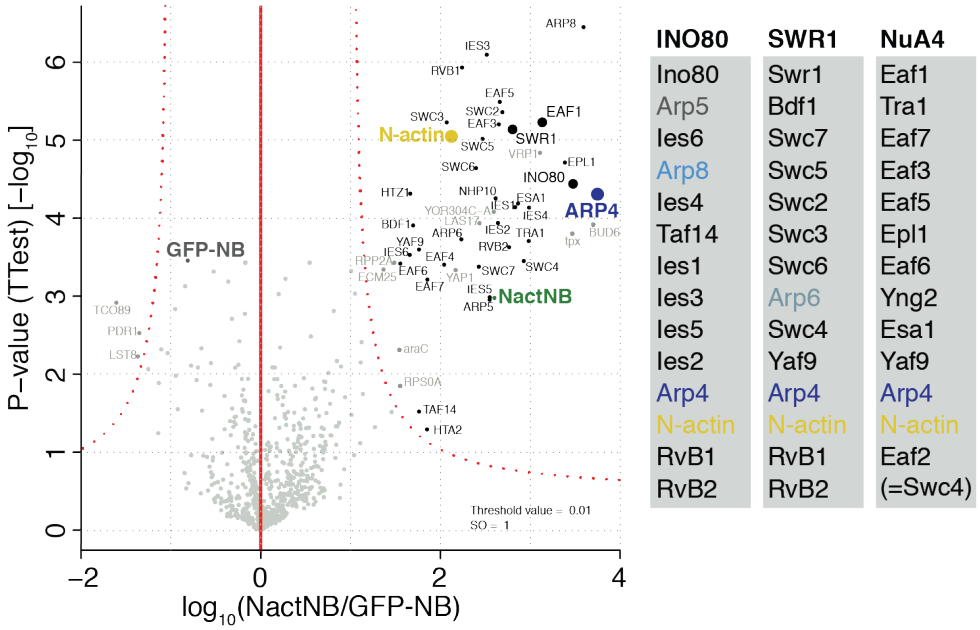

Figure 18 Arp4 and N-actin build a conserved heterodimer in INO80, SWR1 and NuA4.

NactNB binds the endogenous Arp4-N-actin heterodimer in chromatin-associated complexes. Yeast whole cell extract was subjected to AE MS experiments using NactNB and GFP-NB as a control. Pull-downs shown in Figure 17c were measured by mass spectrometry and label-free quantification data analysis was applied (see section 5.2.6). A two-sided and two sampled t-test shows in a volcano plot representation significant enrichment of all subunits of INO80, SWR1 and NuA4. The table on the right lists all components of the individual complexes. Adapted from (Knoll et al., 2018).

Optimized pull-down experiments from yeast whole cell extract were performed in triplicates with the Arp4-N-actin specific (NactNB) and an unspecific (GFP-NB) control binder (Figure 17c). Samples were further processed by 'on-bead digestion' and prepared for tandem mass spectrometry measurement (see section 5.2.6). Data were analyzed and evaluated using a label-free quantification algorithm (Cox et al., 2014) (mass spectrometry measurements and data analysis were performed by Dr. Gabriele Stoehr).

In yeast, the Arp4-N-actin heterodimer builds a conserved entity in the chromatin-associated complexes INO80, SWR1 and NuA4 (Olave et al., 2002) (Figure 5). Strikingly,

NactNB enriches all 35 proteins of the three chromatin-associated complexes in the AE MS experiment (Figure 18), indicating the presence of a conserved and solvent-accessible NactNB binding epitope in the Arp4-N-actin dimer in all three complexes. Interestingly, H2A.Z, a known interaction partner of SWR1, was also co-purified by NactNB. Additionally, ten unexpected proteins that were so far not linked to INO80, SWR1 and NuA4 were also enriched in the pull-down, indicating that they might be new interaction partners of chromatin-associated complexes. In contrast, highly abundant cytoplasmic actin interacting proteins involved in actin cytoskeleton formation, such as gelsolin and the Arp2/3 complex, were not enriched by NactNB. Consequently, NactNB recognizes the Arp4-N-actin heterodimer within endogenous INO80, SWR1 and NuA4 in a highly specific manner.

In summary, the AE MS results indicate the presence of a conserved and solvent-exposed binding epitope of NactNB in all three complexes and accordingly a similar architecture of the Arp4-N-actin dimer in endogenous INO80, SWR1 and NuA4.

3.4 Crystal structure of the NactNB-Arp4-N-actin complex

NactNB recognizes INO80, SWR1 and NuA4 via the same solvent-accessible binding epitope on the conserved Arp4-N-actin heterodimer. In order to reveal this common feature of N-actin containing chromatin associated complexes, the crystal structure of the ternary 120 kDa complex formed by NactNB together with Arp4 and N-actin was determined.

3.4.1 Purification and crystallization of the NactNB-Arp4-N-actin complex

3.4.1.1 Purification of the NactNB-Arp4-N-actin complex

Arp4 and N-actin were heterologously expressed in insect cells and affinity purified using NactNB bound to Strep-Tactin resin (previously described in section 3.3; Figure 17a). Following the NactNB affinity pull-down, the ternary complex was eluted from the Strep-Tactin resin and subjected to anion-exchange chromatography with Q Sepharose resin to remove residual nucleic acid contaminations. The final size-exclusion chromatography step with Superdex 200 resin resulted in a pure and monodisperse sample (Figure 19 and section 5.2.2.4). Purification from 2 L of insect cell expression yielded typically 2 mg of the ternary complex. Expression and purification produced protein sample in sufficient amounts and purity for crystallization.

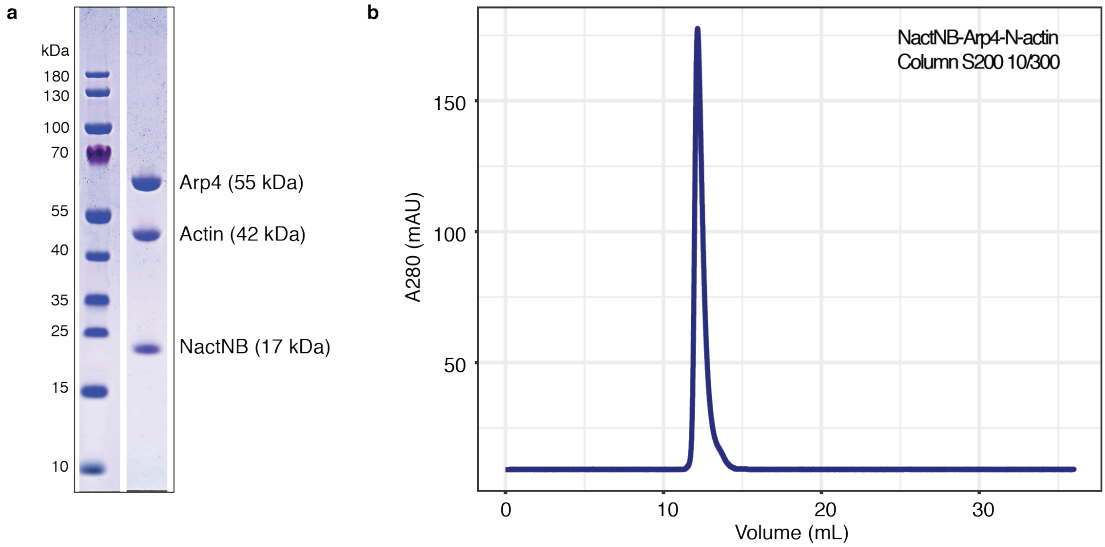

Figure 19 Purification of the NactNB-Arp4-N-actin complex.

a, SDS-PAGE and Coomassie brilliant blue staining of the purified NactNB-Arp4-N-actin complex used for crystallization. **b**, Size-exclusion chromatography elution profile of the NactNB-Arp4-N-actin complex on a S200 10/300 column. Adapted from (Knoll et al., 2018).

3.4.1.2 Crystallization of the NactNB-Arp4-N-actin complex

A stoichiometric 130 kDa complex comprising NactNB, Arp4 and N-actin was produced for crystallization through expression in insect cells (Figure 19). Applying 'in situ proteolysis' and high-throughput crystallization screening resulted in an initial crystallization condition for the complex. NactNB-Arp4-N-actin (20 mg/mL) was mixed with subtilisin [1:8000; (w(protease):w(sample)] prior to sitting-drop vapour-diffusion crystallization against 1.4 M sodium maloante at pH 6.0. Crystal optimization resulted in the final crystallization condition with 16 mg/mL protein mixed with subtilisin [1:8000; w(protease):w(sample)] in hanging-drop vapour-diffusion experiments against 1.2 M sodium maloante pH 6.0 at 20°C. Crystals were harvested after 4–8 days and cryo-protected with 15% D-(-)-2,3-butandiol.

The best diffracting crystal was used to determine an initial structure of the NactNB-Arp4-N-actin complex, however there was only weak electron density for a bound nucleotide in the nucleotide binding pocket of N-actin. To reveal the nucleotide state of N-actin in the complex, co-crystallization experiments with ADP and ATP (see section 5.2.3.2) were performed. Addition of ADP or ATP to the NactNB-Arp4-N-actin complex prior to crystallization did not alter crystal growth. The best diffracting crystals were harvested after 4–8 days and cryo-protected with 23% glycerol.

3.4.2 Crystal structure determination of the NactNB-Arp4-N-actin complex

Diffraction data from single crystals were used to determine the crystal structure of the NactNB-Arp4-N-actin complex by molecular replacement, with N-actin in the nucleotide free (apo) state and in the ATP-bound state. The initial structure derived from crystals grown without the addition of any nucleotide was used as search model to solve the two structures (section 5.2.3.5). The crystal grown in the presence of ADP diffracted up to 2.8 Å resolution and resulted, despite the addition of ADP, in the NactNB-Arp4-N-actin(apo) structure with N-actin in a nucleotide-free state. For crystals grown with ATP, diffraction data up to 3.4 Å resolution were collected, resulting in the NactNB-Arp4-N-actin(ATP) structure. Iterative rounds of model building and refinement resulted in final models for the NactNB–Arp4–N-actin(apo) complex (PDB 5NBL) at 2.8 Å resolution with R_{work}/R_{Free} values of 17.1%/20.4% and the NactNB–Arp4–N-actin(ATP) complex (PDB 5NBM) at 3.4 Å resolution with R_{work}/R_{Free} values of 15.2%/19.3% (Table 3 and section 5.2.3.5).

3.4.3 Conserved architecture of the Arp4-N-actin heterodimer

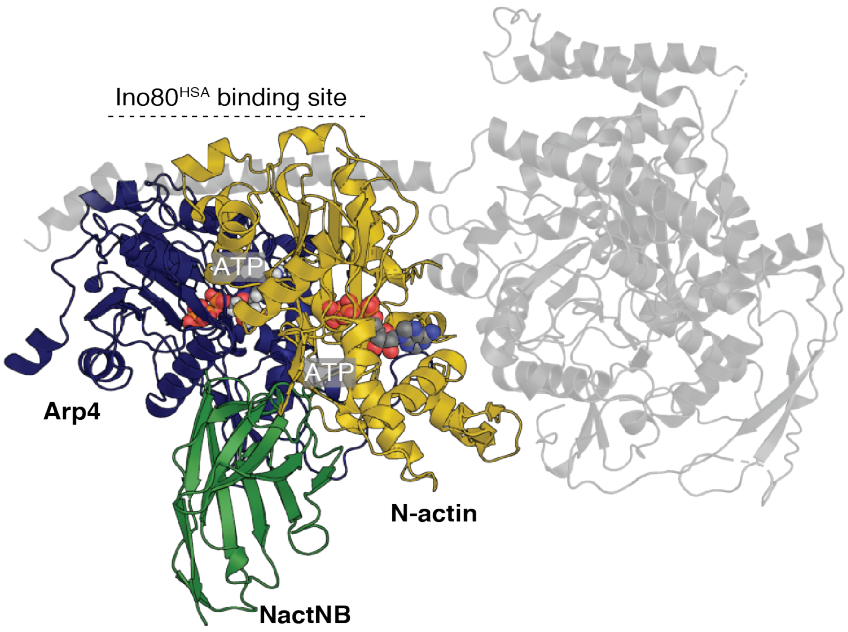

Figure 20 Crystal structure of the NactNB-Arp4-N-actin(ATP) complex.

Structure of the NactNB-Arp4–N-actin(ATP) complex shown as cartoon representation. The Arp8 module structure aligned on the Arp4–N-actin dimer is shown in light gray. N-actin and Arp4 are ATP-bound (colored spheres). Adapted from (Knoll et al., 2018).

NactNB pull-downs from yeast lysate indicated the presence of a conserved architecture for the Arp4-N-actin heterodimer and a solvent-accessible binding epitope for NactNB in endogenous chromatin-associated complexes. The crystal structures of the NactNB-Arp4-N-actin complex match these observations. The arrangement of the Arp4-N-actin heterodimer captured by NactNB is analogous to that of Arp4 and N-actin in the Arp8 module structure and the Swr1^{HSA}-Arp4-N-actin structure. Using secondary structure matching (Krissinel and Henrick, 2004) in COOT (Emsley et al., 2010), the NactNB bound Arp4-N-actin dimer superimposes to Arp4 and N-actin in the two related structures with a low backbone RMSD of 0.68 Å (N_{align} 753) to the dimer in the Arp8 module and 0.96 Å (N_{align} 724) to the Swr1^{HSA} bound dimer. The architectural similarity of the Arp4-N-actin interaction in those structures validates the conclusion that NactNB recognizes an integral physiological arrangement of both proteins.

NacNB binds the dimer into a pocket formed by the pointed ends of the two actin-fold proteins. The main interactions of NactNB are made between the N-actin sub-domains 1, 2 and 4 and its three complementary defining regions (CDR1 (residues 27-35), CDR2 (residues 53-60) and CDR3 (residues 101-114)), whereas Arp4 SD2 and SD1 are contacted by CDR1 and two additional regions of the nanobody framework (FR) (N-term (residues 1-3) and FR3 residues 75-79) (Figure 21).

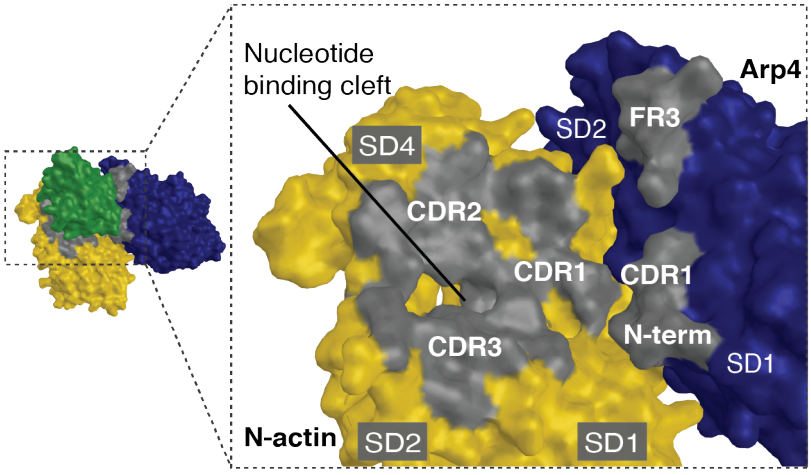

Figure 21 NactNB binding epitope on the Arp4-N-actin heterodimer.

Surface representation of the NactNB-Arp4-N-actin complex showing the NactNB binding epitope on the Arp4-N-actin dimer. Grey regions indicate recognition sites of the respectively labeled NactNB binding element. CDR, complementarity-determining region; N-term, N-terminus; FR, framework region. Adapted from (Knoll et al., 2018).

In summary, the crystal structure of the NactNB-Arp4-N-actin complex in conjunction with AE MS using NactNB provides direct evidence for an evolutionarily conserved mode by which the Arp4-N-actin pair is incorporated into SWR1, INO80 as well as NuA4. In this model the NactNB binding site is surface-exposed in all Arp4-N-actin containing complexes in yeast.

3.4.4 NactNB probes N-actin in an ATP state

In the cytoplasm the nucleotide state of actin is tightly linked to actin filament formation and drives 'actin treadmilling' (Merino et al., 2018). In contrast, the N-actin nucleotide state and its role in context of chromatin remodelers is less clear. Since NactNB probes N-actin within its native environment in entire endogenous chromatin-associated complexes, the nucleotide state of N-actin in the crystal structures represents a physiological feature of N-actin.

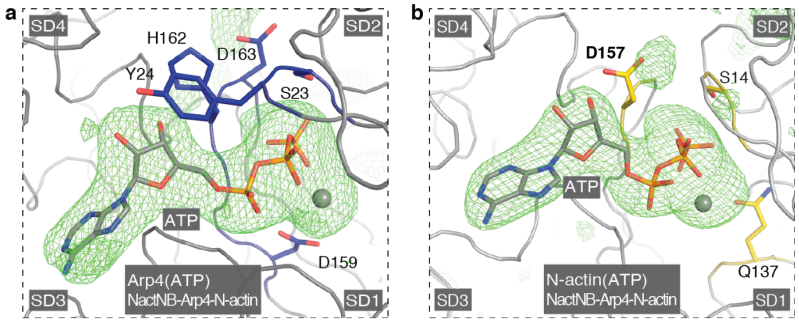

Figure 22 Nucleotide states of Arp4 and N-actin in the NactNB-Arp4–N-actin complex.

a, and **b**, Close-ups of the NactNB-Arp4-N-actin structure N-actin(ATP) and Arp4(ATP) nucleotide-binding pockets with electron density (green mesh) for the bound ligands (mFo-DFc difference map with a carving radius of 20 Å around each ligand; contoured at 3 sigma; resulting from structure refinement with phenix.refine (Adams et al., 2010) lacking ligands). Adapted from (Knoll et al., 2018).

In a first structure of the NactNB-Arp4–N-actin complex, only weak density for a bound nucleotide was visible in the nucleotide binding cleft of N-actin. The following co-crystallization experiments with either ADP or ATP revealed, however, that NactNB probes N-actin in the ATP state. Co-crystallization with ATP results in unambiguous electron density for ATP in the nucleotide-binding pocket of N-actin (Figure 22), whereas addition of ADP results in nucleotide-free N-actin. The two structures of the NactNB-Arp4-N-actin complex with N-actin in the ATP and apo states do not display any differences compared

to one other in the overall architecture of the complex and the N-actin conformation is also similar.

NactNB appears to specifically recognize N-actin in the ATP state and to stabilize this state, by binding to the two actin lobes formed by SD2-SD1 and SD4-SD3 and preventing further movement between lobes, which is directly linked to the nucleotide state of actin (Dominguez and Holmes, 2011). In addition, Arg104 of NactNB-CDR3 inserts deeply into the actin nucleotide-binding cleft between SD2 and SD4 and contacts via a tripartite interaction Asp157$^{N\text{-actin}}$ of the phosphate binding loop P1, Ser14$^{N\text{-actin}}$ of P2 as well as Glu72$^{N\text{-actin}}$ and Tyr69$^{N\text{-actin}}$ of the ATP sensor loop. P1, P2 and the ATP sensor loop are critical elements for actin nucleotide binding and hydrolysis. Overall the interactions of NactNB with the two actin lobes and within the nucleotide binding pocket seem to specifically recognize the ATP state of N-actin.

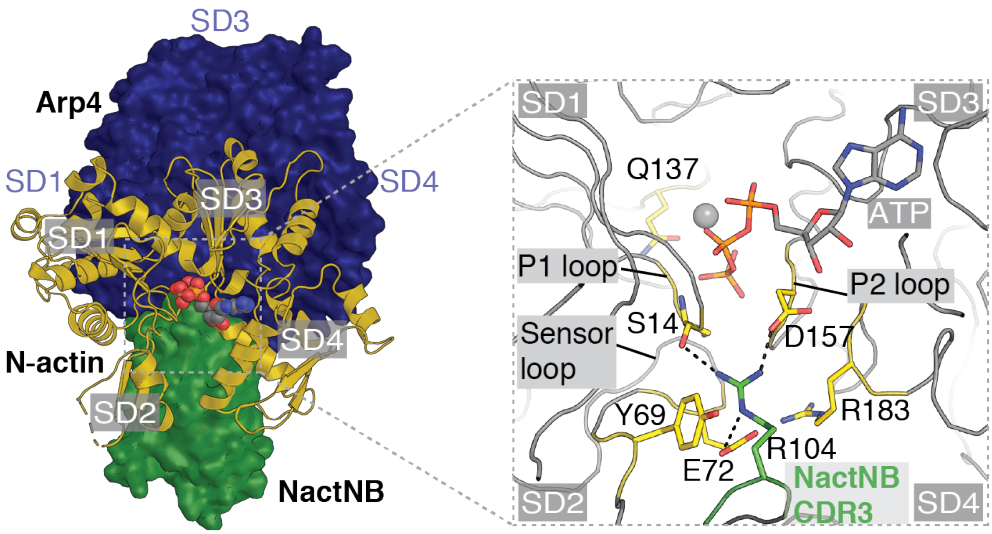

Figure 23 NactNB captures the ATP state of N-actin.

Crystal structure of the NactNB-Arp4–N-actin complex is displayed as cartoon (N-actin) and surface representation (NactNB and Arp4). ATP (colored sphere) is bound in the nucleotide-binding cleft of N-actin. Zoomed image (right panel) shows that Arg104 of NactNB binds deep in the nucleotide-binding pocket of N-actin, thereby contacting all three critical nucleotide-binding elements of actin - P1, P2 and the sensor loop. Adapted from (Knoll et al., 2018).

Previous studies and the results above showed that Arp4 binds ATP tightly and lacks detectable ATP hydrolysis activity (Fenn et al., 2011a; Gerhold et al., 2012) (see section 3.1.4). In line with these observations, Arp4 is in an ATP-bound state in both of the NactNB-Arp4–N-actin structures (Figure 22). Of note, the excess of ADP in the co-

crystallization experiment did not displace ATP from nucleotide-binding cleft of Arp4, indicating a strong binding preference for ATP. Coordination of ATP in the Arp4 nucleotide-binding pocket is analogous to that described before for Arp4 within the Arp8 module structure in section 3.1.4 (Figure 12 and Figure 22).

In summary, NactNB specifically recognizes the ATP state of N-actin in INO80, SWR1 and NuA4. Accordingly, ATP binding seems to be a conserved and common feature of N-actin in chromatin-associated complexes. In order to investigate whether the nucleotide state of N-actin plays a functional role for chromatin remodeling additional experiments were performed (see section 3.6).

3.5 Biochemical characterization of the INO80 Arp8 module

In vitro ChIP-exo mapping of Arp8 and the recent cryoEM structure of the INO80-nucleosome complex indicated binding of extranucleosomal DNA by the Arp8 module (Eustermann et al., 2018; Yen et al., 2013). Additionally, the crystal structure of the Arp8 module revealed large positively-charged patches on the solvent-accessible side of Ino80^{HSA}, indicative of a potential DNA binding function (section 3.1.6). In order to characterize the Ino80^{HSA} as a possible DNA binding platform of INO80, biochemical and mutational analysis of the Ino80^{HSA} in context of the Arp8 module only and in context of the whole INO80 remodeler were performed. This work focused on the characterization of the Arp8 module only.

3.5.1 Purification of Arp8 module Ino80^{HSA} mutants

Based on the crystal structure of the Arp8 module, Ino80^{HSA} mutants with a less negatively-charged surface were designed. Conserved lysine and arginine residues on the surface of the Ino80^{HSA} were mutated into non-charged glutamine residues (Figure 14), resulting in three mutants; two with either of the two helical segments, HSAα1 and HSAα2, and one with both helices, HSAα1/HSAα2, mutated (Figure 24a).

The first expression and purification experiments of the Arp8 module Ino80^{HSA} mutants showed significantly lower expression yields and stability of the mutant complexes compared to the wild type (WT) complex, pointing to a destabilizing effect of the Ino80^{HSA} mutations. However, size-exclusion chromatography experiments showed that NactNB increases the stability on WT and Ino80^{HSA} mutant Arp8 module complexes. Addition of NactNB directly to the insect lysate prior to purification yielded stable WT and HSAα2 Arp8 module-NactNB complexes, whereas the Ino80^{HSA} mutations HSAα1 and

HSAα1/HSAα2, despite the presence of NactNB, did not form a stable Arp8 module complex (Figure 24b). Purification of the WT and HSAα2 Arp8 module-NactNB complexes was performed analogous to that described previously for the Arp8 module only (see section 3.1.1 and 5.2.2.5) and yielded per 2 L of insect cell expression typically 1-2 mg of pure and stoichiometric protein sample (Figure 24c). WT and HSAα2 Arp8 module-NactNB complexes were then used for the further analysis of the DNA and nucleosome binding properties of Ino80^{HSA}.

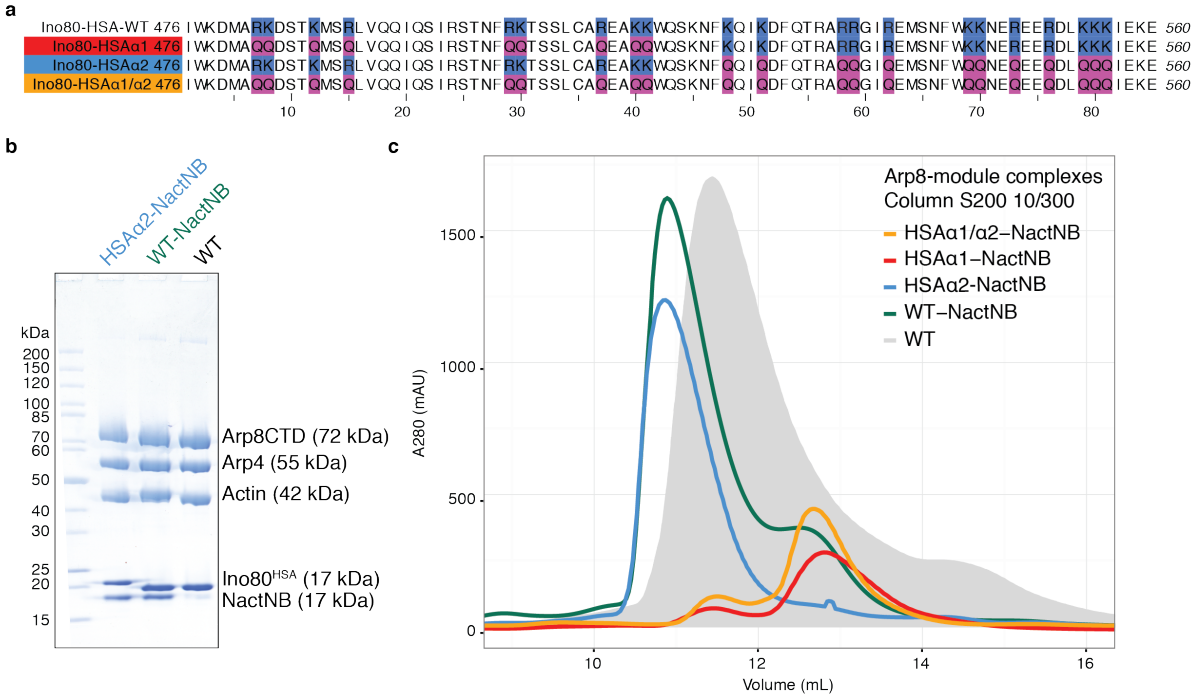

Figure 24 Purification of Ino80^{HSA} mutant Arp8 module complexes.

a, Sequence alignment of Ino80^{HSA} (res 476 – 560) WT and the three Ino80^{HSA} mutants. Mutated residues are highlighted in purple. **b**, SDS-PAGE and Coomassie brilliant blue staining of the Arp8 module (WT) and the Arp8 module in complex with NactNB (WT and the Ino80^{HSA} mutant HSAα2). **c**, Size-exclusion chromatography elution profiles for the different Arp8 module-NactNB complexes on a S200 10/300 column.

3.5.2 Extranucleosomal DNA binding by the Arp8 module

Previous studies showed the direct binding of Arp8 to histones (Saravanan et al., 2012; Shen et al., 2003), others showed binding to DNA (Gerhold et al., 2012; Osakabe et al., 2014) and more recent studies located the Arp8 module, in context of INO80 nucleosome binding, in the extranucleosomal linker DNA region (Eustermann et al., 2018; Yen et al., 2013). In order to characterize the nucleosome binding specificity of Arp8 module, competition

electro mobility shift assays (EMSAs) were performed using a 1:1 mixture of fluorophore-labeled nucleosomes with either an 80 bp extranucleosomal DNA overhang (0N80) or none (0N0).

EMSAs were performed with a concentration of 20 nM of each nucleosome species, lower than the assumed equilibrium dissociation constant (Kd) of the Arp8 module for nucleosome binding (Gerhold et al., 2012). WT Arp8 module showed a clear binding preference for 0N80 nucleosome, indicating that the Arp8 module binds extranucleosomal DNA (Figure 25). At a concentration of 400 nM WT complex, most of the 0N80 nucleosome is shifted to the Arp8 module bound species, whereas most of the 0N0 nucleosome is unbound. Of note, the Arp8 module in complex with NactNB shows similar nucleosome-binding properties to the Arp8 module only, suggesting that binding of NactNB to the complex does not interfere with extranucleosomal DNA binding. In contrast, mutations on Ino80^{HSA} change the nucleosome binding affinity of the Arp8 module drastically. The HSAα2 Arp8 module-NactNB complex shows a substantially reduced affinity for its nucleosomal substrate (Figure 25). Only at the highest titration point, with 1000 nM Arp8 module complex, most of the 0N80 nucleosome is bound by the Arp8 module, implying that the affinity of the HSAα2 mutant is more than twofold decreased compared to the WT complex.

Overall, nucleosome competition EMSAs indicate that the Arp8 module binds the extranucleosomal linker DNA region of the nucleosome and mutational analysis identified the Ino80^{HSA} as the responsible DNA binding element.

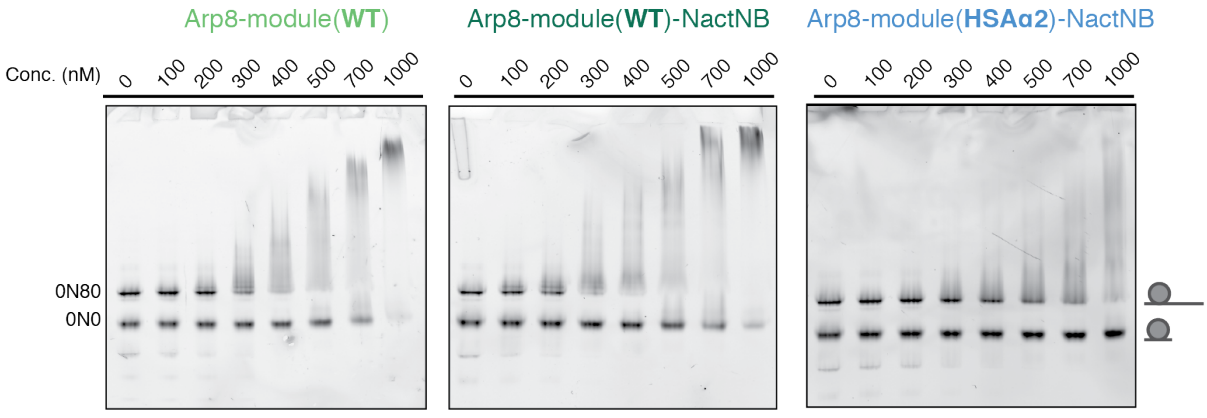

Figure 25 Extranucleosomal DNA binding by the Arp8 module.

Competition electromobility shift assays with two nucleosome species (20 nM each), one with an 80 bp extranucleosomal DNA overhand (0N80) and one without a DNA overhang (0N0), and increasing concentration of the indicated Arp8 module complex (Conc., concentration). Adapted from (Knoll et al., 2018).

3.5.3 DNA binding properties of the Arp8 module

In context of an entire nucleosome with an 80 bp DNA overhang, competition EMSA experiments demonstrated that the Arp8 module of INO80 binds via the Ino80^{HSA} to extranucleosomal DNA. In order to measure binding affinity of the Arp8 module to a double-stranded DNA substrate only, fluorescence anisotropy experiments were performed with a fluorophore-labeled dsDNA. The Arp8 module DNA binding platform, Ino80^{HSA}, extends to a length of around 120 Å, corresponding to a DNA footprint of approximately 40 bp. Therefore, the experiments were done with a 40 bp dsDNA oligomer at a concentration of 20 nM.

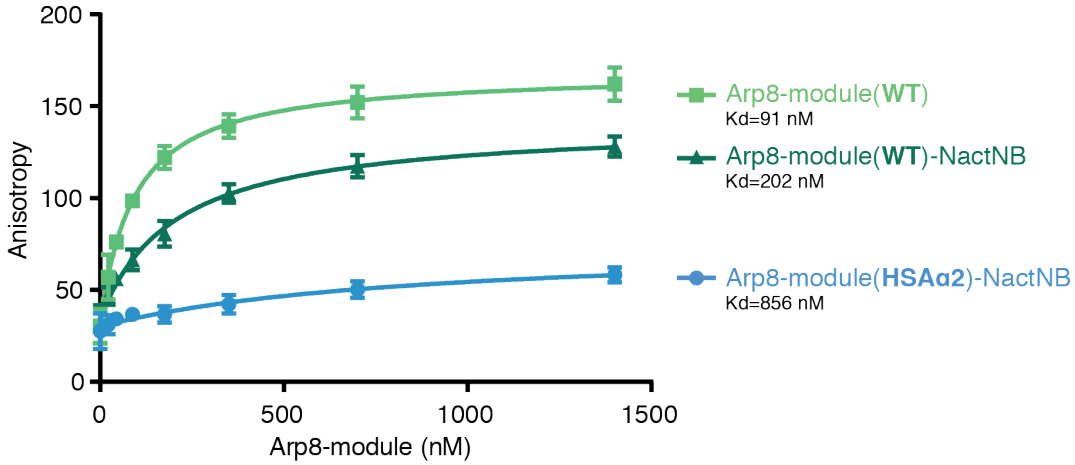

Figure 26 Arp8 module dsDNA binding

Arp8 module 40 bp dsDNA binding affinity measured by fluorescence anisotropy (with 20 nM dsDNA). Anisotropy is plotted against Arp8 module protein concentration and fitted to a non-linear non-cooperative 1:1 binding model. Data points and error bars represent the means ± s.d. from three independent experiments. Adapted from (Knoll et al., 2018).

In the first experiments different salt concentrations (150, 100 and 50 mM KCl) were tested to find ideal buffer conditions. Optimal binding was observed at 50 mM KCl and higher ionic strengths seemed to disrupt all DNA protein interaction. Subsequent measurements were performed at 50 mM KCl. All binding experiments were performed in triplicates and produced reproducible results. Anisotropy measurements were fitted to a 1:1 binding model without any cooperativity to calculate Kd values for the three complexes; the WT Arp8 module, WT Arp8 module-NactNB and HSAα2 Arp8 module-NactNB (Figure 26 and section 5.2.4.1). The WT Arp8 module binds dsDNA with a Kd of ~90 nM, whereas the Arp8 module in complex with NactNB showed weaker binding of dsDNA with an Kd

of ~200 nM. This observation is surprising, since the competition EMSAs with nucleosomes did not show large variations between the Arp8 module only and the NactNB-bound complex (Figure 25). Nevertheless, the mutation of the potential Ino80^{HSA} DNA binding site substantially reduced the dsDNA binding affinity compared to both WT complexes. The measured Kd, ~850 nM, for HSAα2 Arp8 module-NactNB ds DNA binding is more than four-fold increased compared with the WT Arp8 module-NactNB complex.

In summary, the anisotropy measurements show similar results for Arp8 module DNA binding as the competitions EMSAs for nucleosome binding. Mutations in Ino80^{HSA} clearly decrease its binding affinity for DNA. Accordingly, positively-charged amino acids on the solvent-exposed side of Ino80^{HSA} form the DNA-binding element of the Arp8 module.

3.6 N-actin nucleotide state during INO80 chromatin remodeling

N-actin is a key subunit of chromatin-associated complexes, pointing to an important functional role. The structural and functional work on N-actin described above demonstrated that N-actin can adopt an ATP-bound state in chromatin remodelers (see section 3.1.4 and 3.4.4), furthermore the nucleotide-free state of N-actin was previously visualized in the Swr^{HSA}-Arp4-N-actin complex (Cao et al., 2016). Although the different structures do not reveal any large conformational changes in N-actin between the apo and the ATP-bound states, studies on the human BAF complex indicated that the N-actin nucleotide state allosterically regulates the remodeler activity (Zhao et al., 1998). It was proposed that N-actin and ARPs might function as a conformational switch in chromatin remodelers (Boyer and Peterson, 2000). The structural studies on the Arp8 module and the NactNB-Arp4-N-actin complex demonstrated that NactNB and LatA can be used as molecular tools to trap N-actin in an ATP state. In order to investigate a possible ATP-dependent function of N-actin as a conformational switch during chromatin remodeling, INO80 nucleosome binding and remodeling experiments were performed in the presence of either NactNB or LatA.

3.6.1 INO80 nucleosome binding

INO80 nucleosome binding was measured with EMSAs using 20 nM 0N80 fluorophore-labeled nucleosomes and increasing amounts of the entire yeast INO80 complex (see section 5.2.4.2). In order to capture the nucleotide state of N-actin within INO80 either NactNB (90 nM) or LatA (2 µM) was added to the experiment.

All INO80 nucleosome binding experiments were performed in triplicates and produced reproducible results. INO80 showed in all three experiments similar binding to 0N80 nucleosomes (Figure 27a). The presence of either LatA or NactNB did not influence INO80 nucleosome binding. INO80 bound nucleosomes in all three experiments with an Kd of approximately 20 nM (Figure 27b), which is similar to that reported previously for yeast INO80 (Udugama et al., 2011).

Overall, the addition of N-actin binding ligands did not alter the INO80 nucleosome binding affinity.

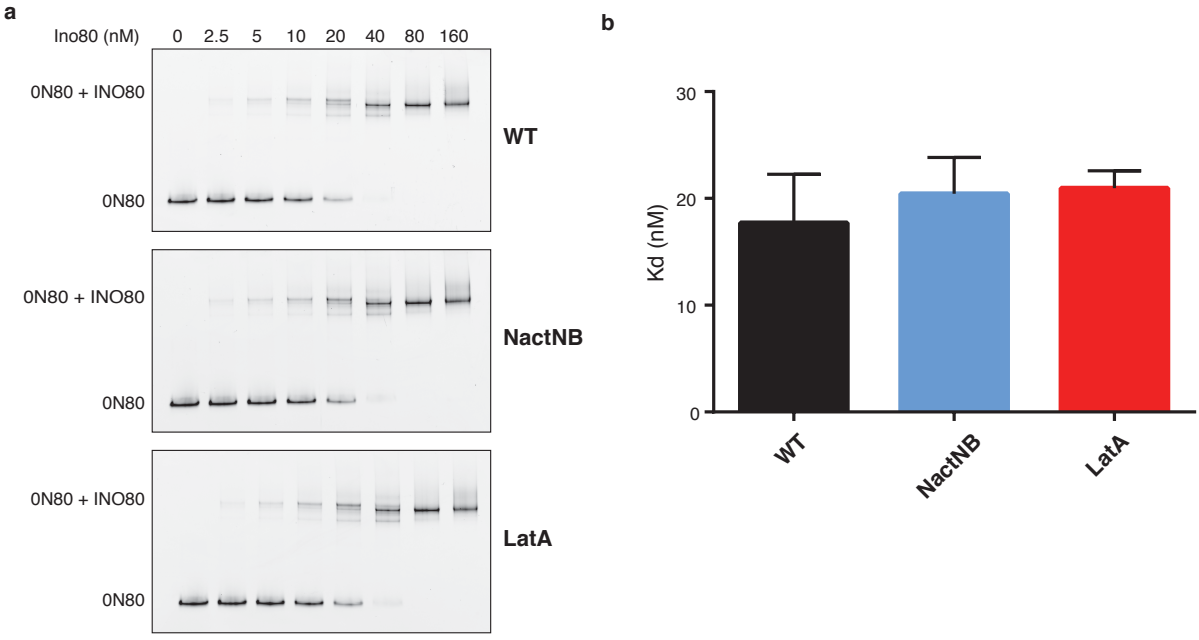

Figure 27 INO80 nucleosome binding in dependence of the N-actin nucleotide state.

a, Electromobility shift assays (EMSAs) with 0N80 nucleosomes (20 nM) and increasing concentration of INO80 complex plus indicated N-actin ligand. WT, INO80 only; NactNB, INO80 and 90 nM NactNB; LatA, INO80 and 2 µM LatA. **b**, The equilibrium binding constants (Kd) calculated from EMSA experiments as shown in panel a, displayed as a bar chart. EMSA experiments were quantified by band density analysis with ImageJ (Schneider et al., 2012). Kd values and error bars represent the means ± s.d. from three independent experiments.

3.6.2 INO80 nucleosome sliding

The ability to slide nucleosomes on DNA is a key feature of INO80 (Shen et al., 2003). Furthermore, INO80 on its own can position nucleosomes on genomic DNA at the +1 position on the transcription start site of a gene, a hallmark of chromatin organization (Krietenstein et al., 2016). The capability of INO80 to slide nucleosomes on the DNA can be tested in a simple assay on a mononucleosomal substrate. INO80 slides end-positioned

mono-nucleosomes to the center of the DNA fragment in an ATP-dependent manner and, due to their different electrophoretic mobilities, end- and center-positioned nucleosomes can be separated by Native-PAGE (Shen et al., 2003). To reveal a possible regulatory role of N-actin in the INO80 nucleosome remodeling activity such gel-based 'sliding assays' were performed in presence of either NactNB (250 nM) or LatA (10 µM).

Using 90 nM 0N80 nucleosomes and 10 nM of INO80 the nucleosome sliding reaction was nearly complete 60 min after ATP addition. Addition of either 250 nM NactNB or 10 µM LatA to such assay did not affect INO80 nucleosome sliding (Figure 28). In the case of all three samples, around 75% of mononucleosomes in the reaction were remodeled. Overall, the addition of the N-actin binding ligands NactNB or LatA did not change the INO80 nucleosome remodeling activity.

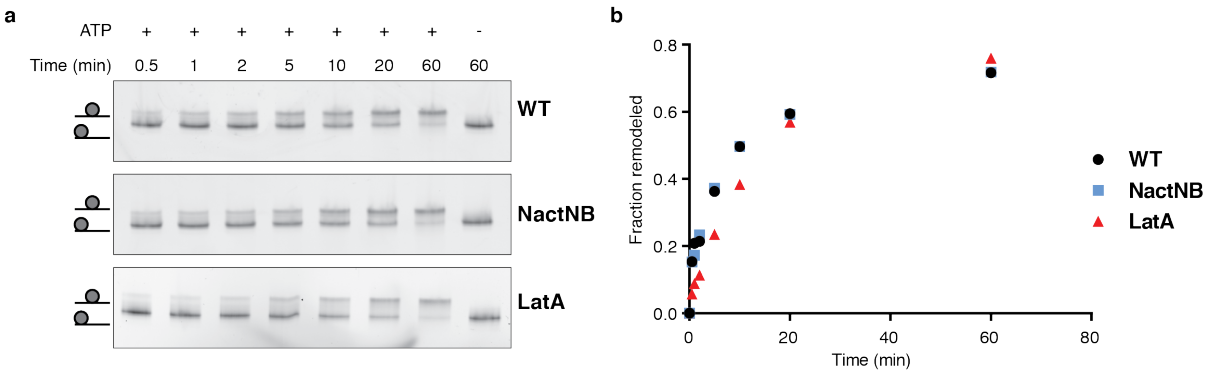

Figure 28 'Locking' the N-actin nucleotide state during INO80 nucleosome remodeling.

a, Time-course of ATP-dependent INO80 nucleosome sliding on a fluorophore-labeled mononucleosome substrate (0N80), with 10 nM IN80 and 90 nM 0N80. End-positioned and center-positioned nucleosome species were resolved by NativePAGE. WT, INO80 only; NactNB, INO80 and 250 nM NactNB; LatA, INO80 and 10 µM LatA. **b**, Quantification of the experiments shown in panel a, by band density analysis with ImageJ (Schneider et al., 2012).

3.7 *In vivo* characterization of Arp4

Arp4 is a critical subunit of INO80, SWR1 and NuA4, three complexes that have key functions in cellular processes such as the organization of chromatin, DNA repair and transcription regulation (Gerhold et al., 2015; Poli et al., 2017; Wang et al., 2018). Consistent with its important role in genome maintenance, the gene coding for the human Arp4 homolog hBAF53a/b is mutated in cancer (Hodges et al., 2016). In yeast, the deletion of the *ARP4* gene is lethal (Harata et al., 1994). However, earlier a yeast Arp4 plasmid shuffling system in BY4743 Δ*ARP4* cells was developed, allowing the relatively fast and easy *in vivo* characterization of Arp4 mutants (Gerhold, 2012) (see section 5.2.5). In order to

identify and confirm functional important residues and interfaces of Arp4, yeast growth assays were performed with Arp4 mutant cells. Given the importance of Arp4 as a critical subunit of INO80 for DNA repair (Poli et al., 2017), the growth of yeast cells was examined under conditions that induce genotoxic stress. Yeast media was supplemented with DNA damaging agents such as the ribonucleotide reductase inhibitor hydroxyurea or the DNA alkylating methyl methanesulfonate. In addition, yeast growth was examined at increased temperature to test for protein stability.

3.7.1 Cancer mutations in the Arp4 nucleotide binding pocket

Biochemical and structural analysis revealed the tight binding of ATP in the nucleotide binding cleft of Arp4 (Fenn et al., 2011a; Sunada et al., 2005) (see section 3.1 and 3.4). It was shown that Arp4 lacks detectable ATPase activity and that ATP binding is critical for Arp4 folding (Fenn et al., 2011a; Gerhold et al., 2012). As in other actin-fold proteins, Arp4 coordinates the phosphate moiety of ATP between the two phosphate binding loops P1 and P2. The P2 loop actin residue Ser14 plays an important role in coordination of the gamma phosphate and is conserved in all nuclear ARPs (Schuler et al., 1999) (Figure 29a). Mutation of Arp4 Ser23, the homologous residue to actin Ser14, results in insoluble protein upon expression in insect cells (Fenn et al., 2011a). Moreover, the residue homologous to Arp4 Ser23 is mutated in human cancer in hBAF53a, as well as other P2 loop residues (Figure 29b). In order to examine the significance of P2 loop cancer mutations, the corresponding Arp4 mutations, S23F (COSMIC ID: COSM3590426) and T25S (COSMIC ID: COSM1632997), were characterized *in vitro* in an Arp4 yeast plasmid shuffling assay.

Arp4 T25S mutant cells did not show any phenotype in growth, indicating that Arp4 stability and function were not affected by the mutation. Moreover, examination of the structure does not indicate that the T25S substitution would sterically restrain ATP binding (Figure 29c). In contrast, Arp4 S23F cells showed even without stress conditions a phenotype in growth and were non-viable under conditions with high genotoxic stress (100 mM HU) (Figure 29d). Matching these observations, the structural analysis reveals that the S23F substitution would lead to a direct clash of the phenyl group and the gamma phosphate of ATP in the structure and consequently block ATP binding (Figure 29c).

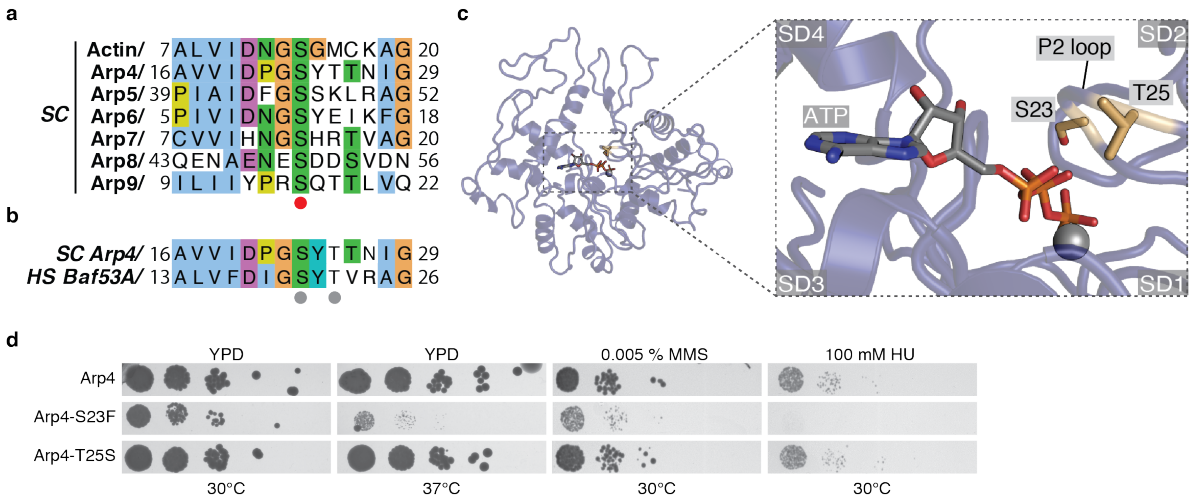

Figure 29 Arp4 nucleotide binding mutations.

a, Sequence alignment of yeast actin and nuclear Arps4-9. Ser14 from the phosphate-binding loop P2 in actin is highly conserved between the different ARPs (indicated by the red dot below). **b**, Sequence alignment of the P2 loop region in yeast Arp4 and the human homolog hBAF53a. Grey dots below highlight residues that are mutated in human cancer and were characterized in yeast growth assays shown in panel d. (*SC*, *Saccharomyces cerevisiae*; *HS*, *Homo sapiens*). **c**, Structure of Arp4 shown as cartoon (PDB 3QB0). Boxed 'zoom' image shows the Arp4 nucleotide-binding pocket with the P2 loop residues homologous to the cancer mutations in panel b displayed as sticks. **d**. Yeast spotting assay to assess cell viability of the Arp4 mutants in comparison to WT Arp4. Overnight culture of yeast cells was serially diluted (1:10), spotted on YPD media and grown for 48 h at the indicated temperature and if indicated supplemented with genotoxic agents. HU, hydroxyurea; MMS, methyl methanesulfonate.

Taken together, the yeast Arp4 growth assays further highlights the critical role of ATP binding in Arp4 stability not only *in vitro* but also *in vivo*. In addition, the experiments showed that a single point mutation in hBAF53a, that was identified in human cancer (COSMIC ID: COSM3590426), directly perturbs Arp4 stability and function, leading to a strong phenotype in yeast cell growth.

3.7.2 Arp4 interface mutations

The structural work on Arp4 reveals two binding interfaces, the lateral side of Arp4 that binds N-actin via mainly electrostatic interactions and the barbed end of Arp4 that binds α1' through hydrophobic interactions. Remarkably, three hydrophobic Arp4 residues at the barbed end that bind to Ino80^{HSA} α1' were mutated previously in the yeast growth assays, without structural knowledge on HSA domain binding (Gerhold, 2012) (Figure 30). In yeast cells these Arp4 mutations (L462E/F465Y/L468E) have a strong negative effect on yeast growth and the cells are hypersensitive to genotoxic stress (Gerhold, 2012), showing

the significance of the hydrophobic interface for the correct assembly of Arp4 into the large chromatin-associated complexes. In order to characterize the Arp4 interface to N-actin, a charge-reversal mutant of three main interacting residues was designed (E59K/R66E/K210E). Growth of the interface mutant cells was similar to WT Arp4 under normal conditions, however slightly impaired upon high genotoxic stress (100 mM HU).

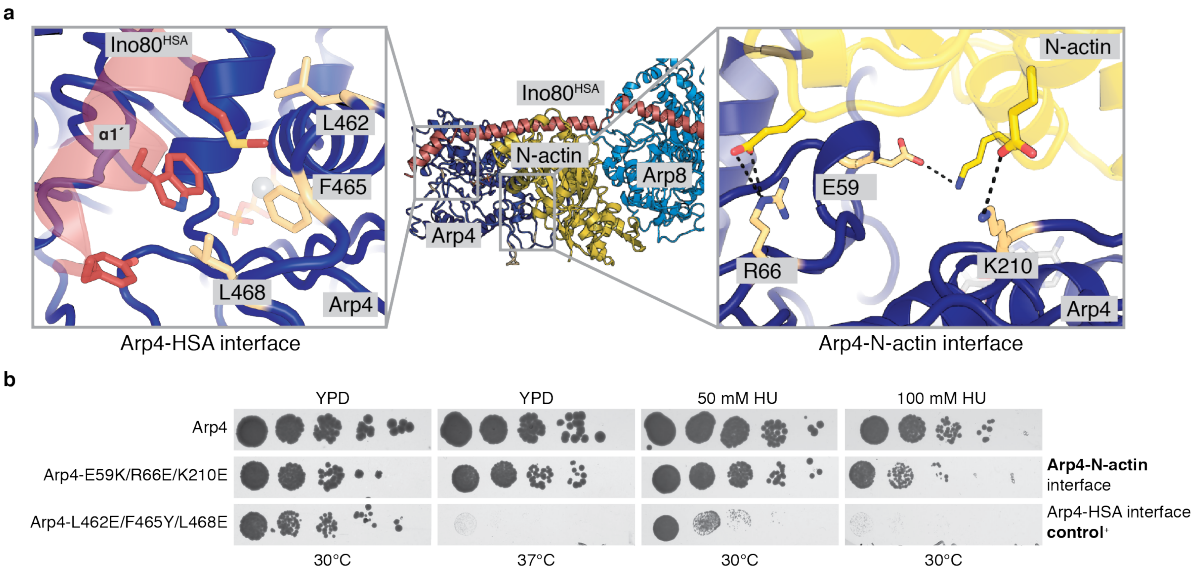

Figure 30 Arp4 interface mutants.

a, Structure of the Arp8 module shown as cartoon. Boxed 'zoom' images show the Arp4 Ino80^{HSA} interface (left box) and the Arp4 N-actin interface (right box). **b**, Yeast spotting assay to assess cell viability of Arp4 interface mutants in comparison to WT Arp4. $^{+}$The Arp4-L462E/F465Y/L468E mutant identified previously (Gerhold, 2012) and was used as a control. Overnight culture of yeast cells was serially diluted (1:10), spotted on YPD media and grown for 48 h at the indicated temperature and if indicated supplemented with genotoxic agents.

Overall, yeast growth assays of the previously identified Arp4-HSA domain interface mutant and the structure based Arp4-N-actin interface mutant confirmed the relevance and importance of the two Arp4 interfaces observed in the Arp8 module and the Swr1^{HSA}-Arp4-N-actin structures. Moreover, the HSA domain interface appeared to be more critical for correct Arp4 function than the N-actin interface.

3.8 Purification and crystallization of the *Chaetomium thermophilum* Arp5

INO80 contains in addition to Arp4, N-actin and Arp8, a fourth actin-fold protein, Arp5. Arp5 is not part of the Arp8 module but was shown to form together with Ies6 a distinct complex, termed the Arp5-module, that directly interacts with the Rvb1/2 heterohexamer

and is part of the INO80^{Core} module (Tosi et al., 2013). Biochemical experiments showed that Arp5 is required to couple INO80 ATP hydrolysis to nucleosome remodeling and binds to DNA (Shen et al., 2003; Tosi et al., 2013). By the time this work started no structural knowledge on Arp5 that could explain its critical function in INO80 remodeling was available. In order to fill this gap, the purification and crystallization of Arp5 was attempted.

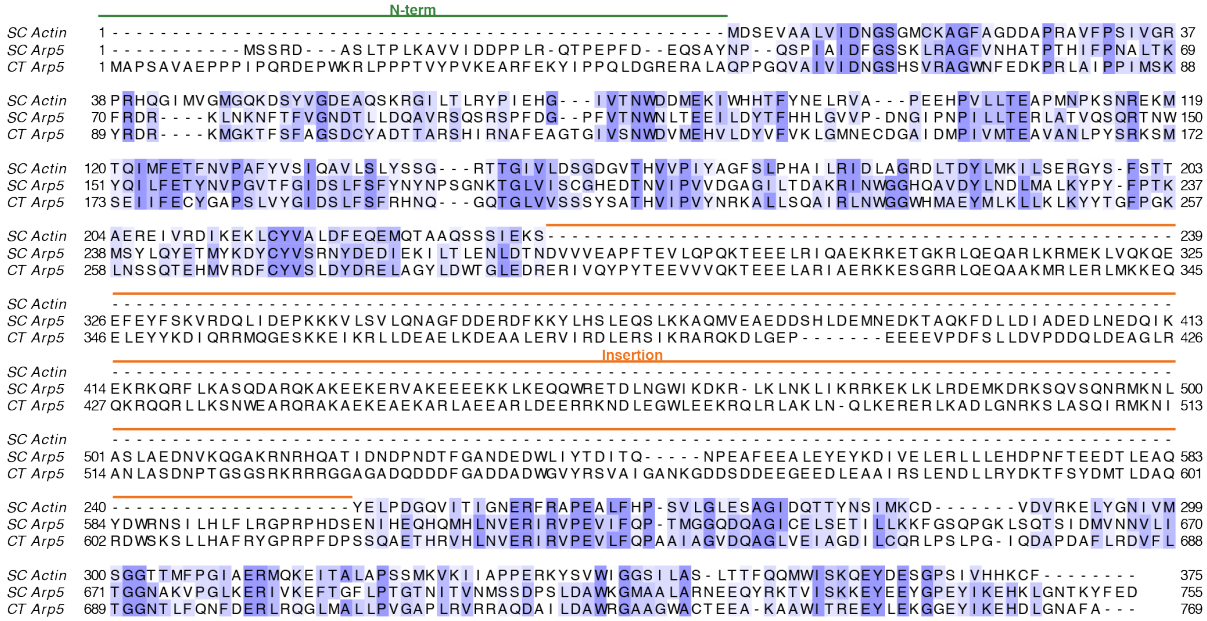

Figure 31 Sequence alignment of yeast actin, Arp5 and *Chaetomium thermophilum* Arp5.

Sequence alignment showing Arp5 regions that are not part of the actin-fold; the N-terminal region (N-term) and the insertion region, are highlighted (*SC*, *Saccharomyces cerevisiae*; *CT*, *Chaetomium thermophilum*).

Proteins from *Chaetomium thermophilum* (*CT*), a thermophilic fungus, emerged to be promising targets in structural biology, due to their increased thermostability. The purification of WT *CT*Arp5 was previously established by Dr. Kristina Lakomek. Arp5 harbors, in addition to the actin-fold, an approximately 50 residue long N-terminal extension and a 320 residue long insertion region (Figure 31). To limit flexibility in the molecule for crystallization, Arp5 variants with a deletion of the insertion element (Arp5ΔI; deletion of residues 311-611) or deletion of both the N-terminal and the insertion element (Arp5ΔIN; deletion of residues 1-51 and 311-611) were designed.

WT Arp5, Arp5ΔI and Arp5ΔIN were heterologously expressed in insect cells. To obtain pure protein for crystallization, proteins were purified from the lysate via a N-terminal Twin-Strep-Tag in a first affinity purification step followed by anion-exchange

chromatography with Q Sepharose resin and size-exclusion chromatography with Superdex 200 resin. Expression and purification of all three Arp5 constructs was successful and produced soluble, pure and monodisperse protein samples (Figure 32). 1 L of insect cell expression yielded around 1 mg of sample for each of the three constructs. Samples were subjected to initial high throughput crystallization screening, but this did not result in crystal growth for any of the Arp5 constructs.

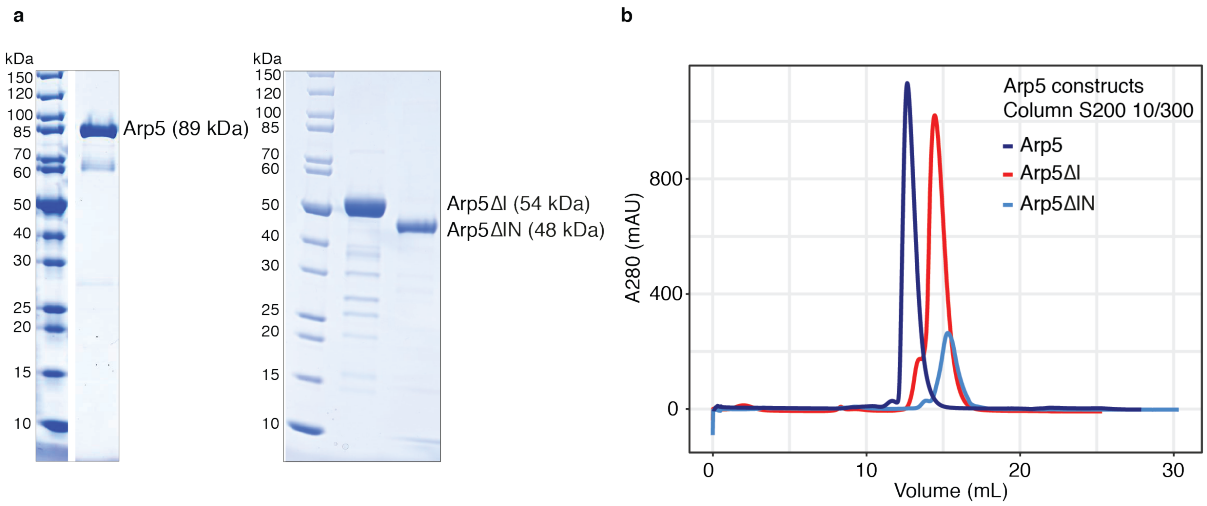

Figure 32 Purification of different Arp5 constructs.

a, SDS-PAGE and Coomassie brilliant blue staining of the purified full length Arp5, Arp5ΔI and Arp5ΔIN. **b**, Size-exclusion chromatography elution profiles of the different Arp5 constructs from panel a on a S200 10/300 column.

3.9 Purification of the human Arp8 module

In order to also characterize N-actin and the ARPs in a human context, the expression and purification of the human Arp8 module was performed. Human Arp4 (hBAF53a; 47 kDa), β-actin (41 kDa), Arp8 (70 kDa) and Ino80^{HSA} (residues 267-484; 27 kDa) carrying a C-terminal Strep-Tag II were combined on a single virus and co-expressed in insect cells. The human complex was purified from the lysate by affinity purification step on Strep-Tactin resin, followed by anion-exchange chromatography with Q Sepharose resin and size-exclusion chromatography with Superdex 200 resin. Purification gave a pure and monodisperse complex, which was stable during size-exclusion chromatography. However, 1 L of insect cell expression yielded only around 0.1 mg of sample, which was not sufficient for the further characterization of the human Arp8 module.

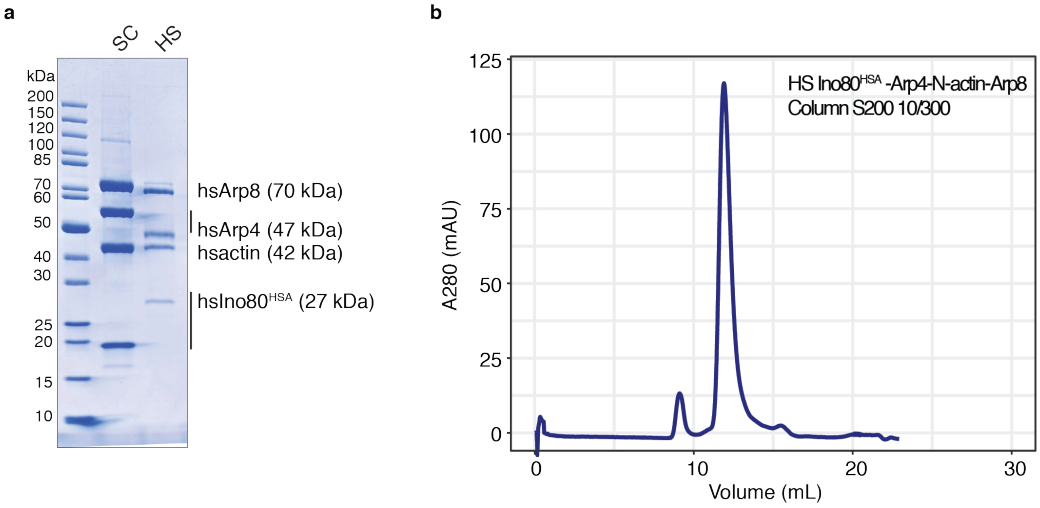

Figure 33 Purification of the human Arp8 module.

a, SDS-PAGE and Coomassie brilliant blue staining of the purified yeast and human Arp8 module, for comparison. **b**, Size-exclusion chromatography elution profile of the human Arp8 module complex, comprising Ino80^{HSA}, Arp4(hBAF53a), N-actin and Arp8, on a S200 10/300 column.

4 Discussion

4.1 Structural model of the INO80^{Core}-Arp8 module-nucleosome complex

N-actin and ARPs are critical components of the large chromatin remodeling complexes (Clapier et al., 2017; Olave et al., 2002; Shen et al., 2003; Szerlong et al., 2008). Although nuclear ARPs were structurally and functionally characterized extensively as individual proteins (Clapier et al., 2017; Fenn et al., 2011a; Gerhold et al., 2012; Saravanan et al., 2012; Szerlong et al., 2008), the function of ARPs and N-actin in chromatin remodelers remained elusive. To uncover how ARPs or N-actin contribute to the conversion of DNA translocation to nucleosome remodeling, insights into the entire structural framework of the remodelers are required.

Of all remodelers, the INO80 complex is particularly intriguing to study N-actin and ARPs as it comprises four actin-fold proteins (Shen et al., 2000; Shen et al., 2003; Szerlong et al., 2008). INO80 is a highly processive chromatin remodeler (Schwarz et al., 2018; Zhou et al., 2018) that can slide (Shen et al., 2003), space (Udugama et al., 2011) and edit (Papamichos-Chronakis et al., 2011) nucleosomes and is involved in diverse cellular processes such as transcription regulation, DNA repair and replication fork progression (Gerhold et al., 2015; Tosi et al., 2013). The Arp8 module and the INO80^{Core} module build together the conserved and functional critical part of the INO80 complex (Chen et al., 2013; Tosi et al., 2013). Recent cryoEM structures on the INO80^{Core}-NCP complex provided together with biochemical and single-molecule studies a first model for nucleosome remodeling by a large multi-subunit chromatin remodeler (Ayala et al., 2018; Brahma et al., 2017; Eustermann et al., 2018; Zhou et al., 2018). INO80 appears to function as a macromolecular ratchet, in which Arp5 acts as a counter-grip to couple DNA translocation by the Ino80 Snf2-type ATPase to nucleosome remodeling (Eustermann et al., 2018). Despite advances in understanding the function of the INO80^{Core} module, the role of the second functionally critical INO80 module, the Arp8 module, remained elusive, mainly due to a lack of structural and functional information. The structure of the Arp8 module and its biochemical characterization now provide important insights into this critical INO80 module.

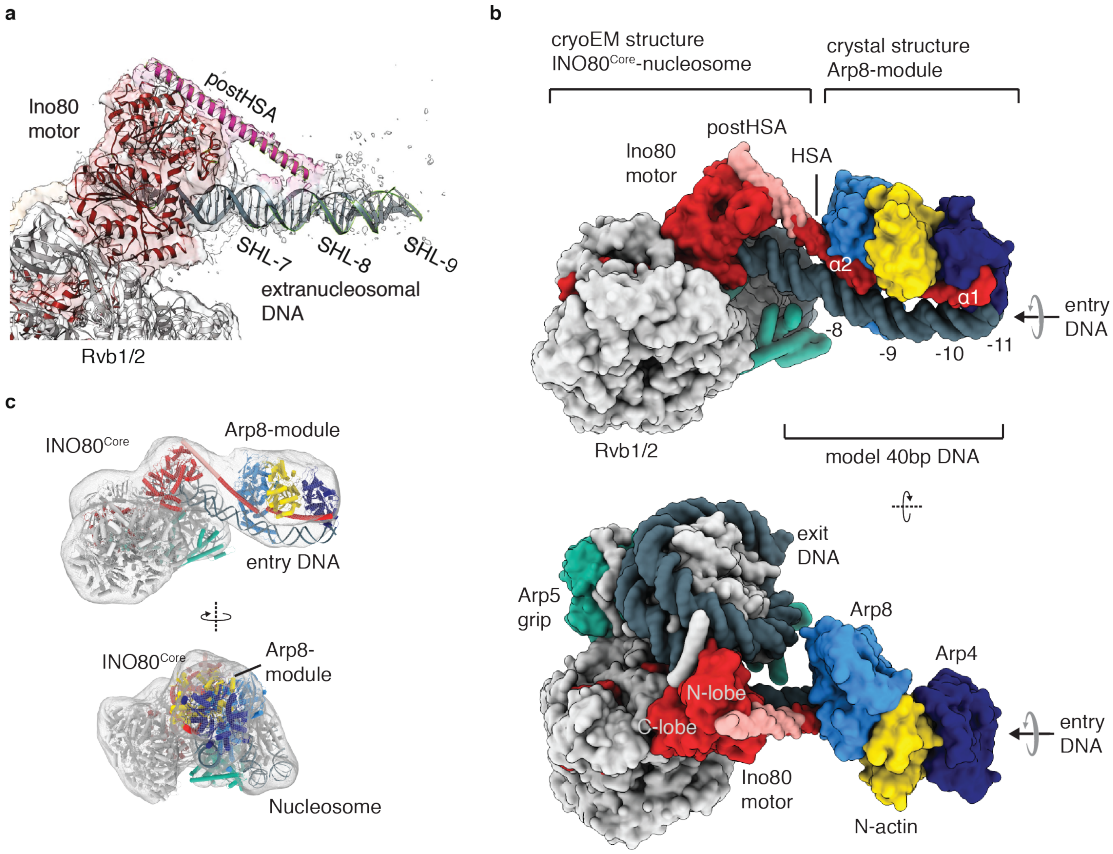

Figure 34 Structural model of the INO80^{Core}-Arp8 module-nucleosome complex.

a, Structure and cryoEM density map of the INO80^{Core}-NCP complex. Displayed is the region around the Ino80 motor domain showing cryoEM density for the Ino80$^{post\text{-}HSA}$. Adapted from (Eustermann et al., 2018). **b**, Structural model of the INO80^{Core}-Arp8 module-NCP complex created by combining the 4.3 Å INO80^{Core}-NCP cryoEM structure (Eustermann et al., 2018) and the 4 Å Arp8 module crystal structure. **c**, Low resolution cryoEM density map of the INO80^{Core}-Arp8 module-nucleosome complex (Eustermann et al., 2018). The model shown in panel b fitted into the map. Panel b and c are adapted from (Knoll et al., 2018).

Moreover, the Arp8 module crystal structure and the INO80^{Core}-NCP cryoEM structure (Eustermann et al., 2018) can be combined to build a structural model of the entire conserved part of the INO80 complex bound the nucleosome. The post-HSA domain, a highly conserved region in remodelers of the SWI/SNF and the INO80 families (Szerlong et al., 2008), forms a continuous helix C-terminal of the HSA domain (Figure 6a and Figure 36). Structures of the SWI/SNF remodeler motor domain revealed, that the post-HSA domain binds directly to the N-lobe of the Snf2-type ATPase domain (Liu et al., 2017; Xia et al., 2016). Moreover, the Ino80 post-HSA domain (Ino80$^{post\text{-}HSA}$) is visible in the 4.3 Å INO80^{Core}-NCP cryoEM structure (Eustermann et al., 2018) (Figure 34a). Consequently, by simply extending the helical Ino80^{HSA} by 35 residues the two structures can be combined to a model for the entire INO80^{Core}-Arp8 module-nucleosome complex (Figure 34b).

Importantly the resulting structural model fits the previously published low resolution cryoEM density map of the *Chaetomium thermophilum* INO80^{Core}-Arp8 module complex bound to the nucleosome (Eustermann et al., 2018) (Figure 34c). Moreover, density in the low resolution cryoEM map is also in agreement with the modeled 40 bp DNA of extranucleosomal DNA (Figure 34c). This is also consistent with nucleosome competition EMSA experiments (Figure 25), which demonstrated extranucleosomal DNA binding of the Arp8 module. Notably, the Arp8 module is oriented to contact the extranucleosomal DNA via the conserved positively-charged side of Ino80^{HSA} that was identified as a DNA binding element (Figure 15 and Figure 25). In addition, the model agrees with genome-wide *in vivo* data that localized the Arp8 module at promoter sites (Yen et al., 2013), and with *in vitro* experiments where the Arp8 module was crosslinked to SHL-10 and SHL-11 of extranucleosomal DNA (Brahma et al., 2018). In summary, the combination of the two structures resulted in a model that shows for the first time the entire structural framework of a remodeler complex that includes all actin-fold proteins and can remodel nucleosomes.

In addition to the extended extranucleosomal DNA binding conformation of the Arp8 module described above (Figure 34), alternative conformations of INO80 during the nucleosome remodeling cycle and in the nucleosome-free state are likely. Indeed, EM studies of entire yeast INO80 complex indicated compact and more extended conformations of the remodeler (Tosi et al., 2013; Watanabe et al., 2015). Moreover, a recent cryoEM study of the human INO80^{Core}-Arp8 module complex revealed a 'closed conformation' of the Arp8 module in the nucleosome-free state, although the resolution of the cryoEM map was limited to 10 Å – 15 Å (Aramayo et al., 2018). In this conformation the Arp8 module accommodates the place of the NCP in the INO80^{Core}–NCP structure with Arp4 turned towards Arp5. Therefore, it is tempting to speculate about a possible lateral actin-fold interaction between Arp4 and Arp5 in the inactive compact state of INO80, however there is so far no evidence for such a contact. Additional studies will be necessary to reveal all the different conformations of INO80 and the Arp8 module during a complete nucleosome remodeling cycle.

4.2 Arp8 module DNA binding drives INO80 nucleosome remodeling

In parallel to this work the function of extranucleosomal DNA binding by the Arp8 module in INO80 nucleosome remodeling was examined by mutational analysis in context of the entire INO80 complex (work done by Vanessa Niebauer) (Knoll et al., 2018). A recombinant expression system allowed the generation of the 15-subunit INO80 complex containing Ino80^{HSA} mutations that do not bind extranucleosomal DNA; these mutations are similar to the Ino80^{HSA} mutations described for the Arp8 module in section 3.5.

Mutating the conserved lysine and arginine residues on either of the helical Ino80^{HSA} segments (HSAα1 and HSAα2) or on both (HSAα1/α2) resulted in three INO80 mutants. Interestingly, all INO80 HSA domain mutants still bind nucleosomes comparably to WT INO80. This is in agreement with the observation in the INO80^{Core}–NCP cryoEM structure, that the main interactions to the NCP are made by the INO80^{Core} module only (Eustermann et al., 2018). In contrast, mononucleosome sliding assays reveal drastic effects of the Ino80^{HSA} mutations on INO80 nucleosome remodeling. While the HSAα1 and HSAα2 mutants show residual nucleosome sliding activity, the HSAα1/α2 mutant is completely deficient in nucleosome remodeling. Moreover, the dsDNA stimulated INO80 ATPase activity of all three Ino80^{HSA} mutants is clearly decreased, whereas the 0N80 nucleosome stimulated ATPase activity is comparable to WT INO80. Similar effects have been observed before for the INO80 ΔArp8 mutant, which lacks the entire Arp8 module (Shen et al., 2003; Tosi et al., 2013).

As the Arp8 module binds the linker DNA region of nucleosomes, a possible function of Ino80^{HSA} DNA binding in promoter recognition during +1 nucleosome positioning on yeast genes was examined with an *in vitro* 'genome wide nucleosome positioning assay' (Krietenstein et al., 2016). Interestingly, although nucleosome sliding of HSAα1 and HSAα2 INO80 mutants was clearly decreased in a mononucleosome context, nucleosome positioning on genomic DNA was comparable to WT INO80, indicating that mobilization of nucleosomes on genomic DNA might be easier than on the strong positioning '601' sequence (Lowary and Widom, 1998), that was used to assemble the mononucleosomes. This idea is further supported by the observation that the HSAα1 and HSAα2 INO80 mutants also show also drastically reduced nucleosome sliding activity compared to WT INO80 in a multinucleosome context where 25 nucleosomes are positioned on an array of '601' sequences separated by 50 bp linker DNA. Mutation of both helical Ino80^{HSA} segments (HSAα1/α2) abolishes mobilization of nucleosomes on all tested substrates and also +1 nucleosome positioning on yeast genes.

Overall, the binding of the Arp8 module to the extranucleosomal DNA region is a critical part of the chemomechanical INO80 nucleosome remodeling cycle. Although Arp8 module binding to the linker DNA hints towards a role in promoter sequence recognition during +1 nucleosome positioning, the mutational analysis of the Ino80^{HSA} domain instead indicates an important function in the coupling of Ino80 ATP-dependent DNA translocation to nucleosome remodeling.

Additional factors might be involved in promoter recognition such as the species-specific N-terminal submodule of INO80 (such as the Nhp10 module in yeast) and the non-conserved subunits of the Arp8 module, for example hYY1 in human INO80 (Cai et al.,

2007). Furthermore, the unconserved N-terminal region of Arp8, which was shortened in the Arp8 module used for crystallization might be an element involved in +1 nucleosome positioning. Consistent with this idea, DNA crosslinking of the yeast INO80 complex revealed that this region of Arp8 binds directly to linker DNA (Brahma et al., 2018). Moreover, truncation of the Arp8 N-terminus renders yeast cells hypersensitive to genotoxic stress, similar to Δ*ARP8* cells (Brahma et al., 2018). Further experiments are required to reveal which part of the INO80 complex is required for promoter recognition and +1 nucleosome positioning.

4.3 Model for INO80 nucleosome remodeling including the Arp8 module

Mutational analysis of the Ino80^{HSA} domain demonstrated that extranucleosomal DNA binding by the Arp8 module is critical for INO80 nucleosome remodeling. These new insights together with the structural model of the INO80^{Core}-Arp8 module-nucleosome complex suggest a mechanism that directly links Arp8 module extranucleosomal DNA sensing to INO80 nucleosome remodeling.

The molecular model for INO80 nucleosome remodeling can now be completed by including the functional critical Arp8 module (Figure 35). In the macromolecular ratchet model INO80 binds the NCP via Arp5-Ies6 and the Ino80^{ATPase} that contact the nucleosomal DNA at SHL-2 and SHL-6 respectively. DNA translocation facilitated by Ino80^{ATPase} at the DNA entry site pumps the DNA in 1-2 bp steps towards Arp5-Ies6. Continuous DNA pumping would lead to a bulge formation and exposure of the H2A-H2B dimer proximal to the motor domain, as Arp5-Ies6 functions as 'counter grip' that prevents further propagation of the DNA around the histone octamer (Eustermann et al., 2018). In fact, formation of such a bulge between SHL-2 and SHL-6 was detected for INO80 remodeling (Brahma et al., 2017). After around 10-15 bp of DNA translocation the tension is probably sufficient that the bulge slips over the Arp5-Ies6 'counter grip' resulting in a large translocation step size for INO80 driven nucleosome movement, as observed by DNA crosslinking and smFRET experiments (Brahma et al., 2017; Zhou et al., 2018). Moreover, INO80 nucleosome movement is strictly dependent on the length of the flanking DNA region and more than 40 bp of DNA are required for effective nucleosome translocation (Udugama et al., 2011; Zhou et al., 2018). Indeed, the length requirement of 40 bp matches exactly the footprint of the Arp8 module in the structural model of the INO80^{Core}-Arp8 module-nucleosome complex. Previously INO80 was proposed to directly couple the sensing of linker DNA to nucleosome movement, and unless more than 40 bp of linker DNA is sensed, the already translocated DNA might collapse backwards (Zhou et al., 2018). This situation is similar to the INO80 HSA domain mutants, in which the disruption of

linker DNA sensing leads to uncoupling of the Ino80^{ATPase} activity and nucleosome sliding. Binding of the Arp8 module to the linker DNA appears to prevent 'back-slippage' of the translocated DNA and thereby promotes propagation of the DNA bulge between Ino80^{ATPase} and Arp5-Ies6 towards the dyad and around the histone octamer (Figure 35).

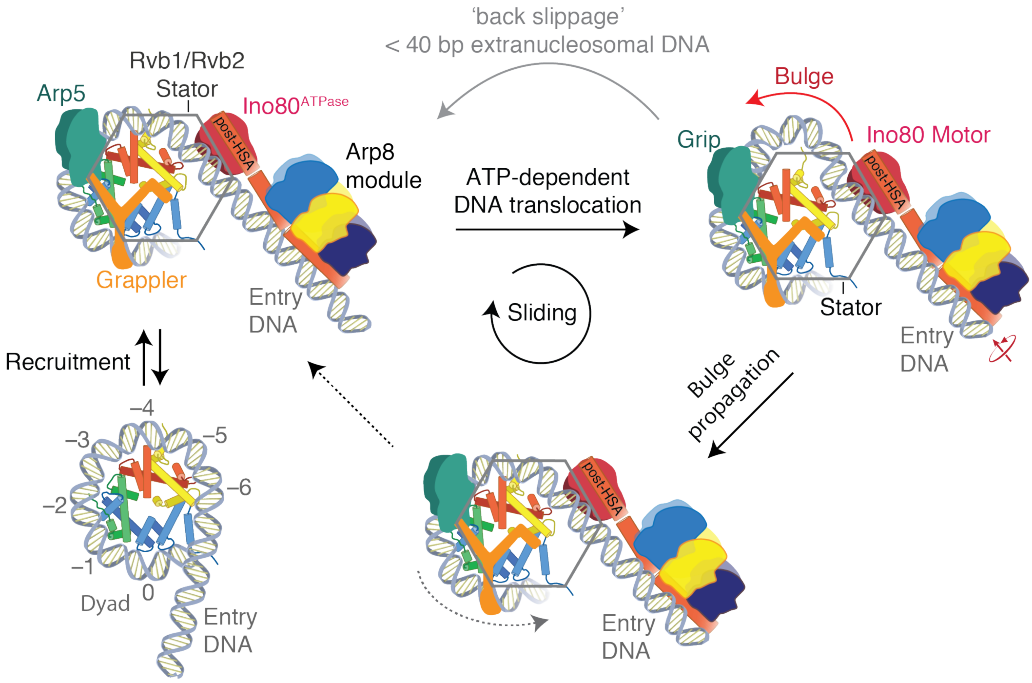

Figure 35 Model for INO80 nucleosome remodeling including the Arp8 module.

Model for INO80 nucleosome sliding including the Arp8 module, based on the 'macromolecular ratchet model' for INO80 nucleosome remodeling shown in Figure 7 (Eustermann et al., 2018). The Arp8 module functions as an extranucleosomal DNA sensor that couples Ino80 DNA translocation to nucleosome remodeling by promoting DNA bulge propagation around the histone octamer. Adapted and modified from (Eustermann et al., 2018).

Accordingly, the Arp8 module functions as a linker DNA sensor that drives INO80 nucleosome remodeling unless less than 40 bp of extranucleosomal DNA are available. Future studies are needed to elucidate how extranucleosomal DNA binding by the Arp8 module exactly contributes to the mechanochemical nucleosome remodeling cycle of INO80.

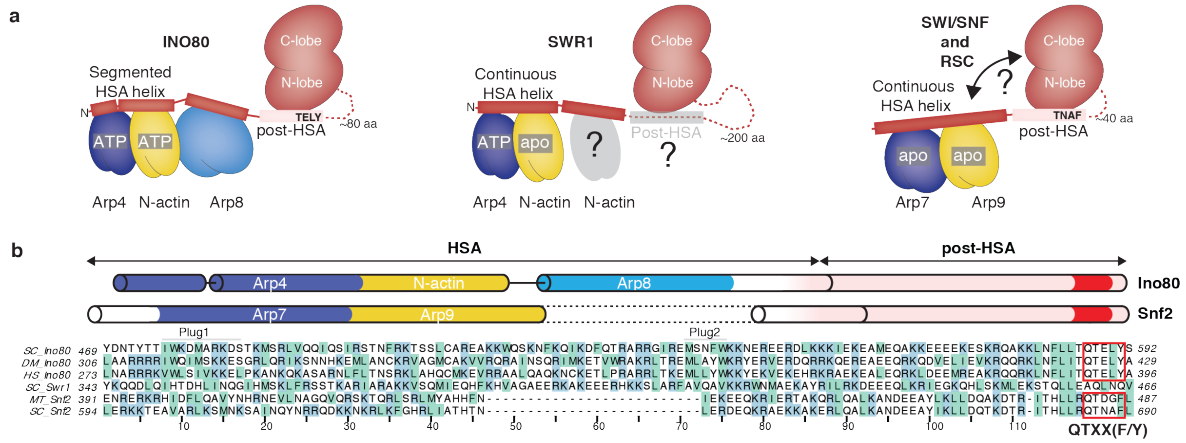

Figure 36 Conserved architecture of 'Arp modules' in INO80 and SWI/SNF family chromatin remodelers.

a, Schematic representation of the organization of 'Arp modules' in INO80, SWR1, SWI/SNF and RSC with respect to the Snf2-type motor domain. The scheme is based on a structure-guided sequence alignment shown in panel b and the crystal structures of Arp4–N-actin–Swr1^{HSA} (PDB 5I9E), Arp7–Arp9–Snf2^{HSA} (PDB 4I6M), the Arp8 module and the Snf2 motor domain in the resting state (PDB 5HZR). Conformations of the respective HSA domains (red) are illustrated as continuous or segmented helices. The post-HSA of Ino80 and Snf2 (pink) interacts with N-lobe of the Snf2-type ATPase (red) and is connected by a linker region with the Snf2-type motor domain (dotted line; aa, amino acids). The nucleotide state of the actin-fold proteins is indicated according to the respective crystal structure. Notably, biochemical analysis of the SWR1 remodeler indicated that the Swr1^{HSA} is bound by Arp4 and two N-actin molecules (Lin et al., 2017). **b**, Top of the panel: Illustration of the HSA and post-HSA domains of Ino80 and Snf2. Binding sites of the actin-fold proteins are highlighted. Bottom of the panel: Sequence alignment of the HSA and post-HSA domains from Ino80, Swr1 and Snf2 from different organisms (*SC*, *Saccharomyces cerevisiae*; *DM*, *Drosophila melanogaster*; HS *Homo sapiens*; MT, *Myceliophthora thermophila*). The alignment reveals that the Ino80$^{post\text{-}HSA}$ (Q)TELY motif (Shen et al., 2000) is related to the Snf2$^{post\text{-}HSA}$ QTXX(F/Y) motif. Adapted from (Knoll et al., 2018).

Similar to the results for the INO80 Arp8 module, studies on related remodelers of the SWI/SNF class indicate an allosteric regulation of the Snf2-type ATPase motor by ARPs and the HSA domain. Interactions between the highly conserved post-HSA domain and the N-lobe of the Snf2-type ATPase appear to be a critical element for the regulation of the ATPase motor activity (Clapier et al., 2016; Liu et al., 2017; Turegun et al., 2018; Xia et al., 2016). Structures of the Snf2 ATPase domain and the INO80^{Core} together with biochemical experiments revealed that the post-HSA domain directly interacts with a conserved structural element, termed protrusion-1, at the N-lobe of the Snf2-type motor domains in the INO80, SWI/SNF and RSC remodelers (Clapier et al., 2016; Eustermann et al., 2018; Liu et al., 2017; Turegun et al., 2018). Moreover, sequence alignments show that the conserved Ino80$^{post\text{-}HSA}$ (Q)TELY motif (Shen et al., 2000) is also present as QTXX(F/Y) motif in the post-HSA domains of Sth1 and Snf2, the motor subunits of the RSC and

SWI/SNF remodelers, respectively (Figure 36), implying a conserved role for the post-HSA protrusion-1 interaction. Mutational analysis of Sth1 demonstrated that interactions of the post-HSA domain and protrusion-1 directly regulate the ATPase activity and the DNA translocation rate of the motor domain (Clapier et al., 2016). Additionally, genetic studies directly linked the function of ARPs to the post-HSA domain and protrusion-1. In yeast Sth1 mutations in the post-HSA domain or protrusion-1 region that alter the ATPase motor activity rescue the lethal double-deletion of *ARP7* and *ARP9* (Clapier et al., 2016). Biochemical analysis further confirmed that binding of ARPs to the Sth1 HSA domain weakens the interaction of the post-HSA domain and protrusion-1 (Turegun et al., 2018). These results suggest a conserved intramolecular interplay of HSA, post-HSA and protrusion-1 in allosterically regulating the Snf2-type motor domain, which can be modulated by the ARPs and N-actin.

Overall, the sensing of linker DNA is a critical feature of chromatin remodelers that is required to establish ordered nucleosome patterns, such as nucleosomal arrays around genes. This study reveals that the Arp8 module functions as an extranucleosomal DNA sensor that drives INO80 nucleosome remodeling. The binding of linker DNA by the Arp8 module might allosterically regulate the Ino80 motor activity, via the post-HSA protrusion-1 interaction. Further studies are needed to reveal the exact interplay of different structural motifs within the Snf2-type ATPase motor domain that regulates the DNA translocation rate.

4.4 Is there a conserved task of ‘Arp modules’ in chromatin remodelers?

The organization of ARPs and N-actin by the HSA domain appears to be similar between INO80 and SWI/SNF chromatin remodelers (Figure 36). Structures and sequence alignments suggest a conserved arrangement of the ‘Arp module’ and Snf2-type motor domain in the different complexes. In addition, current insights (described in section 4.3) point towards a conserved mechanism for how ‘Arp modules’ allosterically regulate the Snf2-type ATPase motor activity by modulating the post-HSA domain and protrusion-1 interaction.

The mechanism of the ‘Arp7-Arp9 module’ dependent regulation of the Snf2-type motor was characterized widely in SWI/SNF and RSC remodelers (Clapier et al., 2016; Turegun et al., 2018), but it is not yet known which, if any, substrate is sensed by the ‘Arp7-Arp9 module’. Similar to the Arp8 module, the ‘Arp7-Arp9 module’ of the SWI/SNF remodeler preferentially binds to free DNA and nucleosomes with DNA overhang, rather than to nucleosomes without DNA overhang (Schubert et al., 2013). However, sensing of

extranucleosomal entry DNA by the 'Arp modules' of the SWR1, SWI/SNF and RSC remodelers appears to be unlikely, as nucleosome binding compared to INO80 is different. Whereas the Ino80 motor domain contacts the NCP at SHL-6, the SWR1, SWI/SNF and RSC remodelers bind the NCP with the Snf2-type motor at SHL-2 (Clapier et al., 2017), opposite to the nucleosomal entry site in spatial distance from the extranucleosomal linker DNA region where the INO80 Arp8 module binds.

Apart from INO80, there are no structural models of remodelers including both the ATPase domain and 'Arp module'. CryoEM studies on the different remodeler complexes have so far failed to resolve both 'Arp module' and Snf2-type motor domain at high resolution (Ayala et al., 2018; Eustermann et al., 2018; Willhoft et al., 2018). The structure of the $Snf2^{ATPase}$-NCP complex (Liu et al., 2017) alone reveals an orientation of $Snf2^{ATPase}$ motor and the post-HSA domain, which would be incompatible with nucleosomal DNA or extranucleosomal DNA binding by the SWI/SNF 'Arp module'. Interestingly, comparison of the $Snf2^{ATPase}$-NCP complex cryoEM structure and the crystal structure of the $Snf2^{ATPase}$ in the resting state reveals movement of the post-HSA domain upon nucleosome binding (Liu et al., 2017; Xia et al., 2016). Other conformations of the post-HSA domain are possible, but the spatial distance between $Snf2^{ATPase}$ and nucleosomal DNA entry site in the $Snf2^{ATPase}$-NCP complex cryoEM structure (Liu et al., 2017) is too large for a 'Arp module' linker DNA binding mode similar to INO80.

In summary, for chromatin remodelers that bind nucleosomal DNA with the motor domain at SHL-2, a direct interaction of the particular 'Arp module' with extranucleosomal entry DNA at the same nucleosome appears to be unlikely without larger conformational changes. However, also the sensing of other substrates, such as histones or neighbouring nucleosomal DNA, needs to be considered. Future studies are required to reveal a possible 'substrate' for 'Arp module' dependent regulation of the Snf2-type motor in the SWI/SNF, RSC and SWR1 remodelers.

4.5 Actin-fold proteins: Regulatory elements in chromatin remodelers?

The actin-fold is a conserved structural-motif with a prominent central nucleotide-binding cleft (Kabsch and Holmes, 1995). Several crystal structures of actin indicate a conformational change of the protein upon ATP hydrolysis and phosphate release (Kudryashov and Reisler, 2013). Moreover, cryoEM studies of actin filaments observed small but important conformational changes of actin during the transition from ATP F-actin to ADP F-actin, involving a slight rotation of the two actin lobes with regard to each other (Merino et al., 2018).

In chromatin remodelers nuclear ARPs and N-actin are functionally critical components (Clapier et al., 2017; Olave et al., 2002). The structural model of the INO80^{Core}-Arp8 module-nucleosome complex, crystal structures of the Arp8 module, the Swr1^{HSA}-Arp4-N-actin (Cao et al., 2016) and the Snf2^{HSA}-Arp7-Arp9 complexes (Schubert et al., 2013) and cryoEM structures of INO80^{Core} (Ayala et al., 2018; Eustermann et al., 2018) and SWR1^{Core} (Willhoft et al., 2018) revealed that N-actin and ARPs are important building blocks of chromatin remodelers. In 'Arp modules' the actin-fold proteins organize the helical HSA domain. Moreover, Arp4, Arp5, Arp6 and Arp8 directly interact with nucleosomal or extranucleosomal DNA within the structural framework of a particular remodeler during nucleosome binding (Ayala et al., 2018; Brahma et al., 2018; Brahma et al., 2017; Eustermann et al., 2018; Willhoft et al., 2018). In addition to these static functions, early studies also proposed a role for actin-fold proteins as a conformational switch that might regulate the remodeler activity (Boyer and Peterson, 2000). In fact, nucleotide binding by N-actin and ARPs seems to have important roles. Arp4 ATP binding is critical for protein stability and folding (Fenn et al., 2011a). In yeast assays, mutations of the Arp4 ATP-binding cleft, that occur in human cancer in the human Arp4 homolog hBAF53a, resulted in cells that are hypersensitive to genotoxic stress (section 3.7.1). Mutations that prevent ATP-binding most probably lead to misfolding of Arp4 and hBAF53a and consequently to dysfunction of the entire remodeler. Notably, hBAF53a is a critical subunit of the BAF remodeler, an important tumor suppressor. In the RSC remodeler, ATP binding of Arp7 seems to allosterically regulate the DNA translocation efficiency (Turegun et al., 2018). Although Arp7 does not hydrolyse ATP, the binding of ATP by Arp7 seems to stabilize the 'Arp7-Arp9 module' in a conformation that might result in an altered translocation efficiency of the Sth1^{ATPase} motor (Turegun et al., 2018). Most of the so far characterized nuclear ARPs do not display significant ATPase activity (Cairns et al., 1998; Gerhold et al., 2012; Turegun et al., 2018). Only for N-actin in the human BAF complex and Arp8 alone has low ATP hydrolysis activity been detected (Gerhold et al., 2012; Zhao et al., 1998). While there is no evidence yet for an ATP-dependent regulatory role of Arp8, N-actin apparently allosterically regulates the activity of the BAF remodeler. The addition of the actin binding drug latrunculin, which captures actin in an ATP state, to the human BAF complex inhibits the chromatin-stimulated ATPase activity of the remodeler (Zhao et al., 1998). Furthermore, the addition of latrunculin to crystallization screens of the Arp8 module resulted in the formation of diffracting crystals, which did not grow under the same conditions without latrunculin, indicating that conformational flexibility of N-actin in the Arp8 module was indeed inhibited by latrunculin. However, the addition of the N-actin binding ligands, latrunculin and NactNB, that capture N-actin in an ATP state did not alter INO80 nucleosome binding and sliding activity (section 3.6). Accordingly, no evidence was

found for an ATP-dependent regulatory role of N-actin in INO80. Moreover, the comparison of the nucleotide-free N-actin structure in the Swr1^{HSA}-Arp4-N-actin complex (Cao et al., 2016) with the ATP-bound N-actin structure in either the Arp8 module or the NactNB-Arp4-N-actin complex reveals no major conformational changes (the structures align with a RMSD of less than 1 Å) that could trigger a allosteric regulation.

In filaments actin was also described as a 'molecular clock' with the nucleotide state function as a 'local age tag' which is specifically recognized by actin binding proteins (Merino et al., 2018). It is also conceivable that actin-binding proteins might directly interact with N-actin within the remodeler and thereby modulate the remodeler activity or recruit the remodeler to specific loci. Indeed, the AE-MS approach with NactNB, which specifically targets N-actin within yeast remodelers, also enriched proteins that are not known subunits of INO80, SWR1 and NuA4 but might be specific interaction partners of N-actin. In light of the recent findings that nuclear actin filaments relocalize DNA double strand breaks form heterochromatic regions to the nuclear periphery (Caridi et al., 2018; Schrank et al., 2018), an interaction of chromatin remodelers with actin filaments might also be possible. Intriguingly, the yeast homologue Las17 of the Wiskott–Aldrich syndrome protein (WASP), which was identified as coregulator of nuclear actin filament mediated double strand breaks DNA repair (Schrank et al., 2018), was one of the unknown proteins enriched by NactNB.

Overall, N-actin and ARPs are key components of chromatin remodelers and are important for the structural integrity of the complexes and substrate binding by the remodeler. Nucleotide binding is important for the stability of some of the ARPs. Moreover, the nucleotide state of N-actin or ARPs also seems to contribute to the allosteric regulation of remodelers in some cases. Future studies are required to reveal the role of nucleotide binding and hydrolysis by actin-fold proteins in chromatin remodeling more in depth. Moreover, studying actin-binding proteins as possible co-regulators of chromatin remodelers should be considered.

5 Materials and Methods

5.1 Materials

5.1.1 Chemicals and enzymes

Chemicals for buffers and other solutions were obtained from Merck (Darmstadt, Germany), Roth (Karlsruhe, Germany) and Sigma-Aldrich (St. Louis, USA), unless otherwise stated. Enzymes for molecular biology techniques were purchased from Thermo Fischer Scientific (Waltham, USA) and New England Biolabs (NEB, Frankfurt, Germany), unless otherwise stated. Kits for extraction of DNA fragments, plasmids and baculovirus genomes were purchased from Macherey-Nagel (Düren, Germany).

Chromatographic media and columns were acquired from GE Healthcare (München, Germany). Crystallization screens and crystallization tools were obtained from Jena Bioscience (Jena, Germany), Qiagen (Hilden, Germany) and Hampton Research (Aliso Viejo, USA).

5.1.2 Oligonucleotides

Synthetic oligonucleotides used for molecular cloning techniques and biochemical assays were purchased from Metabion (Planegg, Germany).

Table 4 Synthetic DNA oligonucleotides used for biochemical assays.

Name	Sequence (direction 5' - 3')	bp	5' - modification
YGL167_20_fwd	TTCTTAGCAAATATTCTTTC	20	fluoresceine
YGL167_20_rev	GAAAGAATATTTGCTAAGAA	20	-
YGL167_40_fwd	TTCGCCTCGTTTTGGCGATTTTCTTAGCAAATATTCTTTC	40	fluoresceine
YGL167_40_rev	GAAAGAATATTTGCTAAGAAAATCGCCAAAACGAGGCGAA	40	-

5.1.3 Bacterial strains

Table 5 *Escherichia coli* strains used for molecular cloning and protein expression.

Strain name	Genotype	Source
XL21 Blue	recA1 endA1 gyrA96 thi-1 hsdR17 supE44 relA1 lac [F´proAB lacIqZΔM15 Tn10 (Tetr)]	Agilent, Santa Clara USA
Rosetta (DE3)	F– ompT hsdSB (rB– mB-) gal dcm (DE3) pRARE2 (CamR)	Merck Millipore, Burlington USA
DH10MultiBac	Not specified	Imre Berger (Berger et al., 2004)

5.1.4 Yeast strains

Table 6 *Saccharomyces cerevisiae* strains used for pull-down experiments and *in vivo* studies on Arp4 and N-actin.

Strain name	Genotype	Source
Y21342	BY4743; Mat a/alpha ura3delta0/ura3delta0 leu2delta0/leu2delta0 his3delta1/his3delta1 met15delta0/ MET15 LYS2/lys2delta0 YJL081c::kanMX4/YJL081c	Euroscarf, Frankfurt Germany
INO80-FLAG2	MATa INO80-FLAG$_2$ his3delta200 leu2delta0 met15delta0 trp1delta63 ura3delta0	Shen et al., 2000

5.1.5 Insect cell lines

Table 7 Insect cell lines used for virus generation and recombinant protein expression.

Strain name	Origin	Source
High Five insect cells	Clonal isolated, derived from *Trichopulsia ni*	Invitrogen, Karlsruhe
Sf21 insect cells	Clonal isolate, derived from *Spodoptera frugiperda*	Invitrogen, Karlsruhe

5.1.6 Plasmids

Table 8 Plasmids used in this study.

Name	Application	Source
pHEN6	Nanobody expression in *E. coli*	(Conrath et al., 2001)
pFBDM	Protein expression in insect cells.	(Berger et al., 2004)
pACEBac1	Protein expression in insect cells	Geneva Biotech, Geneva Switzerland
pIDC	Protein expression in insect cells	Geneva Biotech, Geneva Switzerland
pIDK	Protein expression in insect cells	Geneva Biotech, Geneva Switzerland
pIDS	Protein expression in insect cells	Geneva Biotech, Geneva Switzerland
pRS315	Yeast plasmid shuffling assay	(Sikorski and Hieter, 1989)
pRS316	Yeast plasmid shuffling assay	(Sikorski and Hieter, 1989)

5.1.7 Media and additives

Escherichia coli strains were cultured in Lysogeny Broth (LB) media or on LB agar plates. LB media was prepared according to standard protocols (Sambrook, 2012) (Table 9). Media was supplemented with respective antibiotics (Table 10).

Table 9 Medium for *Escherichia coli* cultivation.

Name	Composition
LB media	10 g/L tryptone, 5 g/L yeast extract, 10 g/L NaCl, pH 7.5 Solid LB-agar-plates with1.5% (w/v) agar

Table 10 Supplements to *Escherichia coli* cultivation media.

Name	Typical concentration	Application
Plus X-gal	100 µg/mL	DH10MultiBac Blue-White screening
Ampicillin	100 µg/mL	Antibiotic
Chloramphenicol	50 µg/mL	Antibiotic
Gentamycin	10 µg/mL	Antibiotic
Kanamycin	50 µg/mL	Antibiotic
Tetracycline	12.5 µg/mL	Antibiotic

Saccharomyces cerevisiae strains were cultivated in yeast-extract-peptone-dextrose (YPD) media or synthetic defined (SD) selection media. YPD media was prepared according to standard protocols (Sambrook, 2012) and SD selection media according to the manufacturer's protocol (Formedium, Norfolk, UK)

Table 11 Media for *Saccharomyces cerevisiae* cultivation.

Name	Composition
YPD media	10 g/L yeast extract, 20 g/L peptone, 20 g/L glucose Solid YPD-agar-plates with 2% (w/v) agar
SD -Ura media	6.9 g/L "yeast nitrogen base without amino acids" (Formedium), 0.72 g/L "Complete supplement mixture" (CSM) drop-out: -Ura (Formedium), 20 g/L raffinose Solid SD-agar-plates with 2% (w/v) agar
SD -Leu media	6.9 g/L "yeast nitrogen base without amino acids" (Formedium), 0.72 g/L CSM drop-out: -Leu (Formedium), 20 g/L raffinose Solid SD-agar-plates with 2% (w/v) agar

Table 12 Supplements to *Saccharomyces cerevisiae* cultivation media.

Name	Final concentration	Application
5-fluorooretic acid	1% (w/v)	Selection against the URA3 marker gene on the pRS316 plasmid
Hydroxyurea	50 mM or 100 mM	Induction of genotoxic stress
Methyl methane sulfonate	0.005%	Induction of genotoxic stress

Express Five insect cell media (Invitrogen) was solubilized according to manufacturer's protocol and supplemented with gentamycin (10 µg/mL) and glutamine (18 mM), before use for High Five insect cell cultivation. Sf-900 III SFM liquid media (Invitrogen) was supplemented with gentamycin (10 µg/mL) and used for Sf21 cell cultures.

5.1.8 Buffers and solutions

Table 13 Buffers and solutions used for SDS-PAGE, gel electrophoresis and protein purifications.

Application	Name	Composition
SDS-PAGE	4x sample buffer	50% glycerol, 250 mM Tris/HCl pH 6.8, 7.5% SDS, 5 mM EDTA, 10 mM DTT, 0.5% bromophenol blue
	Coomassie stain	50% (v/v) ethanol, 7% (v/v) acetic acid, 0.2% Coomassie Brilliant blue R-250
Gel electrophoresis	6x DNA loading dye	1.5 g/l bromophenol blue, 1.5 g/l xylene cyanol, 50% (v/v) glycerol
	1x TAE buffer	40 mM Tris, 20 mM acetic acid, 1 mM Na_2EDTA
Nanobody purification	NB-lysis-buffer	50 mM Tris pH 8.0, 300 mM NaCl, protease inhibitor cocktail (PI) (Sigma-Aldrich), 1 mg/mL lysozyme, 12.5 units/mL benzonase
	NB-wash-buffer	50 mM Tris pH 8.0, 300 mM NaCl
	NB-elution-buffer	50 mM Tris pH 8.0, 300 mM NaCl, 2.5 mM d-Desthiobiotin
NactNB-Arp4-N-actin purification	C1-lysis-buffer	50 mM Tris pH 8, 300 mM NaCl, 5% glycerol, PI
	C1-wash-buffer	50 mM Tris pH 8, 300 mM NaCl, 5% glycerol
	C1-elution-buffer	50 mM Tris pH 8, 300 mM NaCl, 5% glycerol, 2.5 mM Desthiobiotin
	C1-IEX-buffer-A	50 mM Tris pH 8, 100 mM NaCl, 5% glycerol
	C1-IEX-buffer-B	50 mM Tris pH 8, 1 M NaCl, 5% glycerol
	C1-SEC-buffer	20 mM HEPES pH 8, 200 mM NaCl
Arp8 module and Arp5 purification	C2-lysis-buffer	20 mM HEPES pH 8, 100 mM KCl, 2.5% glycerol, 1 mM DTT, 1x PI
	C2-wash-buffer	20 mM HEPES pH 8, 100 mM KCl, 2.5% glycerol, 1 mM DTT, 2.5 mM Desthiobiotin
	C2- elution -buffer	20 mM HEPES pH 8, 100 mM KCl, 2.5% glycerol, 1 mM DTT
	C2-IEX-buffer-A	20 mM HEPES pH 8, 100 mM KCl, 2.5% glycerol, 1 mM DTT
	C2-IEX-buffer-B	20 mM HEPES pH 8, 800 mM KCl, 2.5% glycerol, 1 mM DTT
	C2-SEC-buffer	20 mM HEPES pH 8, 150 mM KCl, 2.5% glycerol, 1 mM DTT

5.2 Methods

5.2.1 Molecular cloning

For blunt-end cloning, primers were phosphorylated on the 5'-end with T4 polynucleotide kinase (NEB) according to manufacturer's protocol, before polymerase chain reactions (PCR).

PCRs were performed with Phusion Flash High-Fidelity PCR Master Mix (Thermo Fischer Scientific) as 20 µL reactions according to the manufacturer's protocol. The annealing temperature and the extension time of the PCR program were adjusted based upon the melting temperature of the primer and the length of the template. PCRs were afterwards digested with DpnI restriction enzyme (NEB) to degrade the methylated template plasmid. Therefore, DpnI was directly added to the PCR reaction product and incubated for at least 1 h at 37˚C. PCRs were analyzed by agarose gel electrophoresis according to a standard protocol (Sambrook, 2012). PCR products were purified from agarose gels using a Gel Extraction Kit (Machery Nagel). The insertion of DNA fragments into vectors was performed by standard restriction enzyme cloning (Sambrook, 2012) or In-Fusion cloning. For In-Fusion cloning, the In-Fusion HD cloning Kit (Takara Bio, Moutian View USA) was used. Primers were designed and In-Fusion cloning reactions were performed according to the manufacturer's protocol. DNA ligation reactions were performed using T4 DNA ligase (NEB) according to the manufacturer's protocol.

Plasmids or ligation products were transformed into chemically competent *Escherichia coli* cells (Sambrook, 2012). 50 ng of plasmid DNA or 5 µL ligation product was added to 50 µL of chemically competent cells. Cells were incubated for 15 min on ice and heat-shocked at 42°C for 45 sec. Subsequently the cells were cooled on ice for 2 min. After the addition of 950 µL LB medium, cells were incubated for 1 h at 37°C with shaking. Next the cell-suspension was distributed onto an LB-agar-plate supplemented with respective antibiotic. The plate was incubated at 37°C overnight. For plasmid amplification, 5 mL LB medium (with respective antibiotic) was inoculated with a single colony and grown overnight at 37°C with shaking. The cells were pelleted by centrifugation (5 min, 4K x g). Plasmid DNA was extracted from the cell pellet using a plasmid extraction kit (NucleoSpin Plasmid EasyPure, Machery-Nagel). DNA sequences of interest were verified by sequencing (GATC Biotech, Konstanz, Germany).

5.2.2 Protein expression and purification

5.2.2.1 Insect cell virus generation

For the expression of multiprotein complexes in insect cells the MultiBac expression system is a powerful tool. The genes of interest are incorporated into a transfer vector as a 'polycistronic' expression cassette via a multiplication module. Via *cre-lox* site-specific recombination the expression cassette is introduced into the engineered baculoviral genome (DH10MultiBac bacmid) in *Escherichia coli* DH10MultiBac cells (Berger et al., 2004; Trowitzsch et al., 2010).

The transfer vector with genes of interest was transformed (see section 5.2.1 for the transformation protocol) into chemically competent DH10MultiBac cells with 8 h regeneration phase. Transformed cells were grown on LB agar-plates containing gentamycin (10 µg/mL), kanamycin (50 µg/mL), tetracycline (12.4 µg/mL), IPTG (1 mM) and Plus X-gal (100 µg/mL). Successful integration of the expression cassette into the DH10MultiBac bacmid was detected by blue-white screening. Positive clones were used to inoculate 250 mL of LB media (supplemented with gentamycin and kanamycin) and cultivated overnight at 37°C shaking. Cells were harvested by centrifugation (15 min, 4K x g). Baculoviral DNA was isolated from the cells using a standard plasmid extraction kit (NucleoBond Xtra Midi, Machery-Nagel). Bacmid DNA was isopropanol precipitated from the eluate and centrifuged (10 min, 11K x g). The supernatant was removed and the pellet washed with 200 µL 70% ethanol. Next 50 µL 70% ethanol were added to the pellet and removed under a laminar flow hood. The bacmid DNA was dried on air and afterwards solved in sterile water. Sf21 insect cells were seeded in a 6-well tissue plate (0.4×10^6 number of cells/well). Cells were transfected with ~ 2 µg of bacmid DNA mixed with 3 µL FuGENE HD Transfection Reagent (Promega, Madison, USA) according to manufacturer's protocol. Transfected cells were incubated for 60 h at 27˚C. 1 mL of the supernatant (viral generation 0; V_0) was collected and used to transfect 10 mL Sf21 cells (1.3×10^6 cells/mL). The cells were cultured for 60 h at 27˚C with shaking (95 rpm). The supernatant V_1 was separated from cells by centrifugation (10 min, 3K x g). For a second round of viral amplification 50 mL Sf21 cells (1.3×10^6 cells/mL) were transfected with 0.5 mL of V_1. The cells were cultured for 60 h at 27˚C with shaking (95 rpm). The supernatant was harvested by centrifugation (10 min, 3K x g) and filtrated (0.22 µM filter). V_2 was stored at 4˚C and used for protein expression in High Five insect cells.

5.2.2.2 SDS-PAGE

Sodium dodecyl sulfate polyacrylamide gel electrophoresis (SDS-PAGE) is an analytical method to separate proteins in a particular sample by size. Hence it is an easy and fast method to monitor protein purifications and to check the purity of protein samples.

Protein samples were mixed with 4xSDS-loading-buffer and incubated for 10 min at 95°C for denaturing. Samples were analyzed on precast gradient (4-20% acrylamide) protein gels (expedeon, San Diego, USA) according to the manufacturer's protocol. Gels were stained with Coomassie Brilliant Blue.

5.2.2.3 Nanobody expression and purification

Nanobodies were produced by periplasmic expression in *Escherichia coli*. The DNA sequence coding for the respective nanobody carrying a C-terminal Twin-Strep-Tag was cloned into a pHEN6 vector downstream of the pelB leader sequence (The pHEN6-NactNB-Twin-Strep-Tag vector coding for the Arp4-N-actin binding nanobody was cloned previously by Dr. Sebastian Eustermann) (Conrath et al., 2001). *Escherichia coli* Rosetta (DE3) cells were transformed (see section 5.2.1 for the transformation protocol) with the pHEN6-nanobody vector. Freshly transformed cells were cultured at 37°C in LB media containing ampicillin (100 µg/mL). Protein was expressed for 2 h at 22°C after induction with 0.3 mM IPTG at an optical density at a wavelength of 600 nm (OD600) of 0.6.

All protein purification steps were performed at 4°C.

Cells were harvested by centrifugation (15 min, 4K x g) and subsequently incubated for 30 min in NB-lysis-buffer for periplasmic lysis. The cell debris was separated by centrifugation (30 min, 16K x g). The nanobody was purified from the soluble extract via the C-terminal double Strep-Tag. Strep-Tactin Sepharose was incubated with the lysate for 1 h on a rotary mixer. Next, the resin was applied to a gravity flow column and washed with 20 column volumes (CVs) of NB-wash-buffer. NactNB bound to Strep-Tactin Sepharose was stored at 4°C and used within two days for pull-down assays or eluted with 3 x 2 CVs NB-elution-buffer.

5.2.2.4 Expression and purification of the Arp4-Nactin-NactNB complex

In order to obtain a complex consisting of Arp4, N-actin and NactNB, the previously prepared purified NactNB-saturated Strep-Tactin resin (see section 5.2.2.3) was used to

immunopurify the recombinantly overexpressed Arp4-N-actin dimer from insect cell lysate.

A baculovirus coding for the ten yeast INO80 subunits: Arp4, Arp8, actin, Taf14, Ies1, Ies2, Ies3, Ies4, Ies5 and Nhp10 was generated previously by Dr. Sebastian Eustermann. For the expression of the ten INO80 subunits, High Five cells (1 x 10^6 cells/mL) were transfected 1/100 (v/v) with baculovirus. Cells were cultured for 60 h at 27°C until they were harvested by centrifugation (15 min, 3K x g).

All protein purification steps were performed at 4°C.

Cells were lysed by sonication in C1-lysis-buffer. The raw cell lysate was cleared by centrifugation. NactNB bound Strep-Tactin Sepharose was used to isolate the Arp4-N-actin heterodimer from the soluble cell extract. The Arp4-N-actin-NactNB complex was washed with 3x 10 CVs C1-wash-buffer using gravity flow and C1-elution-buffer. The ternary complex was further purified by ion-exchange chromatography with a HiTrapQ HP column by applying and linear gradient form C1-IEX-buffer-A to C1-IEX-buffer B. Peak fractions were concentrated (Amicon Ultra-15, 10 kDa, Merck Millipore) and subjected to gel filtration on a Superdex 200 column equilibrated with C1-SEC-buffer. Pure protein was concentrated to a final concentration of 16-20 mg/ml, flash frozen in liquid nitrogen and stored at -80˚C.

5.2.2.5 Expression and purification of the INO80 Arp8 module

For the generation of Arp8 module protein crystals many different protein constructs were screened. In order to simplify this screening process, which in context of a protein complex becomes more challenging, a combinatorial approach was designed. By using two baculoviruses it was easier and faster to test the expression of different subunit constructs and compositions. Initial 10 mL test-expressions are described in section 3.1.1.1.

For the final Arp8 module complex used for crystallization, genes encoding yeast Arp4 and actin were cloned into one pFBDM vector and those encoding yeast Arp8 (residues 255-881) and $Ino80^{HSA}$ (residues 462-598) carrying a C-terminal Strep-Tag II were combined on a second pFBDM vector. Baculoviruses for the respective vectors were generated as described in section 5.2.2.1.

For the co-expression of the four proteins, High Five insect cells (1 x 10^6 cells/mL) were co-infected with the two viruses (1/100 (v/v) each), cultivated for 60 h at 27°C and harvested by centrifugation (15 min, 3K x g).

All protein purification steps were performed at 4°C.

High Five cells were lysed by sonication in C2-lysis-buffer. The complex was separated from the cleared cell lysate by affinity chromatography using Strep-Tactin Sepharose. The resin was washed with 3x 10 CVs C1-wash-buffer and protein eluted with 3x 2CVs C1-elution-buffer. Eluted protein was further purified by anion-exchange chromatography with a HiTrapQ HP column using a linear gradient form C2-IEX-buffer-A to C2-IEX-buffer-B. Peak fractions were concentrated (Amicon Ultra-15, 10 kDa, Merck Millipore) and subjected to gel filtration on a Superdex 200 column equilibrated with C2-SEC-buffer. Peak fractions containing homogenous Arp8 module complex were pooled, concentrated, flash frozen and stored at -80°C.

For the Arp8 module Ino80-HSA mutants, a single pACE-BacI vector encoding expression cassettes for yeast Arp4, actin, Arp8 and the respective Ino80-HSA mutant was generated using the latest MultiBac system according to published protocols. Generation of the baculovirus, expression in High Five insect cells and purification of respective Arp8 module complex was performed as described above for WT Arp8 module (Eustermann et al., 2018; Trowitzsch et al., 2010).

Purification of the Arp8 module NactNB complex was performed by adding 1 mg of freshly purified NactNB to 20 mL cleared Arp8 module expression insect cell lysate prior to purification. Further purification followed the procedure described above for the WT Arp8 module.

5.2.2.6 Expression and purification of Arp5

Chaetomium thermophilum Arp5 was expressed in insect cells and affinity purified by a N-terminal Strep-Tag II.

Baculovirus containing an expression cassette encoding *Chaetomium thermophilum* Arp5 was generated as described in section 5.2.2.1. High Five insect cells (1 x 10^6 cells/mL) were infected with the virus 1/100 (v/v), cultivated for 60 h at 27°C and harvested by centrifugation (15 min, 3K x g).

All protein purification steps were performed at 4°C.

Cell were lysed in C2-lysis-buffer by sonication. Raw lysate was cleared by centrifugation (30 min, 16K x g). Arp5 was isolated from the cleared lysate by affinity chromatography using Strep-Tactin Sepharose (IBA). Insect cell lysate was incubated with the Strep-Tactin resin for 1 h on a rotary mixer. The resin was applied to gravity flow column and washed with 3x 20 CVs C2-washing-buffer and eluted with 3x CVs C2-elution-buffer. Eluted protein was applied to a HiTrapQ HP column and eluted using a linear gradient, C2-IEX-buffer-A to C2-IEX-buffer-B. Peak fractions were concentrated (Amicon Ultra-15, 30 kDa,

Merck Millipore) and subjected to gel filtration on a Superdex 200 column equilibrated with C2-SEC-buffer. Peak fractions containing monodisperse and pure protein were pooled, concentrated, flash frozen in liquid nitrogen and stored at -80°C.

5.2.2.7 Expression and purification of the human Arp8 module

For the human Arp8 module a single pACE-BacI vector encoding expression cassettes for human Arp4 (hBAF53a), β-actin, Arp8 and Ino80^{HSA} (residues 267-484) carrying a C-terminal Strep-Tag II was generated by using the latest MultiBac system according to published protocols (Eustermann et al., 2018; Trowitzsch et al., 2010). Generation of the baculovirus, expression in High Five insect cells and purification of complex was performed as described in section 5.2.2.5 for the yeast Arp8 module.

5.2.3 X-ray crystallography

5.2.3.1 Initial crystallization screening

A major challenge in protein crystallography is the identification of conditions under which a protein sample of interest forms a crystal that diffracts x-rays. Therefore, screening of multiple different crystallization conditions is necessary. High-throughput crystallization screening in a 96 well plate format based on a robotic dispenser system is a powerful tool for testing a multitude of conditions.

High-throughput screening for initial crystallization conditions was performed in a 96 well plate sitting-drop format (MRC 2-well crystallization plate, Jena Bioscience, Jena, Germany). Crystal screens were set up either in-house by using a Phoenix (ARI – Art Robbins Instruments, Mountain View, USA) dispensing system or with the assistance of the Max Planck Institute of Biochemistry (MPIB) Crystallization Facility (Martinsried, Germany). Sample-reservoir drop size varied between 100-300 nL with a reservoir volume of 55 µL. Commercial crystallization or MPIB in-house crystallization screens were used. Protein concentration and incubation temperature were varied during the screening process. Refinement screens were used to optimize initial crystals and resulted in the final crystallization condition.

5.2.3.2 Crystallization of the Arp4-N-actin-NactNB complex

Prior to crystallization the Arp4-N-actin-NactNB complex protein sample (16 mg/mL) was mixed with subtilisin 1:6000 [w(protease):w(complex)] for in-drop proteolysis, 0.2 mM

$CaCl_2$ and either 1 mM ATP (buffered at pH 7.5 in 100 mM Tris) for the N-actin ATP-bound structure or 1 mM ADP (buffered at pH 7.5 in 100 mM Tris) for the nucleotide-free (apo) structure. Crystals were grown by hanging-drop vapour diffusion at 20˚C in 1.4-1.5 M sodium malonate at pH 6.0. The best diffracting crystals were harvested after 4-8 days and cryo-protected with 23% glycerol.

5.2.3.3 Crystallization of the INO80 Arp8 module

For the crystallization of the $Ino80^{HSA}$-Arp4-N-Actin-Arp8 complex, protein solution (13 mg/mL) was mixed with latrunculin A (LatA) (For the LatA stock solution LatA was dissolved in 100% DMSO to a final concentration of 10 mM) at a molar ratio of 1:1.5 (Complex : LatA). Crystals were grown by hanging-drop vapour diffusion at 4˚C against 0.1 M sodium citrate tribasic dihydrate and 18% w/v polyethylene glycol 3,350. The crystals were harvested after 30 days and cryo-protected with 20% glycerol.

5.2.3.4 Data collection and processing

Diffraction data from all crystals were collected at 100 K with a wavelength of 1.0 Å at the SLS (Swiss Light Source, Villigen, Switzerland) beamline X06SA. Data were processed with XDS (Kabsch, 2010), analysed with POINTLESS and scaled with AIMLESS (Evans and Murshudov, 2013) within the CCP4 suite (Winn et al., 2011).

5.2.3.5 Structure determination of the Arp4-Nactin-NactNB complex

The two structures of the Arp4-N-actin-NactNB complex with N-actin ATP bound (PDB 5NBM) and nucleotide free (apo) (PDB 5NBL) were determined by molecular replacement with Phaser (McCoy et al., 2007). For a first model, structures of *S. cerevisiae* actin (PDB 1YAG) and Arp4 (PDB 3QB0) were used as search models following the removal of any nucleotides, water molecules or metal atoms. A homology model of NactNB was generated using the PHYRE server (Kelley et al., 2015) and the three CDR loops were deleted prior its use as a search model. Sequential search analysis with two copies of each of the search models for Arp4, actin and NactNB resulted in a unique solution for two copies of the ternary complex per asymmetric unit. The initial model was used as search model for the analysis of the diffraction data sets from crystals grown in presence of ATP or ADP, giving immediately a single solution with two complexes per asymmetric unit for both structures (N-actin ATP-bound and nucleotide-free). The initial models were then improved through

iterative rounds of model refinement with phenix.refine (Adams et al., 2010) and manual model building with COOT (Emsley et al., 2010). Both electron density maps contained density for a peptide of unknown source that we could not assign to any sequence of the expressed proteins. This density was therefore modelled as a poly-UNK (unknown amino acid) peptide. The final model of the N-actin(ATP)-Arp4-NactNB complex (PDB 5NBM) at 3.4 Å resolution has R_{work}/R_{Free} values of 15.2/19.3% and the model of the N-actin(apo)-Arp4-NactNB complex (PDB 5NBL) at 2.8 Å resolution has R_{work}/R_{Free} values of 17.1/20.4% (Table 3).

5.2.3.6 Structure determination of the INO80 Arp8 module

The $Ino80^{HSA}$-Arp4-N-Actin-Arp8 module structure (PDB 5NBN) was determined by molecular replacement with Phaser (McCoy et al., 2007). The Arp4-N-actin-NactNB structure (PDB 5NBM) without NactNB and the yeast Arp8CTD structure (PDB 4AM6) were used as search models following the removal of any ligands or waters molecules. A single solution containing two copies of the Arp4-N-actin-Arp8 complex per asymmetric unit was found. Clear difference density for the $Ino80^{HSA}$ domain was visible in the initial map after molecular replacement. The model was improved through iterative rounds of refinement with phenix.refine (Adams et al., 2010), applying secondary structure restraints and NCS restraints, and manual model building with COOT (Emsley et al., 2010). The $Ino80^{HSA}$ domain was built manually with COOT (Emsley et al., 2010) using B-factor sharpening and feature-enhanced-maps (Afonine et al., 2015) (calculated by phenix.fem (Adams et al., 2010)) for model building. The final model of the $Ino80^{HSA}$-Arp4-N-Actin-Arp8 module model at 4.0 Å resolution has R_{work}/R_{Free} values of 19.3%/24.2% (Table 3).

5.2.3.7 Structure analysis and presentation

Structures were analysed using COOT (Emsley et al., 2010) and PISA (Krissinel and Henrick, 2007). Figures of structures were prepared with PyMOL (Schrodinger, 2015) and ChimeraX (Goddard et al., 2018).

5.2.4 Protein biochemistry

5.2.4.1 Fluorescence anisotropy

Fluorescence anisotropy was used to determine the Arp8 module binding affinity to fluorophore-labeled DNA. Measurements were performed in principle as described before (Favicchio et al., 2009).

Fluorescein-labeled ssDNA was ordered from Metabion and resuspended in water. For generation of dsDNA, equimolar amounts (25 µL with 80 µM each strand) of the two complementary DNA strands (only one strand was fluorescein labeled; see Table 4) were mixed, heated to 95°C for 10 min and slowly cooled to room temperature to anneal the two DNA strands. The Arp8 module was diluted to the respective working concentration and incubated with 20 nM dsDNA on ice for 30 min in 20 mM Tris pH 7.8, 50 mM KCl and 2.5% glycerol in a total volume of 100 µL.

Fluorescence anisotropy was measured in a black flat-bottomed non-binding 96 well plate (Greiner-Bio) on a Tecan Infinite M1000 plate reader (settings are listed in Table 14). Blank wells contained only buffer.

Table 14 Tecan Infinite M1000 plate reader settings for fluorescence anisotropy.

Mode	Fluorescence anisotropy
Excitation wavelength	470 nM
Emission Wavelength	520 nM
Excitation Bandwidth	5 nM
Emission Bandwidth	10 nM
Gain	129
Number of Flashes	10
Settle Time	0 ms
Z-Position (Manual)	20000 μm
G-Factor	1

Data was analysed and fitted to a non-linear non-cooperative 1:1 binding model (Equation 1) with the program Prism (GraphPad) to calculate the dissociation constants for the respective complex. Experiments were performed in triplicate.

$$y = A_f - (A_f - A_b)\,\frac{x}{K_d + x}$$

Equation 1 Non-linear non-cooperative 1:1 binding model (y anisotropy; A_f anisotropy of free ligand; A_b Anisotropy of bound ligand; K_d dissociation constant; x receptor concentration).

5.2.4.2 Electro mobility shift assays

The Arp8 module binding preference for mononucleosomes with 80 bp extranucleosomal DNA overhang (0N80) or without extranucleosomal DNA (0N0) was examined with competition electro-mobility shift assays (EMSAs). Nucleosomes were prepared by Kevin Schall.

Increasing amounts of the respective Arp8 module complex were titrated against a 1:1 mixture of 0N0 and 0N80 (20 nM each) mononucleosomes in 10 mM HEPES pH 8.0, 2 mM $MgCl_2$, 60 mM NaCl, 8% glycerol and incubated for 20 min on ice. 15 µL of each titration step was loaded on a precast native polyacrylamide gel (NativePAGE Novex™ 4-16% Bis-Tris Protein Gels; Invitrogen). Arp8 module bound and unbound nucleosomes were resolved by Native-PAGE in 1x NativePAGE™ Running Buffer (Invitrogen) according to the manufacturer's protocol at 120 V for 120 min at 4°C. Gels were analysed on a Typhoon FLA 9000 plate reader (GE Healthcare) using FITC fluorescence scan.

The INO80 binding affinity to 0N80 nucleosomes with N-actin binding ligands was measured in EMSAs, similar as described above, with the small modification that only one nucleosome species (0N80) was added. In order to calculate equilibrium binding constant (Kd), the experiment was quantified by band density analysis with ImageJ (Schneider et al., 2012) and fitted to a one site specific binding model with the program Prism (GraphPad). Kd values and error bars represent the means ± s.d. from three independent experiments.

5.2.4.3 Nucleosome sliding assays

The nucleosome sliding activity of INO80 in the presence of the N-actin nucleotide state stabilizing ligands, LatA and NactNB, was monitored on 0N80 mononucleosomes. The

entire yeast INO80 complex was prepared by Dr. Sebastian Eustermann and nucleosomes by Kevin Schall.

18 nM INO80 was incubated with 90 nM 0N80 nucleosome in sliding buffer (25 mM Hepes, pH 8.0, 60 mM KCl, 7% glycerol, 0.10 mg/mL BSA, 0.25 mM DTT, 2 mM $MgCl_2$) at 26°C. The sliding reaction was started by the addition of ATP and $MgCl_2$ (final concentrations: 1 mM ATP and 2 mM $MgCl_2$). At the respective time points (30, 60, 120, 300, 600, 1800 and 3600 s) the reaction was stopped by adding lambda DNA (NEB) to a final concentration of 0.2 mg/mL. 1.5 µL 15% Ficoll was added to 11 µL of the quenched remodeling reaction and analyzed by Native PAGE (NativePAGE™ Novex™ 4-16% Bis-Tris Protein Gels; Invitrogen) to separate distinct nucleosome species. Gels were analysed on a Typhoon FLA 9000 plate reader (GE Healthcare) using FITC fluorescence scan.

5.2.5 Yeast methods

5.2.5.1 Yeast transformation

Competent yeast cells were prepared and transformed based on a polyethylene glycol (PEG)/LiAcetate-method. Transformed cells were selected by an auxotrophy marker on SD selection media.

5 mL of YPD medium was inoculated with a single yeast colony from a YPD-agar plate and cultivated under shaking overnight at 30°C. 1-2 mL of the overnight culture was used to inoculate 40 mL YPD media. Cells were cultivated at 30°C under shaking until an OD600 of 0.6–1.0 was reached.

For the following steps working at 4°C with precooled solutions was critical for the competence of the cells. Yeast was harvested by centrifugation (1K x g, 5 min). Cells were washed with 40 mL sterile water and pelleted again (1K x g, 5 min). Cells were treated with 40 mL sterile Li-buffer (100 mM LiAcetate, 10 mM Tris-HCl pH 7.4, 1 mM EDTA) and pelleted again (1K x g, 5 min). Cells were resuspended in 200 µL Li-buffer and stored at 4°C until transformation, but maximally for one day.

For the transformation 2 µL salmon sperm carrier DNA (10 µg/mL, Thermo Fisher Scientific), 2-5 µL of plasmid DNA (0.2-1 µg) and 15 µL of competent yeast cells were mixed and incubated for 15 min at 30°C. Cells were mixed with 150 µL pre-warmed sterile PEG-buffer (40% (w/v) PEG4000, 10 mM Tris-HCl pH 7.4, 1 mM EDTA) and incubated for 15 min at 30°C. Next, cells were heat shocked at 42°C for 8 min, chilled on ice (1-2 min) and pelleted (10K x g, 10-15 sec). Cells were suspended in 100 µL sterile water, spread on a

SD selection medium agar plate and incubated for 3 to 5 days at 30°C. In general, after 4 days the first colonies were visible.

5.2.5.2 Arp4 plasmid shuffling assay

For studying the essential *ARP4* (YJL081c) gene in yeast the plasmid shuffling technique was used (Sikorski and Hieter, 1989).

Dr. Christian B. Gerhold previously generated a haploid *Saccharomyces cerevisiae ARP4* deletion strain from a heterozygous *Saccharomyces cerevisiae ARP4* (YJL081c) deletion strain (Table 6; obtained from EUROSCARF) by sporulation. The *ARP4* deletion strain was rescued with a plasmid carrying the essential *ARP4* gene plus the flanking genomic regions (+500 Arp4 -300) (Gerhold, 2012).

In a yeast plasmid shuffling assay WT Arp4 was replaced with the particular mutant variant of Arp4. Hereby the respective Arp4 mutant plus the genomic flanking regions (+500 mutant Arp4 -300) was encoded on a pRS315 vector. The pRS315 vector harbors the *LEU2* marker gene, allowing positive selection for pRS315 on SD -Leu media. Wild type Arp4 on a pRS316 vector harbors the *URA3* marker gene which encodes for orotidine 5'-phosphate decarboxylase (ODCase). ODCase degrades 5-fluorooretic acid (5-FOA) to toxic 5-fluorouracil, allowing counter-selection against the pRS316 vector in the presence of 5-FOA containing medium. Transformation of pRS315-mutant-Arp4 in the yeast Δ*ARP4* pRS316-WT-Arp4 cells and subsequent cultivation on SD-Leu+5-FOA medium allowed the selection against wild type Arp4 and for the Arp4 mutant variant.

Competent Δ*ARP4* pRS316-WT-Arp4 yeast cells were prepared and transformed as described in section 5.2.5.1 with the pRS315-mutant-Arp4 plasmid. Cells were plated on solid SD-Leu+5-FOA medium (1% (w/v) 5-FOA) and incubated for up to five days at 30°C in order to select for Arp4 mutants and against WT Arp4. Colonies were tested on SD-Leu media and SD-Ura media for successful counter-selection against the pRS316 vector.

5.2.5.3 Yeast growth and survival assays

The phenotype of Arp4 mutant cells was compared to WT Arp4 cells by monitoring yeast growth under normal conditions (YPD media at 30°C), at increased temperature (YPD media at 37°C) and under genotoxic stress (YPD media supplemented with HU or MMS at 30°C).

For yeast growth and survival assays 5 mL of YPD medium were inoculated with a single yeast colony of a particular Arp4 variant from a YPD-agar plate and cultivated by shaking overnight at 30°C. The cell density of the cultures was diluted to an OD600 of 0.1 in water. Subsequently, cultures were further diluted in a serial dilution series with a dilution factor of 1/10. 3 µL of each dilution step was spotted on a YPD agar plate and incubated at the appropriate temperature for 48 h.

5.2.6 Affinity-enrichment mass spectrometry from whole cell yeast extract

Yeast with a double FLAG-tagged INO80 (Genotype: MATa INO80-FLAG$_2$ his3Δ200 leu2Δ0 met15Δ0 trp1Δ63 ura3Δ0) (Shen et al., 2000) were grown for 2 days in YPD medium at 30°C. Cells were harvested by centrifugation. Pellets were re-suspended 5:1 (w(yeast): w(buffer)) in 20 mM HEPES pH 7.8. The cell suspension was dripped into liquid nitrogen and the frozen cells were lysed using a freezer mill (SPEX SamplePrep). The frozen cell powder was stored at -80°C until usage.

20 g of frozen yeast cell powder was thawed in 20 mL lysis buffer (25 mM HEPES pH 8.0, 500 mM KCl, 10% glycerol, 0.05% NP40, 1 mM EDTA, 4 mM $MgCl_2$ and 1x PI (Sigma-Aldrich)). Chromatin was fragmented with a polytron homogenizer (Kinematica; Fisher Scientific) and by sonication (Branson). The raw cell lysate was cleared by centrifugation and 250 µg/mL avidin (IBA) was added.

Both the specific-binder nanobody (NactNB) and the control nanobody (enhancer GFP nanobody; eGFP-NB) (Kirchhofer et al., 2010) have a C-terminal Twin-Strep-Tag and were expressed and purified as described for NactNB in section 5.2.2.3. NactNB or eGFP-NB immobilized on Strep-Tactin Sepharose were incubated with equal amounts of cleared yeast cell lysate. Unbound protein was removed by washing with buffer W1 (25 mM HEPES pH 8.0, 500 mM KCl, 10% glycerol, 0.05% NP40, 1 mM EDTA, 4 mM $MgCl_2$) followed by buffer W2 (25 mM HEPES pH 8.0, 200 mM KCl, 10% glycerol, 1 mM EDTA and 4 mM $MgCl_2$).

Samples for LC-MS/MS measurement were in prepared as published before (Keilhauer et al., 2015). Briefly, equal amounts of the nanobody Strep-Tactin Sepharose beads from each pull-down were incubated in buffer E1 (50 mM Tris-HCl pH 7.5, 2 M urea, 5 µg/ml trypsin (Promega) and 1 mM DTT) for 30 min at 30°C for on-bead digest. Any remaining peptides were eluted from the beads and alkylated with buffer E2 (50 mM Tris-HCl pH 7.5, 2 M urea, 5 mM iodoacetamide). Elution fractions were pooled and incubated in the dark overnight at 32°C. The digestion was stopped by the addition of 1% trifluoroacetic acid. Samples were loaded on self-made C18 reversed-phase StageTips for purification and enrichment following a standard protocol (Rappsilber et al., 2007). Peptides were eluted

with 2x20 µL buffer B (80% ACN and 0.5% AcOH) and concentrated using a SpeedVac concentrator to a final volume of 5-10 µL. Finally, 2.5 µL of buffer A* (2% ACN, and 1% TFA) and 2.5 µL buffer A (0.5% AcOH) were added to the sample.

Sample measurement and data analysis was performed by Dr. Gabriele Stoehr. Peptide samples were measured on a liquid chromatography-tandem mass spectrometry system using an ultra-high-performance liquid chromatography system (EASY-nLC 1000) coupled to an LTQ Orbitrap Elite (both Thermo Scientific) equipped with a standard nanoelectrospray source. Peptides were loaded onto a 15-cm × 0.050-mm inner diameter reversed phase column packed with 2 µm C18 beads (Acclaim PepMap RSLC analytical column, Thermo Scientific) and subsequently separated using a 90-min gradient of solvent B (98% ACN, 0.1% FA) from 2% to 35% at a flow rate of 250 nl min−1. *.RAW files from the eGFP-NB (mock) and NactNB triplicate experiments were analyzed together using the MaxQuant software suite (version 1.5.2.18) including the label-free algorithm for label-free quantification intensity calculation (Cox et al., 2014). Downstream data analysis was performed in the Perseus environment (version 1.5.0.9.) (Tyanova et al., 2016). Briefly, label-free quantification intensity values were log10 transformed, the data were filtered for at least two valid values in at least one of the two conditions, and missing values were imputed using a normal distribution at the noise level (width: 0.3 s.d. of the data; down shift: 1.8 s.d. of the valid data). To reveal significant outliers, a two-sample t-test was performed and data were visualized using an in-house R script.

6 References

Adams, P.D., Afonine, P.V., Bunkoczi, G., Chen, V.B., Davis, I.W., Echols, N., Headd, J.J., Hung, L.W., Kapral, G.J., Grosse-Kunstleve, R.W., *et al.* (2010). PHENIX: a comprehensive Python-based system for macromolecular structure solution. Acta Crystallogr D Biol Crystallogr *66*, 213-221.

Afonine, P.V., Moriarty, N.W., Mustyakimov, M., Sobolev, O.V., Terwilliger, T.C., Turk, D., Urzhumtsev, A., and Adams, P.D. (2015). FEM: feature-enhanced map. Acta Crystallogr D Biol Crystallogr *71*, 646-666.

Alatwi, H.E., and Downs, J.A. (2015). Removal of H2A.Z by INO80 promotes homologous recombination. EMBO Rep *16*, 986-994.

Allshire, R.C., and Madhani, H.D. (2018). Ten principles of heterochromatin formation and function. Nat Rev Mol Cell Biol *19*, 229-244.

Aramayo, R.J., Willhoft, O., Ayala, R., Bythell-Douglas, R., Wigley, D.B., and Zhang, X. (2018). Cryo-EM structures of the human INO80 chromatin-remodeling complex. Nat Struct Mol Biol *25*, 37-44.

Ayala, R., Willhoft, O., Aramayo, R.J., Wilkinson, M., McCormack, E.A., Ocloo, L., Wigley, D.B., and Zhang, X. (2018). Structure and regulation of the human INO80-nucleosome complex. Nature *556*, 391-395.

Badis, G., Chan, E.T., van Bakel, H., Pena-Castillo, L., Tillo, D., Tsui, K., Carlson, C.D., Gossett, A.J., Hasinoff, M.J., Warren, C.L., *et al.* (2008). A library of yeast transcription factor motifs reveals a widespread function for Rsc3 in targeting nucleosome exclusion at promoters. Mol Cell *32*, 878-887.

Baker, N.A., Sept, D., Joseph, S., Holst, M.J., and McCammon, J.A. (2001). Electrostatics of nanosystems: application to microtubules and the ribosome. Proc Natl Acad Sci U S A *98*, 10037-10041.

Bannister, A.J., and Kouzarides, T. (2011). Regulation of chromatin by histone modifications. Cell Res *21*, 381-395.

Bartholomew, B. (2013). Monomeric actin required for INO80 remodeling. Nat Struct Mol Biol *20*, 405-407.

Bartholomew, B. (2014). Regulating the chromatin landscape: structural and mechanistic perspectives. Annu Rev Biochem *83*, 671-696.

Berger, I., Fitzgerald, D.J., and Richmond, T.J. (2004). Baculovirus expression system for heterologous multiprotein complexes. Nat Biotechnol *22*, 1583-1587.

Boyer, L.A., and Peterson, C.L. (2000). Actin-related proteins (Arps): conformational switches for chromatin-remodeling machines? Bioessays *22*, 666-672.

Brahma, S., Ngubo, M., Paul, S., Udugama, M., and Bartholomew, B. (2018). The Arp8 and Arp4 module acts as a DNA sensor controlling INO80 chromatin remodeling. Nat Commun *9*, 3309.

Brahma, S., Udugama, M.I., Kim, J., Hada, A., Bhardwaj, S.K., Hailu, S.G., Lee, T.H., and Bartholomew, B. (2017). INO80 exchanges H2A.Z for H2A by translocating on DNA proximal to histone dimers. Nat Commun *8*, 15616.

Cai, Y., Jin, J., Yao, T., Gottschalk, A.J., Swanson, S.K., Wu, S., Shi, Y., Washburn, M.P., Florens, L., Conaway, R.C., *et al.* (2007). YY1 functions with INO80 to activate transcription. Nat Struct Mol Biol *14*, 872-874.

Cairns, B.R., Erdjument-Bromage, H., Tempst, P., Winston, F., and Kornberg, R.D. (1998). Two actin-related proteins are shared functional components of the chromatin-remodeling complexes RSC and SWI/SNF. Mol Cell *2*, 639-651.

Cao, T., Sun, L., Jiang, Y., Huang, S., Wang, J., and Chen, Z. (2016). Crystal structure of a nuclear actin ternary complex. Proc Natl Acad Sci U S A *113*, 8985-8990.

Caridi, C.P., D'Agostino, C., Ryu, T., Zapotoczny, G., Delabaere, L., Li, X., Khodaverdian, V.Y., Amaral, N., Lin, E., Rau, A.R., *et al.* (2018). Nuclear F-actin and myosins drive relocalization of heterochromatic breaks. Nature *559*, 54-60.

Carlier, M.F., and Shekhar, S. (2017). Global treadmilling coordinates actin turnover and controls the size of actin networks. Nat Rev Mol Cell Biol *18*, 389-401.

Chen, L., Cai, Y., Jin, J., Florens, L., Swanson, S.K., Washburn, M.P., Conaway, J.W., and Conaway, R.C. (2011). Subunit organization of the human INO80 chromatin remodeling complex: an evolutionarily conserved core complex catalyzes ATP-dependent nucleosome remodeling. J Biol Chem *286*, 11283-11289.

Chen, L., Conaway, R.C., and Conaway, J.W. (2013). Multiple modes of regulation of the human Ino80 SNF2 ATPase by subunits of the INO80 chromatin-remodeling complex. Proc Natl Acad Sci U S A *110*, 20497-20502.

Clapier, C.R., and Cairns, B.R. (2009). The biology of chromatin remodeling complexes. Annu Rev Biochem *78*, 273-304.

Clapier, C.R., Iwasa, J., Cairns, B.R., and Peterson, C.L. (2017). Mechanisms of action and regulation of ATP-dependent chromatin-remodelling complexes. Nat Rev Mol Cell Biol *18*, 407-422.

Clapier, C.R., Kasten, M.M., Parnell, T.J., Viswanathan, R., Szerlong, H., Sirinakis, G., Zhang, Y., and Cairns, B.R. (2016). Regulation of DNA Translocation Efficiency within the Chromatin Remodeler RSC/Sth1 Potentiates Nucleosome Sliding and Ejection. Mol Cell *62*, 453-461.

Conrath, K.E., Lauwereys, M., Galleni, M., Matagne, A., Frere, J.M., Kinne, J., Wyns, L., and Muyldermans, S. (2001). Beta-lactamase inhibitors derived from single-domain antibody fragments elicited in the camelidae. Antimicrob Agents Chemother *45*, 2807-2812.

Cox, J., Hein, M.Y., Luber, C.A., Paron, I., Nagaraj, N., and Mann, M. (2014). Accurate proteome-wide label-free quantification by delayed normalization and maximal peptide ratio extraction, termed MaxLFQ. Mol Cell Proteomics *13*, 2513-2526.

Cremer, T., and Cremer, M. (2010). Chromosome territories. Cold Spring Harb Perspect Biol *2*, a003889.

Crick, F. (1970). Central dogma of molecular biology. Nature *227*, 561-563.

Cutter, A.R., and Hayes, J.J. (2015). A brief review of nucleosome structure. FEBS Lett *589*, 2914-2922.

de la Mata, M., and Grosshans, H. (2018). Turning the table on miRNAs. Nat Struct Mol Biol *25*, 195-197.

Deal, R.B., Henikoff, J.G., and Henikoff, S. (2010). Genome-wide kinetics of nucleosome turnover determined by metabolic labeling of histones. Science *328*, 1161-1164.

Deindl, S., Hwang, W.L., Hota, S.K., Blosser, T.R., Prasad, P., Bartholomew, B., and Zhuang, X. (2013). ISWI remodelers slide nucleosomes with coordinated multi-base-pair entry steps and single-base-pair exit steps. Cell *152*, 442-452.

Dion, V., Shimada, K., and Gasser, S.M. (2010). Actin-related proteins in the nucleus: life beyond chromatin remodelers. Curr Opin Cell Biol *22*, 383-391.

Dixon, J.R., Gorkin, D.U., and Ren, B. (2016). Chromatin Domains: The Unit of Chromosome Organization. Mol Cell *62*, 668-680.

Dominguez, R., and Holmes, K.C. (2011). Actin structure and function. Annu Rev Biophys *40*, 169-186.

Doyon, Y., and Cote, J. (2004). The highly conserved and multifunctional NuA4 HAT complex. Curr Opin Genet Dev *14*, 147-154.

Durr, H., Korner, C., Muller, M., Hickmann, V., and Hopfner, K.P. (2005). X-ray structures of the Sulfolobus solfataricus SWI2/SNF2 ATPase core and its complex with DNA. Cell *121*, 363-373.

Eaton, M.L., Galani, K., Kang, S., Bell, S.P., and MacAlpine, D.M. (2010). Conserved nucleosome positioning defines replication origins. Genes Dev *24*, 748-753.

Ebbert, R., Birkmann, A., and Schuller, H.J. (1999). The product of the SNF2/SWI2 paralogue INO80 of Saccharomyces cerevisiae required for efficient expression of various yeast structural genes is part of a high-molecular-weight protein complex. Mol Microbiol *32*, 741-751.

Emsley, P., Lohkamp, B., Scott, W.G., and Cowtan, K. (2010). Features and development of Coot. Acta Crystallogr D Biol Crystallogr *66*, 486-501.

Eustermann, S., Schall, K., Kostrewa, D., Lakomek, K., Strauss, M., Moldt, M., and Hopfner, K.P. (2018). Structural basis for ATP-dependent chromatin remodelling by the INO80 complex. Nature *556*, 386-390.

Evans, P.R., and Murshudov, G.N. (2013). How good are my data and what is the resolution? Acta Crystallogr D Biol Crystallogr *69*, 1204-1214.

Falbo, K.B., Alabert, C., Katou, Y., Wu, S., Han, J., Wehr, T., Xiao, J., He, X., Zhang, Z., Shi, Y., *et al.* (2009). Involvement of a chromatin remodeling complex in damage tolerance during DNA replication. Nat Struct Mol Biol *16*, 1167-1172.

Farnung, L., Vos, S.M., Wigge, C., and Cramer, P. (2017). Nucleosome-Chd1 structure and implications for chromatin remodelling. Nature *550*, 539-542.

Favicchio, R., Dragan, A.I., Kneale, G.G., and Read, C.M. (2009). Fluorescence spectroscopy and anisotropy in the analysis of DNA-protein interactions. Methods Mol Biol *543*, 589-611.

Fenn, S., Breitsprecher, D., Gerhold, C.B., Witte, G., Faix, J., and Hopfner, K.P. (2011a). Structural biochemistry of nuclear actin-related proteins 4 and 8 reveals their interaction with actin. EMBO J *30*, 2153-2166.

Fenn, S., Gerhold, C.B., and Hopfner, K.P. (2011b). Nuclear actin-related proteins take shape. Bioarchitecture *1*, 192-195.

Flaus, A., Martin, D.M., Barton, G.J., and Owen-Hughes, T. (2006). Identification of multiple distinct Snf2 subfamilies with conserved structural motifs. Nucleic Acids Res *34*, 2887-2905.

Galarneau, L., Nourani, A., Boudreault, A.A., Zhang, Y., Heliot, L., Allard, S., Savard, J., Lane, W.S., Stillman, D.J., and Cote, J. (2000). Multiple links between the NuA4 histone acetyltransferase complex and epigenetic control of transcription. Mol Cell *5*, 927-937.

Gamarra, N., Johnson, S.L., Trnka, M.J., Burlingame, A.L., and Narlikar, G.J. (2018). The nucleosomal acidic patch relieves auto-inhibition by the ISWI remodeler SNF2h. Elife *7*.

Ganguli, D., Chereji, R.V., Iben, J.R., Cole, H.A., and Clark, D.J. (2014). RSC-dependent constructive and destructive interference between opposing arrays of phased nucleosomes in yeast. Genome Res *24*, 1637-1649.

Gerhold, C.-B. (2012). Structural biochemistry of actin-related protein 8 within its INO80 chromatin remodeler environment. . In Faculty for Chemistry und Pharmacy (LMU Munich).

Gerhold, C.B., and Gasser, S.M. (2014). INO80 and SWR complexes: relating structure to function in chromatin remodeling. Trends Cell Biol *24*, 619-631.

Gerhold, C.B., Hauer, M.H., and Gasser, S.M. (2015). INO80-C and SWR-C: guardians of the genome. J Mol Biol *427*, 637-651.

Gerhold, C.B., Winkler, D.D., Lakomek, K., Seifert, F.U., Fenn, S., Kessler, B., Witte, G., Luger, K., and Hopfner, K.P. (2012). Structure of Actin-related protein 8 and its contribution to nucleosome binding. Nucleic Acids Res *40*, 11036-11046.

Goddard, T.D., Huang, C.C., Meng, E.C., Pettersen, E.F., Couch, G.S., Morris, J.H., and Ferrin, T.E. (2018). UCSF ChimeraX: Meeting modern challenges in visualization and analysis. Protein Sci *27*, 14-25.

Gu, M., and Rice, C.M. (2010). Three conformational snapshots of the hepatitis C virus NS3 helicase reveal a ratchet translocation mechanism. Proc Natl Acad Sci U S A *107*, 521-528.

Harada, B.T., Hwang, W.L., Deindl, S., Chatterjee, N., Bartholomew, B., and Zhuang, X. (2016). Stepwise nucleosome translocation by RSC remodeling complexes. Elife *5*.

Harata, M., Karwan, A., and Wintersberger, U. (1994). An essential gene of Saccharomyces cerevisiae coding for an actin-related protein. Proc Natl Acad Sci U S A *91*, 8258-8262.

Hartley, P.D., and Madhani, H.D. (2009). Mechanisms that specify promoter nucleosome location and identity. Cell *137*, 445-458.

Ho, L., and Crabtree, G.R. (2010). Chromatin remodelling during development. Nature *463*, 474-484.

Hodges, C., Kirkland, J.G., and Crabtree, G.R. (2016). The Many Roles of BAF (mSWI/SNF) and PBAF Complexes in Cancer. Cold Spring Harb Perspect Med *6*.

Hofmann, W.A., Stojiljkovic, L., Fuchsova, B., Vargas, G.M., Mavrommatis, E., Philimonenko, V., Kysela, K., Goodrich, J.A., Lessard, J.L., Hope, T.J., *et al.* (2004). Actin is part of pre-initiation complexes and is necessary for transcription by RNA polymerase II. Nature Cell Biology *6*, 1094.

Hopfner, K.P., Gerhold, C.B., Lakomek, K., and Wollmann, P. (2012). Swi2/Snf2 remodelers: hybrid views on hybrid molecular machines. Curr Opin Struct Biol *22*, 225-233.

Hota, S.K., and Bruneau, B.G. (2016). ATP-dependent chromatin remodeling during mammalian development. Development *143*, 2882-2897.

Hsieh, T.H., Weiner, A., Lajoie, B., Dekker, J., Friedman, N., and Rando, O.J. (2015). Mapping Nucleosome Resolution Chromosome Folding in Yeast by Micro-C. Cell *162*, 108-119.

Hu, P., Wu, S., and Hernandez, N. (2004). A role for beta-actin in RNA polymerase III transcription. Genes Dev *18*, 3010-3015.

Jiang, C., and Pugh, B.F. (2009). Nucleosome positioning and gene regulation: advances through genomics. Nat Rev Genet *10*, 161-172.

Jin, J., Cai, Y., Yao, T., Gottschalk, A.J., Florens, L., Swanson, S.K., Gutierrez, J.L., Coleman, M.K., Workman, J.L., Mushegian, A., *et al.* (2005). A mammalian chromatin remodeling complex with similarities to the yeast INO80 complex. J Biol Chem *280*, 41207-41212.

Jonsson, Z.O., Jha, S., Wohlschlegel, J.A., and Dutta, A. (2004). Rvb1p/Rvb2p recruit Arp5p and assemble a functional Ino80 chromatin remodeling complex. Mol Cell *16*, 465-477.

Jost, D., Vaillant, C., and Meister, P. (2017). Coupling 1D modifications and 3D nuclear organization: data, models and function. Curr Opin Cell Biol *44*, 20-27.

Judith G. Voet , C.W.P., Donald Voet (2012). Principles of Biochemistry (John Wiley & Sons Inc).

Kabsch, W. (2010). Xds. Acta Crystallogr D Biol Crystallogr *66*, 125-132.

Kabsch, W., and Holmes, K.C. (1995). The actin fold. FASEB J *9*, 167-174.

Kalashnikova, A.A., Porter-Goff, M.E., Muthurajan, U.M., Luger, K., and Hansen, J.C. (2013). The role of the nucleosome acidic patch in modulating higher order chromatin structure. J R Soc Interface *10*, 20121022.

Kapoor, P., Bao, Y., Xiao, J., Espejo, A., Yang, L., Bedford, M.T., Peng, G., and Shen, X. (2015). Phosphorylation-Dependent Enhancement of Rad53 Kinase Activity through the INO80 Chromatin Remodeling Complex. Mol Cell *58*, 863-869.

Kapoor, P., Chen, M., Winkler, D.D., Luger, K., and Shen, X. (2013). Evidence for monomeric actin function in INO80 chromatin remodeling. Nat Struct Mol Biol *20*, 426-432.

Keilhauer, E.C., Hein, M.Y., and Mann, M. (2015). Accurate protein complex retrieval by affinity enrichment mass spectrometry (AE-MS) rather than affinity purification mass spectrometry (AP-MS). Mol Cell Proteomics *14*, 120-135.

Kelley, L.A., Mezulis, S., Yates, C.M., Wass, M.N., and Sternberg, M.J. (2015). The Phyre2 web portal for protein modeling, prediction and analysis. Nat Protoc *10*, 845-858.

Kirchhofer, A., Helma, J., Schmidthals, K., Frauer, C., Cui, S., Karcher, A., Pellis, M., Muyldermans, S., Casas-Delucchi, C.S., Cardoso, M.C., *et al.* (2010). Modulation of protein properties in living cells using nanobodies. Nat Struct Mol Biol *17*, 133-138.

Klymenko, T., Papp, B., Fischle, W., Kocher, T., Schelder, M., Fritsch, C., Wild, B., Wilm, M., and Muller, J. (2006). A Polycomb group protein complex with sequence-specific DNA-binding and selective methyl-lysine-binding activities. Genes Dev *20*, 1110-1122.

Knoll, K.R., Eustermann, S., Niebauer, V., Oberbeckmann, E., Stoehr, G., Schall, K., Tosi, A., Schwarz, M., Buchfellner, A., Korber, P., *et al.* (2018). The nuclear actin-containing Arp8 module is a linker DNA sensor driving INO80 chromatin remodeling. Nature Structural & Molecular Biology *25*, 823-832.

Kornberg, R.D. (1974). Chromatin structure: a repeating unit of histones and DNA. Science *184*, 868-871.

Kornberg, R.D. (1977). Structure of chromatin. Annu Rev Biochem *46*, 931-954.

Krietenstein, N., Wal, M., Watanabe, S., Park, B., Peterson, C.L., Pugh, B.F., and Korber, P. (2016). Genomic Nucleosome Organization Reconstituted with Pure Proteins. Cell *167*, 709-721 e712.

Krissinel, E., and Henrick, K. (2004). Secondary-structure matching (SSM), a new tool for fast protein structure alignment in three dimensions. Acta Crystallogr D Biol Crystallogr *60*, 2256-2268.

Krissinel, E., and Henrick, K. (2007). Inference of macromolecular assemblies from crystalline state. J Mol Biol *372*, 774-797.

Krogan, N.J., Keogh, M.C., Datta, N., Sawa, C., Ryan, O.W., Ding, H., Haw, R.A., Pootoolal, J., Tong, A., Canadien, V., *et al.* (2003). A Snf2 family ATPase complex required for recruitment of the histone H2A variant Htz1. Mol Cell *12*, 1565-1576.

Kudryashov, D.S., and Reisler, E. (2013). ATP and ADP actin states. Biopolymers *99*, 245-256.

Kurat, C.F., Yeeles, J.T.P., Patel, H., Early, A., and Diffley, J.F.X. (2017). Chromatin Controls DNA Replication Origin Selection, Lagging-Strand Synthesis, and Replication Fork Rates. Mol Cell *65*, 117-130.

Lademann, C.A., Renkawitz, J., Pfander, B., and Jentsch, S. (2017). The INO80 Complex Removes H2A.Z to Promote Presynaptic Filament Formation during Homologous Recombination. Cell Rep *19*, 1294-1303.

Lai, W.K.M., and Pugh, B.F. (2017). Understanding nucleosome dynamics and their links to gene expression and DNA replication. Nat Rev Mol Cell Biol *18*, 548-562.

Lakomek, K., Stoehr, G., Tosi, A., Schmailzl, M., and Hopfner, K.P. (2015). Structural basis for dodecameric assembly states and conformational plasticity of the full-length AAA+ ATPases Rvb1 . Rvb2. Structure *23*, 483-495.

Lin, C.L., Chaban, Y., Rees, D.M., McCormack, E.A., Ocloo, L., and Wigley, D.B. (2017). Functional characterization and architecture of recombinant yeast SWR1 histone exchange complex. Nucleic Acids Res *45*, 7249-7260.

Liu, X., Li, M., Xia, X., Li, X., and Chen, Z. (2017). Mechanism of chromatin remodelling revealed by the Snf2-nucleosome structure. Nature *544*, 440-445.

Lowary, P.T., and Widom, J. (1998). New DNA sequence rules for high affinity binding to histone octamer and sequence-directed nucleosome positioning. J Mol Biol *276*, 19-42.

Luger, K., Mader, A.W., Richmond, R.K., Sargent, D.F., and Richmond, T.J. (1997). Crystal structure of the nucleosome core particle at 2.8 A resolution. Nature *389*, 251-260.

Luk, E., Ranjan, A., Fitzgerald, P.C., Mizuguchi, G., Huang, Y., Wei, D., and Wu, C. (2010). Stepwise histone replacement by SWR1 requires dual activation with histone H2A.Z and canonical nucleosome. Cell *143*, 725-736.

Malik, H.S., and Henikoff, S. (2003). Phylogenomics of the nucleosome. Nat Struct Biol *10*, 882-891.

McCoy, A.J., Grosse-Kunstleve, R.W., Adams, P.D., Winn, M.D., Storoni, L.C., and Read, R.J. (2007). Phaser crystallographic software. J Appl Crystallogr *40*, 658-674.

Meagher, R.B., Kandasamy, M.K., Smith, A.P., and McKinney, E.C. (2010). Nuclear actin-related proteins at the core of epigenetic control. Plant Signal Behav *5*, 518-522.

Merino, F., Pospich, S., Funk, J., Wagner, T., Kullmer, F., Arndt, H.D., Bieling, P., and Raunser, S. (2018). Structural transitions of F-actin upon ATP hydrolysis at near-atomic resolution revealed by cryo-EM. Nat Struct Mol Biol *25*, 528-537.

Misu, S., Takebayashi, M., and Miyamoto, K. (2017). Nuclear Actin in Development and Transcriptional Reprogramming. Front Genet *8*, 27.

Mizuguchi, G., Shen, X., Landry, J., Wu, W.H., Sen, S., and Wu, C. (2004). ATP-driven exchange of histone H2AZ variant catalyzed by SWR1 chromatin remodeling complex. Science *303*, 343-348.

Morrison, A.J., Kim, J.A., Person, M.D., Highland, J., Xiao, J., Wehr, T.S., Hensley, S., Bao, Y., Shen, J., Collins, S.R., *et al.* (2007). Mec1/Tel1 phosphorylation of the INO80 chromatin remodeling complex influences DNA damage checkpoint responses. Cell *130*, 499-511.

Morton, W.M., Ayscough, K.R., and McLaughlin, P.J. (2000). Latrunculin alters the actin-monomer subunit interface to prevent polymerization. Nat Cell Biol *2*, 376-378.

Mueller-Planitz, F., Klinker, H., and Becker, P.B. (2013). Nucleosome sliding mechanisms: new twists in a looped history. Nat Struct Mol Biol *20*, 1026-1032.

Muyldermans, S. (2013). Nanobodies: natural single-domain antibodies. Annu Rev Biochem *82*, 775-797.

Nemet, J., Vidan, N., and Sopta, M. (2017). A meta-analysis reveals complex regulatory properties at Taf14-repressed genes. BMC Genomics *18*, 175.

Obrdlik, A., Kukalev, A., Louvet, E., Farrants, A.K., Caputo, L., and Percipalle, P. (2008). The histone acetyltransferase PCAF associates with actin and hnRNP U for RNA polymerase II transcription. Mol Cell Biol *28*, 6342-6357.

Ocampo, J., Chereji, R.V., Eriksson, P.R., and Clark, D.J. (2016). The ISW1 and CHD1 ATP-dependent chromatin remodelers compete to set nucleosome spacing in vivo. Nucleic Acids Res *44*, 4625-4635.

Olave, I.A., Reck-Peterson, S.L., and Crabtree, G.R. (2002). Nuclear actin and actin-related proteins in chromatin remodeling. Annu Rev Biochem *71*, 755-781.

Olins, A.L., and Olins, D.E. (1974). Spheroid chromatin units (v bodies). Science *183*, 330-332.

Olins, D.E., and Olins, A.L. (2003). Chromatin history: our view from the bridge. Nat Rev Mol Cell Biol *4*, 809-814.

Osakabe, A., Takahashi, Y., Murakami, H., Otawa, K., Tachiwana, H., Oma, Y., Nishijima, H., Shibahara, K.I., Kurumizaka, H., and Harata, M. (2014). DNA binding properties of the actin-related protein Arp8 and its role in DNA repair. PLoS One *9*, e108354.

Ou, H.D., Phan, S., Deerinck, T.J., Thor, A., Ellisman, M.H., and O'Shea, C.C. (2017). ChromEMT: Visualizing 3D chromatin structure and compaction in interphase and mitotic cells. Science *357*.

Papamichos-Chronakis, M., Watanabe, S., Rando, O.J., and Peterson, C.L. (2011). Global regulation of H2A.Z localization by the INO80 chromatin-remodeling enzyme is essential for genome integrity. Cell *144*, 200-213.

Papoulas, O., Beek, S.J., Moseley, S.L., McCallum, C.M., Sarte, M., Shearn, A., and Tamkun, J.W. (1998). The Drosophila trithorax group proteins BRM, ASH1 and ASH2 are subunits of distinct protein complexes. Development *125*, 3955-3966.

Philimonenko, V.V., Zhao, J., Iben, S., Dingova, H., Kysela, K., Kahle, M., Zentgraf, H., Hofmann, W.A., de Lanerolle, P., Hozak, P., *et al.* (2004). Nuclear actin and myosin I are required for RNA polymerase I transcription. Nat Cell Biol *6*, 1165-1172.

Poli, J., Gasser, S.M., and Papamichos-Chronakis, M. (2017). The INO80 remodeller in transcription, replication and repair. Philos Trans R Soc Lond B Biol Sci *372*.

Qi, T., Tang, W., Wang, L., Zhai, L., Guo, L., and Zeng, X. (2011). G-actin participates in RNA polymerase II-dependent transcription elongation by recruiting positive transcription elongation factor b (P-TEFb). J Biol Chem *286*, 15171-15181.

Rada-Iglesias, A., Grosveld, F.G., and Papantonis, A. (2018). Forces driving the three-dimensional folding of eukaryotic genomes. Mol Syst Biol *14*, e8214.

Ranjan, A., Wang, F., Mizuguchi, G., Wei, D., Huang, Y., and Wu, C. (2015). H2A histone-fold and DNA elements in nucleosome activate SWR1-mediated H2A.Z replacement in budding yeast. Elife *4*, e06845.

Rappsilber, J., Mann, M., and Ishihama, Y. (2007). Protocol for micro-purification, enrichment, pre-fractionation and storage of peptides for proteomics using StageTips. Nat Protoc *2*, 1896-1906.

Rasmussen, S.G., DeVree, B.T., Zou, Y., Kruse, A.C., Chung, K.Y., Kobilka, T.S., Thian, F.S., Chae, P.S., Pardon, E., Calinski, D., *et al.* (2011). Crystal structure of the beta2 adrenergic receptor-Gs protein complex. Nature *477*, 549-555.

Razin, S.V., and Gavrilov, A.A. (2014). Chromatin without the 30-nm fiber: constrained disorder instead of hierarchical folding. Epigenetics *9*, 653-657.

Saha, A., Wittmeyer, J., and Cairns, B.R. (2002). Chromatin remodeling by RSC involves ATP-dependent DNA translocation. Genes Dev *16*, 2120-2134.

Saha, A., Wittmeyer, J., and Cairns, B.R. (2005). Chromatin remodeling through directional DNA translocation from an internal nucleosomal site. Nat Struct Mol Biol *12*, 747-755.

Sambrook, J., and Russell, R.W (2012). Molecular cloning: A laboratory manual (Cold spring harbor laboratory press).

Saravanan, M., Wuerges, J., Bose, D., McCormack, E.A., Cook, N.J., Zhang, X., and Wigley, D.B. (2012). Interactions between the nucleosome histone core and Arp8 in the INO80 chromatin remodeling complex. Proc Natl Acad Sci U S A *109*, 20883-20888.

Sarma, K., and Reinberg, D. (2005). Histone variants meet their match. Nat Rev Mol Cell Biol *6*, 139-149.

Schafer, D.A., and Schroer, T.A. (1999). Actin-related proteins. Annu Rev Cell Dev Biol *15*, 341-363.

Schmidt, T.G., and Skerra, A. (2007). The Strep-tag system for one-step purification and high-affinity detection or capturing of proteins. Nat Protoc *2*, 1528-1535.

Schneider, C.A., Rasband, W.S., and Eliceiri, K.W. (2012). NIH Image to ImageJ: 25 years of image analysis. Nat Methods *9*, 671-675.

Schones, D.E., Cui, K., Cuddapah, S., Roh, T.Y., Barski, A., Wang, Z., Wei, G., and Zhao, K. (2008). Dynamic regulation of nucleosome positioning in the human genome. Cell *132*, 887-898.

Schrank, B.R., Aparicio, T., Li, Y., Chang, W., Chait, B.T., Gundersen, G.G., Gottesman, M.E., and Gautier, J. (2018). Nuclear ARP2/3 drives DNA break clustering for homology-directed repair. Nature *559*, 61-66.

Schrodinger, LLC (2015). The PyMOL Molecular Graphics System, Version 1.8.

Schubert, H.L., Wittmeyer, J., Kasten, M.M., Hinata, K., Rawling, D.C., Heroux, A., Cairns, B.R., and Hill, C.P. (2013). Structure of an actin-related subcomplex of the SWI/SNF chromatin remodeler. Proc Natl Acad Sci U S A *110*, 3345-3350.

Schuler, H., Korenbaum, E., Schutt, C.E., Lindberg, U., and Karlsson, R. (1999). Mutational analysis of Ser14 and Asp157 in the nucleotide-binding site of beta-actin. Eur J Biochem *265*, 210-220.

Schwarz, M., Schall, K., Kallis, E., Eustermann, S., Guariento, M., Moldt, M., Hopfner, K.P., and Michaelis, J. (2018). Single-molecule nucleosome remodeling by INO80 and effects of histone tails. FEBS Lett *592*, 318-331.

Scipion, C.P.M., Ghoshdastider, U., Ferrer, F.J., Yuen, T.Y., Wongsantichon, J., and Robinson, R.C. (2018). Structural evidence for the roles of divalent cations in actin polymerization and activation of ATP hydrolysis. Proc Natl Acad Sci U S A.

Shen, X., Mizuguchi, G., Hamiche, A., and Wu, C. (2000). A chromatin remodelling complex involved in transcription and DNA processing. Nature *406*, 541-544.

Shen, X., Ranallo, R., Choi, E., and Wu, C. (2003). Involvement of actin-related proteins in ATP-dependent chromatin remodeling. Mol Cell *12*, 147-155.

Sheng, W., Chen, Y., Gong, Y., Dong, T., Zhang, B., and Gao, W. (2016). miR-148a inhibits self-renewal of thyroid cancer stem cells via repressing INO80 expression. Oncol Rep *36*, 3387-3396.

Shimada, K., Oma, Y., Schleker, T., Kugou, K., Ohta, K., Harata, M., and Gasser, S.M. (2008). Ino80 chromatin remodeling complex promotes recovery of stalled replication forks. Curr Biol *18*, 566-575.

Sikorski, R.S., and Hieter, P. (1989). A system of shuttle vectors and yeast host strains designed for efficient manipulation of DNA in Saccharomyces cerevisiae. Genetics *122*, 19-27.

Singleton, M.R., Dillingham, M.S., and Wigley, D.B. (2007). Structure and mechanism of helicases and nucleic acid translocases. Annu Rev Biochem *76*, 23-50.

Son, E.Y., and Crabtree, G.R. (2014). The role of BAF (mSWI/SNF) complexes in mammalian neural development. Am J Med Genet C Semin Med Genet *166C*, 333-349.

Strahl, B.D., and Allis, C.D. (2000). The language of covalent histone modifications. Nature *403*, 41-45.

Stunkel, W., Kober, I., and Seifart, K.H. (1997). A nucleosome positioned in the distal promoter region activates transcription of the human U6 gene. Mol Cell Biol *17*, 4397-4405.

Sunada, R., Gorzer, I., Oma, Y., Yoshida, T., Suka, N., Wintersberger, U., and Harata, M. (2005). The nuclear actin-related protein Act3p/Arp4p is involved in the dynamics of chromatin-modulating complexes. Yeast *22*, 753-768.

Swaney, K.F., and Li, R. (2016). Function and regulation of the Arp2/3 complex during cell migration in diverse environments. Curr Opin Cell Biol *42*, 63-72.

Szerlong, H., Hinata, K., Viswanathan, R., Erdjument-Bromage, H., Tempst, P., and Cairns, B.R. (2008). The HSA domain binds nuclear actin-related proteins to regulate chromatin-remodeling ATPases. Nat Struct Mol Biol *15*, 469-476.

Tosi, A. (2013). Dissection of the topology, structure and function of the INO80 chromatin remodeler. In Faculty for Chemistry and Pharmacy (LMU Munich).

Tosi, A., Haas, C., Herzog, F., Gilmozzi, A., Berninghausen, O., Ungewickell, C., Gerhold, C.B., Lakomek, K., Aebersold, R., Beckmann, R., *et al.* (2013). Structure and subunit topology of the INO80 chromatin remodeler and its nucleosome complex. Cell *154*, 1207-1219.

Trojer, P., and Reinberg, D. (2007). Facultative heterochromatin: is there a distinctive molecular signature? Mol Cell *28*, 1-13.

Trowitzsch, S., Bieniossek, C., Nie, Y., Garzoni, F., and Berger, I. (2010). New baculovirus expression tools for recombinant protein complex production. J Struct Biol *172*, 45-54.

Turegun, B., Baker, R.W., Leschziner, A.E., and Dominguez, R. (2018). Actin-related proteins regulate the RSC chromatin remodeler by weakening intramolecular interactions of the Sth1 ATPase. Commun Biol *1*.

Tyanova, S., Temu, T., Sinitcyn, P., Carlson, A., Hein, M.Y., Geiger, T., Mann, M., and Cox, J. (2016). The Perseus computational platform for comprehensive analysis of (prote)omics data. Nat Methods *13*, 731-740.

Udugama, M., Sabri, A., and Bartholomew, B. (2011). The INO80 ATP-dependent chromatin remodeling complex is a nucleosome spacing factor. Mol Cell Biol *31*, 662-673.

Urnavicius, L., Zhang, K., Diamant, A.G., Motz, C., Schlager, M.A., Yu, M., Patel, N.A., Robinson, C.V., and Carter, A.P. (2015). The structure of the dynactin complex and its interaction with dynein. Science *347*, 1441-1446.

van Attikum, H., Fritsch, O., Hohn, B., and Gasser, S.M. (2004). Recruitment of the INO80 complex by H2A phosphorylation links ATP-dependent chromatin remodeling with DNA double-strand break repair. Cell *119*, 777-788.

Venkatesh, S., and Workman, J.L. (2015). Histone exchange, chromatin structure and the regulation of transcription. Nat Rev Mol Cell Biol *16*, 178-189.

Virtanen, J.A., and Vartiainen, M.K. (2017). Diverse functions for different forms of nuclear actin. Curr Opin Cell Biol *46*, 33-38.

Wang, F., Ranjan, A., Wei, D., and Wu, C. (2016). Comment on "A histone acetylation switch regulates H2A.Z deposition by the SWR-C remodeling enzyme". Science *353*, 358.

Wang, X., Ahmad, S., Zhang, Z., Cote, J., and Cai, G. (2018). Architecture of the Saccharomyces cerevisiae NuA4/TIP60 complex. Nat Commun *9*, 1147.

Watanabe, S., Radman-Livaja, M., Rando, O.J., and Peterson, C.L. (2013). A histone acetylation switch regulates H2A.Z deposition by the SWR-C remodeling enzyme. Science *340*, 195-199.

Watanabe, S., Tan, D., Lakshminarasimhan, M., Washburn, M.P., Hong, E.J., Walz, T., and Peterson, C.L. (2015). Structural analyses of the chromatin remodelling enzymes INO80-C and SWR-C. Nat Commun *6*, 7108.

Willhoft, O., Bythell-Douglas, R., McCormack, E.A., and Wigley, D.B. (2016). Synergy and antagonism in regulation of recombinant human INO80 chromatin remodeling complex. Nucleic Acids Res *44*, 8179-8188.

Willhoft, O., Ghoneim, M., Lin, C.-L., Chua, E.Y.D., Wilkinson, M., Chaban, Y., Ayala, R., McCormack, E.A., Ocloo, L., Rueda, D.S., *et al.* (2018). Structure and dynamics of the yeast SWR1-nucleosome complex. Science *362*.

Wilson, B.G., and Roberts, C.W. (2011). SWI/SNF nucleosome remodellers and cancer. Nat Rev Cancer *11*, 481-492.

Winger, J., Nodelman, I.M., Levendosky, R.F., and Bowman, G.D. (2018). A twist defect mechanism for ATP-dependent translocation of nucleosomal DNA. Elife *7*.

Winn, M.D., Ballard, C.C., Cowtan, K.D., Dodson, E.J., Emsley, P., Evans, P.R., Keegan, R.M., Krissinel, E.B., Leslie, A.G., McCoy, A., *et al.* (2011). Overview of the CCP4 suite and current developments. Acta Crystallogr D Biol Crystallogr *67*, 235-242.

Woodcock, C.L., and Ghosh, R.P. (2010). Chromatin higher-order structure and dynamics. Cold Spring Harb Perspect Biol *2*, a000596.

Wu, W.H., Alami, S., Luk, E., Wu, C.H., Sen, S., Mizuguchi, G., Wei, D., and Wu, C. (2005). Swc2 is a widely conserved H2AZ-binding module essential for ATP-dependent histone exchange. Nat Struct Mol Biol *12*, 1064-1071.

Xia, X., Liu, X., Li, T., Fang, X., and Chen, Z. (2016). Structure of chromatin remodeler Swi2/Snf2 in the resting state. Nat Struct Mol Biol *23*, 722-729.

Yarmola, E.G., Somasundaram, T., Boring, T.A., Spector, I., and Bubb, M.R. (2000). Actin-latrunculin A structure and function. Differential modulation of actin-binding protein function by latrunculin A. J Biol Chem *275*, 28120-28127.

Yen, K., Vinayachandran, V., and Pugh, B.F. (2013). SWR-C and INO80 chromatin remodelers recognize nucleosome-free regions near +1 nucleosomes. Cell *154*, 1246-1256.

Yuen, K.C., and Gerton, J.L. (2018). Taking cohesin and condensin in context. PLoS Genet *14*, e1007118.

Zhang, Z., Wippo, C.J., Wal, M., Ward, E., Korber, P., and Pugh, B.F. (2011). A packing mechanism for nucleosome organization reconstituted across a eukaryotic genome. Science *332*, 977-980.

Zhao, K., Wang, W., Rando, O.J., Xue, Y., Swiderek, K., Kuo, A., and Crabtree, G.R. (1998). Rapid and phosphoinositol-dependent binding of the SWI/SNF-like BAF complex to chromatin after T lymphocyte receptor signaling. Cell *95*, 625-636.

Zhao, X., Pendergrast, P.S., and Hernandez, N. (2001). A positioned nucleosome on the human U6 promoter allows recruitment of SNAPc by the Oct-1 POU domain. Mol Cell *7*, 539-549.

Zhou, B., Wang, L., Zhang, S., Bennett, B.D., He, F., Zhang, Y., Xiong, C., Han, L., Diao, L., Li, P., *et al.* (2016). INO80 governs superenhancer-mediated oncogenic transcription and tumor growth in melanoma. Genes Dev *30*, 1440-1453.

Zhou, C.Y., Johnson, S.L., Lee, L.J., Longhurst, A.D., Beckwith, S.L., Johnson, M.J., Morrison, A.J., and Narlikar, G.J. (2018). The Yeast INO80 Complex Operates as a Tunable DNA Length-Sensitive Switch to Regulate Nucleosome Sliding. Mol Cell *69*, 677-688 e679.

Zhou, C.Y., Stoddard, C.I., Johnston, J.B., Trnka, M.J., Echeverria, I., Palovcak, E., Sali, A., Burlingame, A.L., Cheng, Y., and Narlikar, G.J. (2017). Regulation of Rvb1/Rvb2 by a Domain within the INO80 Chromatin Remodeling Complex Implicates the Yeast Rvbs as Protein Assembly Chaperones. Cell Rep *19*, 2033-2044.

7 Abbreviations

(v/v)	(volume/volume)
(w/v)	(weight/volume)
0N0	mononucleosomes without DNA overhang
0N80	mononucleosomes with 80 bp extranucleosomal DNA overhang
3C-techniques	chromosome conformation capture-techniques
5-FOA	5-fluorooretic acid
Å	Ångström (=10^{-10} m)
aa	amino acid
ABP	actin binding proteins
ACN	acetonitrile
AcOH	acetic acid
ADP	adenosine diphosphate
AE MS	affinity enrichment mass spectrometry
Arp8CTD	C-terminal domain of Arp8
ARPs	actin-related proteins
ATP	adenosine triphosphate
bp	base pair
C-term	carboxy-terminus
Ca	calcium
CDR	complementary defining region
cHC	constitutive heterochromatin
CHD	chromodomain helicase DNA-binding
ChiP-Seq	chromatin-immunoprecipitation followed by high-throughput DNA sequencing
ChromEMT	chromatin electron microscopy tomography
COSMIC	Catalogue Of Somatic Mutations In Cancer
CryoEM	cryo-electron microscopy
CT	chromosome territories
CTCF	CCCTC-binding factor

CVC	chromatin volume concentration
CVs	column volumes
DBD	DNA binding domain
DNA	deoxyribonucleic acid
ds	double-stranded
DSB	double strand break
DTT	dithiothreitol
EDTA	ethylenediaminetetraacetic acid
EMSAs	electro mobility shift assays
F-actin	filamentous actin
fHC	facultative heterochromatin
FR	framework
G-actin	globular actin
GFP-NB	green fluorescent protein binding nanobody
H1	histone protein 1
H2A	histone protein 2A
H2B	histone protein 2B
H3	histone protein 3
H4	histone protein 4
HEPES	4-(2-hydroxyethyl)-1-piperazineethanesulfonic acid
HSA	helicase/SANT-associated
HSS	HAND–SANT–SLIDE domain
HU	hydroxyurea
INO80	inositol auxotroph mutant 80
IPTG	isopropyl β-D-1-thiogalactopyranoside
ISWI	imitation switch
KCl	potassium chloride
Kd	equilibrium binding constant
LatA	latrunculin A
LB	lysogeny broth

Mg	magnesium
MMS	methyl methanesulfonate
MW	molecular weight
N-actin	nuclear actin
N-term	amino terminus
NaCl	sodium chloride
NactNB	Arp4-N-actin binding nanobody
$\mathbf{N_{align}}$	number of aligned residues in a SSM alignment
NCP	nucleosome core particle
NDR	nucleosome-depleted regions
NegC	negative regulator of coupling domain
NFRs	nucleosome-free regions
NTP	nucleoside triphosphates
OD600	optical density at a wavelength of 600 nm
ORI	origin of replications
PAGE	polyacrylamide gel electrophoresis
PcG	polycomb group
PCR	polymerase chain reactions
PDB	protein data bank
PEG	polyethylene glycol
Pi	phosphate
PI	protease inhibitor
PTM	posttranslational modifications
RMSD	root-mean-square deviation
RNA	ribonucleic acid
SD	sub-domain
SD medium	synthetic defined medium
SDS	sodium dodecyl sulfate
SF2	superfamily 2
SHL	superhelical location

SMC	structural maintenance of chromosome
smFRET	single molecule fluorescence resonance energy transfer
Snf2	sucrose non-fermenting 2
SSM	secondary structure matching
SWI/SNF	switch/sucrose non-fermenting
TADs	topologically associated domains
TFA	trifluoroacetic acid
Tris	trisaminomethane
TSS	transcription start site
WT	wild type
YPD	yeast-extract-peptone-dextrose

8 Acknowledgements

Without the support from various persons this work would not have been possible. Here I want to thank everybody who helped me to complete this thesis.

First of all, I want to thank my supervisor Karl-Peter Hopfner for providing a supportive research environment, for giving me advise whenever I asked for it but also for enough freedom to develop and complete own ideas. Especially I am grateful to Sebastian Eustermann with whom I was working on the 'INO80 N-actin project' together, who helped me in every situation I have been stuck with unlimited scientific knowledge and who motivated me to start this thesis. I am grateful to Robert Byrne, Kevin Schall and Charlotte Lässig for careful proofreading of this thesis. I am very thankful to Manuela Moldt who introduced me into the lab and who helped me with practical support whenever I asked for it. I want to thank all former and present members of the INO80 subgroup Kevin Schall, Vanessa Niebauer, Marianne Schwarz, Sebastian Eustermann, Kristina Lakomek, Gabriele Stoehr, Sandra Schuller and Stephan Woike for inspiring discussions, daily help in the lab, the motivating and fun environment in our 'INO80-Bay' and the great conference visits we had. I am very grateful to Robert Byrne who helped me with his deep knowledge in all questions I had to him. I want to thank Hinnerk Saathoff for discussions and help with various assays. I am very thankful to Gregor Witte and Katja Lammens for technical advice and the exciting synchrotron trips we had. I want to thank all members of the Hopfner lab for the positive and supportive working atmosphere. I am particularly thankful to Elisa Oberbeckmann and Philipp Korber for our stimulating and productive collaboration. I want to thank Petra Runge-Wollmann for the great organization of our research training group and personal support. I am thankful to the RTG1721 for funding. I am thankful to my second-reviewer Roland Beckman and the co-reviewers Philipp Korber, Johannes Stigler, Julian Stingele and Klaus Förstemann.

I am deeply thankful to you Padmi for your never-ending patience, support and love.

Meinen Eltern und meiner Familie möchte ich für die liebevolle Unterstützung und den starken Rückhalt von ganzem Herzen danken.

My apologies to all other whom I have not mentioned by name – I am thankful to you as well.